Feasibility of inspecting mechanical damage of wind turbine nacelle components by using a mobile-robot equipped with sensor devices

by

Nathalia da Costa Ferreira

Supervisor:

Prof.Dr. Xiu Yan

A thesis submitted in partial fulfillment for the requirement of the degree

Master of Science

Sustainable Engineering: Renewables Energy System and the Environment

University of Strathclyde

Glasgow, Scotland

2013

Copyright Declaration

Abstract

Wind turbine plants have increasingly being installed over the past two decades across the world. However, over the time, as the wind turbine ages, the significance of an efficient inspection and/or components condition assessment has increased tremendously [36]. The issues that arise with the wind turbine inspection are often complex and require sophisticated strategies. A crucial point of the inspection is the limited accessibility of the wind turbine components, which reflects immediately on the energy cost of the wind farm. This concerns in particular the offshore wind turbines, which can partly only be accessed by boat or helicopter, and because of the harsh maritime weather condition, only for a limited time period [22]. Therefore, the concept of inspecting the wind turbine with a mobile-robot has been raised in the recent years. In this connection, it is from great importance that the mobile-robot is reliable and able to complete several inspection tasks autonomously and accurately. Hence, the motivation of this dissertation is to assess the technical and economic feasibility of inspecting the wind turbine mechanical damages by using a mobile-robot equipped with sensor devices. Thereby, only the integrated components in the nacelle interior area of the wind turbine will be considered. The overall evaluation process consists of three main steps. First of all, of a literature analysis, where the research problem and focus will be identified. Secondly, of an experimental analysis, due to experiments with a 3D laser scanner it will be analysed the accuracy of the obtained 3D images and evaluated the potential application of the 3D laser system to inspect the mechanical damages. In the last step of the evaluation process, a feasibility assessment will be performed. Based on the conducted experiments and literature analysis, it will be highlighted, which inspection tasks can be carry out by each sensor device or combination of sensor devices as well the therewith acquired economic benefits.

Acknowledgements

Firstly, I would like to express my sincere thanks to the course supervisor Prof.Dr. Paul Strachan and to John Leabody for their support in the enrolment in the course. I'm very thankful for this great experience and opportunity. In addition, I would like to thank my project supervisor Prof.Dr. Xiu Yan for introducing me to the topic as well for his assistance and advice throughout this project. I also like to thank the participants in my experiments for their generous assistance.

Furthermore, I would like to extend my thanks to my friends and family, especially to my beloved mother, who encouraged and supported me throughout my academic career.

Contents

List of Figures

List of Tables

Latin Letter

Symbol	Comment	Unit
A	Rotor swept area	m^2
C	Capital loaned	£
c_p	Power coefficient	—
C_c	Capacity coefficient	—
D	Rotor diameter	m
E	Energy	W
F	Frequency	T^{-1}
n	Number of years for repayment	—
r	Interest rate	%
RPM	Rotation per minute	—
V_∞	Wind speed	m s^{-1}
V_1	Cut-in wind speed	m s^{-1}
V_2	Rated wind speed	m s^{-1}
V_3	Cut-out wind speed	m s^{-1}
T_1	Number of day at cut-in wind speed	—
T_2	Number of day at rated wind speed	—
T_3	Number of day at cut-out wind speed	—

Greek Letter

Symbol	Comment	Dimension
ρ	Air density	kg m^{-3}

Chapter 1

Introduction

The wind turbine industry has experienced worldwide a rapidly growing market over the last two decades [1]. In the European Union alone, the wind power installations have grown constantly between 2000 and 2012 from 3.2 GW to 11.9 GW with an annual growth rate of approximately 11 percent [2]. With the growth of the wind power installation the inspection and maintenance issues are becoming extremely significant.

Figure 1.1: Maintenance of a Wind Turbine [37].

The life span of a wind turbine is typically around twenty years, however some of the integrated equipments as such the main-shaft, gearbox or the electrical system have a relatively short life span and require frequently inspections, maintenance and potentially replacement. These are costly tasks as for example the cost of replacing the gearbox accounts for about ten percent of the wind turbine construction and installation cost, which eventually results in an increase of the energy production cost [3].

Therefore, a reliable inspection of wind turbine failure is of great importance, in order to ensure the detection of any unexpected damage or degradations to the wind turbine at an early stage and so enable an efficient repair or replacement well ahead. But inspections and maintenance operations in wind turbines are very complex and costly, as the inspections are mostly carried out in the harshest environment, creating also additional risk of personal injury. The currently state-of-art method is a manual and visual inspection of the equipments in the nacelle interior area. Operators have so far rely on two methods [38]:

- The data acquisition by means of condition monitoring systems [38]. This system is responsible for a continuously monitoring of the condition of the plants [38]. In this connection, the system evaluates and records the data collected by the sensors devices, which are available either as stand-alone systems or are integrated into the plant control systems. Due to the information acquired from the monitoring system, the maintenance and repair operations can be planned well ahead [38]. In case of an emergency such as to high vibration or temperature, the system sets an alarm off [38].

- And visual examination by experienced service technicians, although a frequently visual inspection is only in onshore wind turbine feasible [38]. The visual inspection of offshore wind turbine by service technicians requires additionally the use of a helicopter or a boat.

In order to keep the downtime of wind turbines as short as possible and also to facilitate those future preventive inspections, some recent research on new types of mobile-robot system for wind turbine inspections have been done. The mobile-robot system for inspection of the wind turbines can be subdivided into two main types; either it is capable to climb the wind turbine autonomous or it is permanently direct located in the nacelle interior area and so able to continuously conduct inspections of the components [38]. This type of robot system is specially suitable for offshore wind turbine, where the access for inspections are more limited. However, the German Wind Technology Management GmbH in cooperation with the Bremen Institute for structural mechanics and production has developed a mobile-robot system, which is

equipped with a intelligent camera system and is permanently integrated in the wind turbine nacelle interior area [38]. The camera system with an intelligent zoom function has the task to detect any anomaly of the components in the nacelle. In this study it will be evaluated the economic and technical possibility of amplify a wind turbine inspection-robot with several sensor devices.

Aim of this dissertation is therefore to evaluate the technical and economic feasibility of inspecting the wind turbine mechanical damages by using a mobile-robot equipped with sensor devices, in order to improve the accuracy of the inspection and decrease downtimes, maintenance costs and risks. In this connection, only the integrated components in the nacelle interior area of the wind turbine will be considered. Moreover, due to experiments with a 3D laser scanner it will be analysed the accuracy of the obtained 3D images and evaluated the potential application of the 3D laser system to inspect the mechanical damages. Based on the conducted experiments and literature analysis, it will be highlighted which inspection tasks can be carry out by each sensor device or combination of sensor devices as well the therewith gained economic benefits.

Chapter 2

Background

The wind turbine captures the kinetic energy from the wind and converts into mechanical energy by rotating the rotor blades. Consequentially, the produced mechanical energy is transmitted to an assembled generator, which converts this energy into electricity in a process called wind power [43]. The amount of energy obtained from moving air, can be defined from the air mass, which flows through a certain area during a certain time period [4]. The kinetic energy of the wind depends on the air density [45]. Basically it applies, the higher the air density the more energy can be extracted [45]. Furthermore, the energy output of the plant depends on the wind speed and on the rotor blades diameter [45], the great the diameter of the rotor blade is the greater the power output [45]. This is exemplary shown in Figure 2.1. In this chapter, the wind
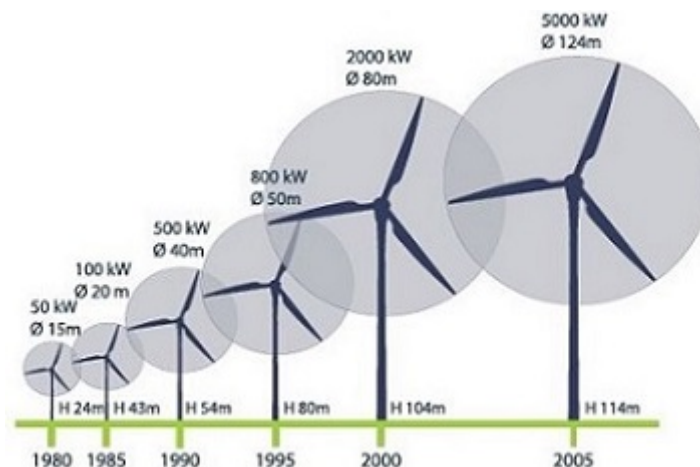
Figure 2.1: Wind turbine sizes [75].

turbine types and the main components of the system, will be explained in more detail.

2.1 Wind Turbine Types

Generally, there are several types of wind turbine, which essentially differ in their construction design. A fundamental distinguishing feature is the arrangements of their rotation axis; vertical axis and horizontal axis [42]. Further distinguishing feature are the number of blades as well the blades design. However, it exists several of available designs for both type and each of them has particular advantages and disadvantages. The Figure 2.2 shows an example of both main types of wind turbine rotation axis.
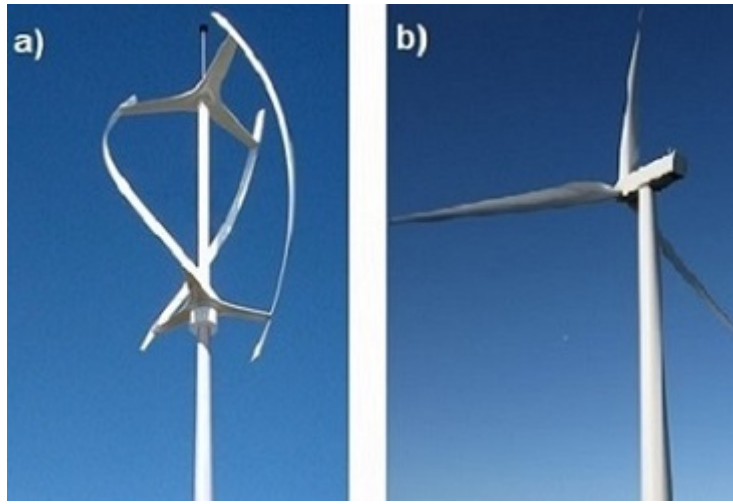
Figure 2.2: Wind turbine types; a) vertical axis wind turbine (Darrieus Wind Turbine) [60], b) horizontal axis wind turbine [61].

2.1.1 Vertical axis wind turbine

The rotor of a vertical axis wind turbine rotates on a vertical shaft perpendicular to the ground and is therefore independent of the wind direction [4]. The most common type of vertical axis wind turbine is the Darrieus wind turbine also known as Eggbeater, which is composed of three vertical parallel stationary blades that are arranged in a triangle [41, 44]. One of the main advantage of wind turbines with vertical axis is that, compared to the horizontal axis wind turbines, they have better flow characteristics [41]. Therefore, the vertical axis wind turbine can be located closer to each other in the wind farms [41]. Besides that, the vertical axis designs are robust and able to operate smoothly and quietly [41]. However, further advantages include their simple machine structure with easily accessible mechanical and electrical components, which are placed

near the ground [4]. While there are some advantages in vertical wind turbine structure there are considerable more disadvantages [44], which overweight making this structure less attractive for the market. The main disadvantage is its low efficiency factor, since the blades are located so close to the ground the vertical axis blades are unable to take advantage of the high speed of the wind at high level [27, 41].

2.1.2 Horizontal axis wind turbine

On the other side, the horizontal axis wind turbine shows as well valuable considerations. To the main advantages of this type of wind turbine include among others, the high technical maturity of the individual components [4]. Further advantages are of this design are the high efficiency, the controllability of the dynamic and vibration problems as well of the control technology [4].

2.1.2.1 Upwind and Downwind Turbines Classification

Basically, the horizontal axis wind turbine can be classified as upwind or downwind turbines [4]. The Figure 2.3 illustrate the two classification for a horizontal axis wind turbine.
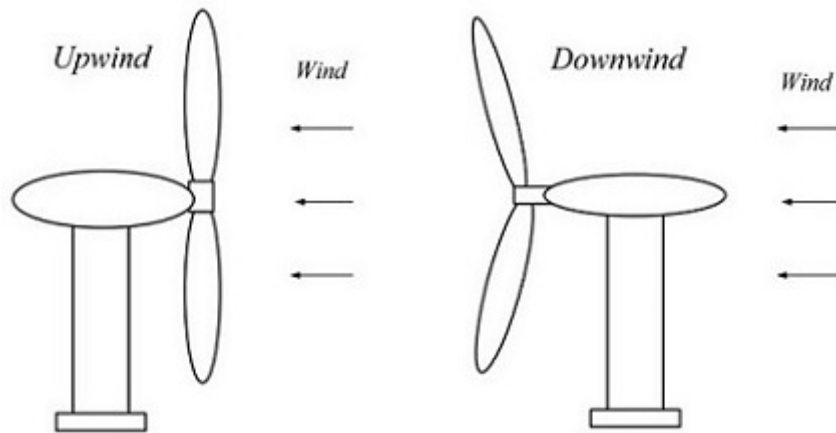
Figure 2.3: Upwind and Downwind Turbines [5].

The upwind turbines design have their rotor facing the wind. Therefore, the blades of the upwind turbine design have to be stiff, in order to avoid the blade from being pushed into the tower by high wind speed [43]. Moreover, the blades have to be mounted a considerable distance in front of the tower [43]. This design has the main advantage of

reducing the wind shade behind the tower [76]. On the contrary of the upwind turbine designs, the downwind turbine have their rotor mounted on the lee side of the tower [5]. Theoretically, the downwind turbines have the advantage that they may not need a additional yaw mechanism [5]. This design allows also the blades to bend, so they are usually made of more flexible materials and thus lighter than the upwind blades[5, 43]. In overall comparison between both type of wind turbine designs, the advantages of the horizontal type overweight the one of the vertical axis wind turbine, making it more competitive in the market. Therefore is the horizontal axis wind turbine the most widely used technology, currently around 99 percent of the systems available on the market are designed in this construction [4]. For this reason, the feasibility study of inspecting wind turbine with a mobile-robot equipped with a sensor devices will focus on the horizontal axis wind turbine. In the following section, the components of a horizontal axis wind turbine will be demonstrated.

2.2 Wind Turbine technical components

A wind turbine consists of several components, as any other technical system, which together enable the full function of the plant [46]. The wind turbine consists essentially of main 12 components. In general, energy is produced as the wind passes through the aerodynamic formed blades and creates thus the rotation movements of the rotor [47]. The individual rotor blades of the wind turbine are fixed on the hub [47]. These transmit the generated torque due to a main shaft into the interior of the nacelle [47]. The main shaft is connected to a multiple stage gearbox, which converts the inputed number of revolutions of the rotor to the required number of revolutions for the generator [47]. The generated electricity is then consequently feed into the grid. The main components of a horizontal axis wind turbine with three rotor blades are illustrated in the Figure 2.4 and are also listed in the Table 2.1. Furthermore, the components of the nacelle are illustrated in the Figure 2.5, showing in more detail the technical equipments.

The model demonstrated in Figure 2.4 and 2.5 have been built as part of this research with a 3D CAD parametric feature solid modeling program (Creo 2.0). It should be

noticed here that only the main technical equipments within the nacelle have been modelled. However, the model of the wind turbine has been built not only with the aim to demonstrate the components of the wind turbine but also with the purpose to demonstrate the inspection procedure with a mobile-robot within the nacelle (See also Chapter 5).

Figure 2.4: Modelled wind turbine.
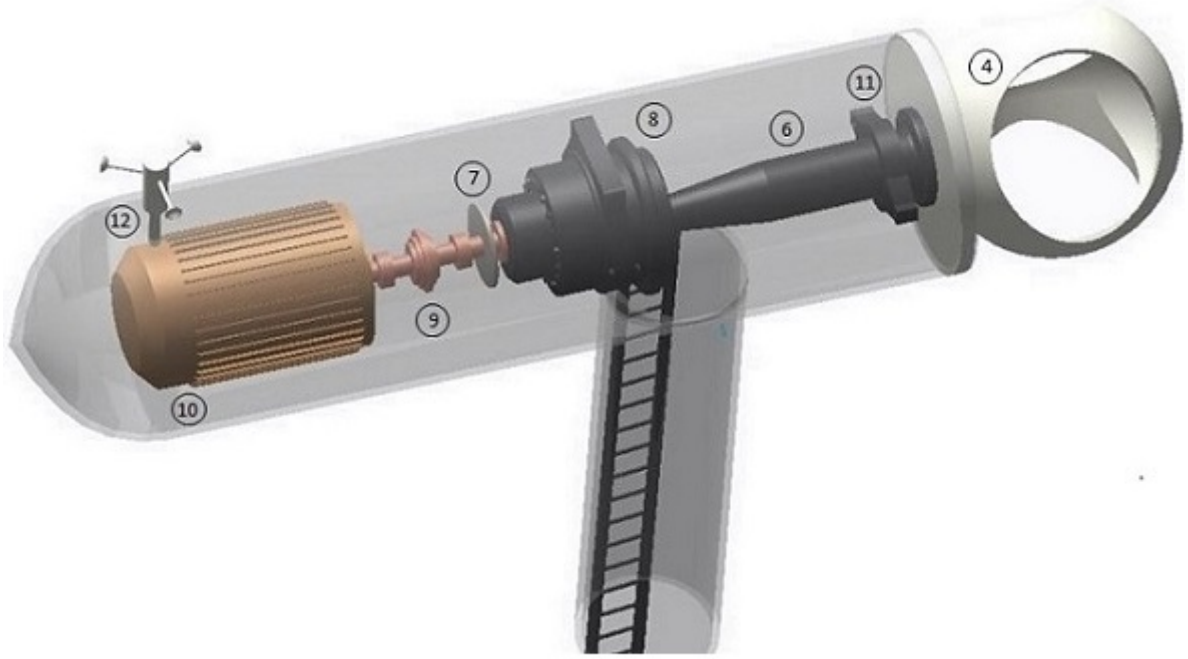
Figure 2.5: Modelled technical equipments within the nacelle.

No.	Components	Comment
1	Base	The base as the foundation of a wind turbine is designed to be very massive [47]. The base has the task to hold a weight of several hundred tons and to give all components secure footing [47]. The base are made of concrete and are additionally strengthened with steel bars. There are two main designs, which basically distinguishes on their dimensions [57].
2	Tower	The tower are mostly made of steel. Depending on the wind turbine type, there are also the option of a hybrid tower, made of steel and concrete [39]. The hybrid tower comprises a concrete tower with a height of about 60 meters which is fixed directly on the base at the site [39]. The steel tower section which has a height of further 60 meter is mounted on top of the concrete tower [39]. The advantages of a hybrid tower is that the concrete part can be produced on site, while the steel tower section can be transported on conventional vehicles [39].
3	Rotor Blade	The rotor blades are designed to capture the kinetic energy in the wind and convert it in rotation energy [47]. Due to its particular shape, the wind generates a pocket of pressure as it goes through the blade [47]. Usually, the rotor blade are made of glass fiber or carbon composite [40]. The blades turns about 5-22 rotation per minute [3].

Table 2.1: Wind Turbine components [40].

No.	Components	Comment
4	Hub	The hub has the task to hold the rotor blades together [40]. In additional to that, the mechanism for the adjustment of the angle of incidence of the rotor blades can be found in the hub [40].
5	Nacelle	In the nacelle are located the technical components, which are responsible for the conversion of mechanical energy in electrical energy. The design or rather the shape of the nacelle changes from manufacturer to manufacturer.
6	Main shaft	The rotor shaft also called rotor shaft or low-speed shaft connects the hub with the gearbox. The main shaft rotates at about 30-60 rpm and has the main task to transmit the rotor energy to the gearbox [40].
7	Rotor Brake	The brake, located behind the gearbox, stops the rotor, mechanically, electronically or hydraulically in case of an emergency.
8	Gearbox	The Gearbox connects the low-speed shaft (main shaft) to the high-speed shaft and it is responsible for increasing the rotational speed from around 5-22 rpm to about 1,000-1,600 rpm, which is the generator-required rotation speed [3].
9	High-speed shaft	The high-speed shaft is located between the gearbox and generator. This rotates at about 1,000-1,600 rpm and has the task of driving the generator [3].
10	Generator	The generator converts the mechanical energy of the high-speed shaft in electrical energy. Synchronous generator are compatible with the main three type of drivetrain (See also Section 2.2.1.4) [35].
11	Transfomation Elements	The transformers elements has the task to convert the low voltage output of the generator to a high voltage, which is better for the transport of the electricity [40]. This voltage level is usually in the range of 15-30 kilovolts, and is appropriate for short and as well for medium distances [40].
12	Anemometer	The Anemometer measures the wind speed and transfers the wind speed data to the controller [40]. However, the wind speed measured by the anemometer does not correspond the actually wind speed in front of the wind turbine, as the anemometer is located behind the rotor [40].

Table 2.2: Wind Turbine components [40].

2.2.1 Wind Turbine Drivetrain

The drivetrain is located in the nacelle of the wind turbine and is basically responsible for the conversion of mechanical energy into electrical energy. The Figure 2.4 shows the within this study constructed model of a drivetrain. In general, there are different types of drivetrain design technology in the market. The drive-train design decision is an essential success factor in the wind turbine system, as the drive-train system has a major impact on the future performance of a wind turbine [7]. The main requirements for a drivetrain and gearbox design are [7]:

- High reliability, of mechanical and electronic equipments [7].

- High efficiency, as the heart of the wind turbine the drivetrain efficiency is one of the most essential factor [7].

- Ease of manufacture, maintenance, assembly and as well of transport [7].

- Low capital and maintenance costs [7].

The different drivetrain design technologies can be classified in three main types: drivetrain with gearbox (high-speed modular drivetrain), hybrid drivetrain (medium speed drivetrain) and direct drivetrain (gearless) [7]. Figure 2.6 shows a systematic illustration of the main three drivetrain types.
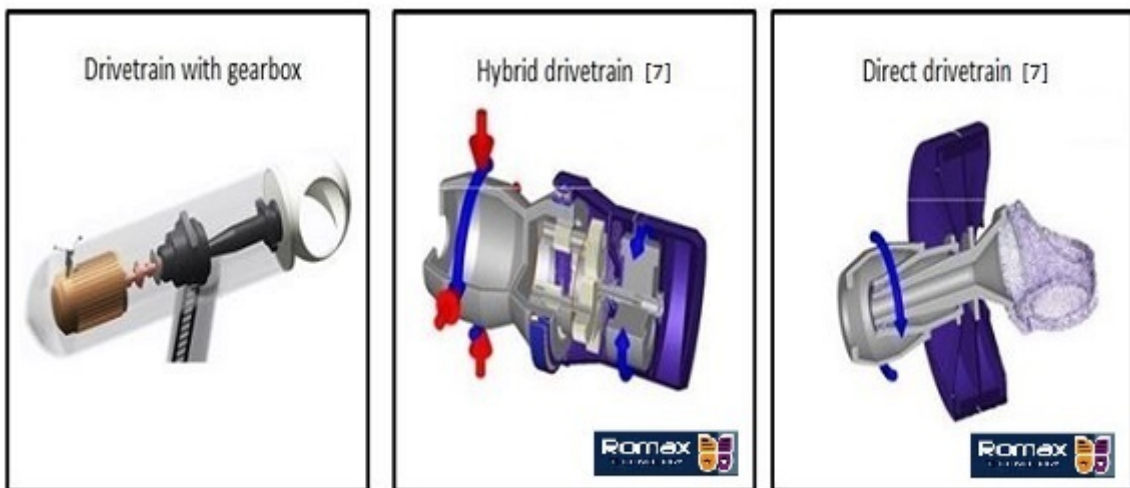
Figure 2.6: Systematic illustration of the main three drivetrain types.

2.2.1.1 Drivetrain with gearbox

The drivetrain with gearbox design is currently the most largely employed drivetrain type and it is usually combined with an asynchronous generator [35]. As previously mentioned, the conversion of mechanical energy into electrical energy is performed by this type of drivetrain by increasing the low rotor blades rotation speed, which is typically between 5-22 rpm (rotation per minute), to the generator-required rotation speed of approximately 1,000 to 1,600 rpm [3]. This results in an average gear ratio or overall ratio of 100:1 [7]. A gear ratio is the relation between the number of revolutions of input to the number of revolutions of output, or in other words the relation among the number of teeth, which are meshed on two or more gears [48, 49].

The increase of revolutions is carried out by an assembled three stage gearbox, which is located between the main shaft also known as low-speed shaft, and the high-speed shaft. The most drivetrain use similar gearbox types which typically consists of different types of gearbox stages. Usually the wind turbine gearboxes comprise of a three-stage spur wheel gearbox, located in lower capacity area, plus an one-stage planetary gearbox with two spur wheel stages, which is located in the middle capacity area and two-stage planetary gearbox with one spur wheel stage that is placed in the higher capacity area [6]. The most common gearbox stage type used by wind turbines are the epicyclic (planetary) gearbox, which has on the one hand the advantage to feature a better load distribution thus compactness [50]. On the other hand, it has problematic regarding the release of heat and also difficulty to employ helical gears, causing therefore more noises [50]. The epicyclic gearing compound of one or more outer gears (planet gear) which turns around a central gear (sun gear) [51]. The Figure 2.7 shows the systematic of a epicyclic gearbox.

As in the Figure 2.7 can be observed, the planet gear carrier, which is here colored in green, is operated by an input torque [51]. The planet gear carrier holds the peripheral planet gears, which are colored in blue [52]. The planet gears have the same dimension and meshes with the central gear (sun gear) [52]. The yellow gear, which is located in the center and hidden by the green gear (planet gear), is called the sun gear and

12
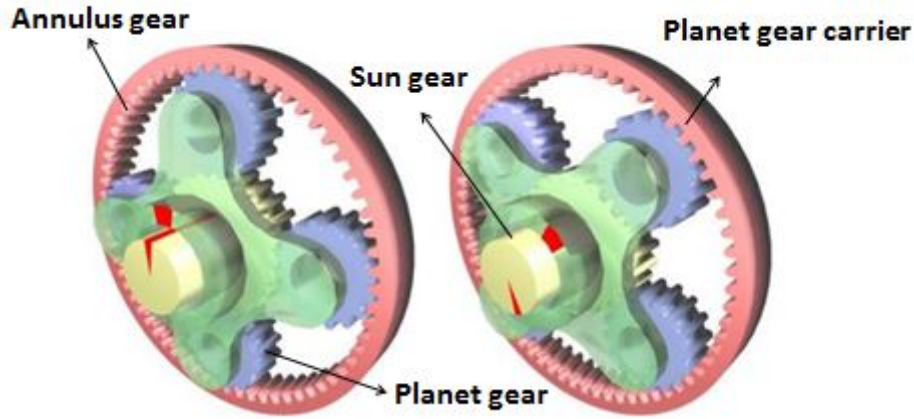
Figure 2.7: Systematic of a epicyclic (planetary) gearbox [51].

supplies the output torque [51]. The ring gear (annulus) colored in pink is fastened [51]. Drivetrain with gearbox have as main advantage, its mature technology, as the most used type [35]. Moreover, the nacelle of this type of drivetrain features a more compact assembling with a better weight sharing and lighter weight [35]. Since the drivetrain with gearbox is equipped with more mechanical components, the system is more vulnerable to fail, especially the gearbox shows problematic [35]. Other disadvantages of this type are the high maintenance and repair cost as well the high level of vibration and flickers [35].

2.2.1.2 Direct drivetrain (gearless)

As the name already implies the direct drivetrain also known as gearless drivetrain excludes the use of a gearbox [53]. The direct drivetrain is combined with a low-speed synchronous generators, which runs with a generator speed of about 12-30 rpm [53, 8]. This type of generator are generally bigger and heavier than the generators assembled in the conventional drivetrain [54]. It is also distinguished by its simple, robust design, which requires no excitation power or control systems as also no slip rings [54]. This mentioned characteristics results in high efficiency at even low loads [54].

As there is no gear in this kind of drivetrain design the overall ratio is equal 1:1 [7]. The direct drivetrain is compared to the conventional geared drivetrain a relative new technology, thats accounts nowadays for approximately 15 percent of the total new

wind turbine installations [8]. Figure 2.8 illustrates direct drivetrain nacelle example.

Figure 2.8: Gearless Wind Turbine [55, 56].

Compared with the conventional drivetrain design the gearless drivetrain holds some competitive benefits. The main one lies in the fact that the gearless design is a simple but sophisticated and reliable system [9]. This consequently makes the need for a gearbox dispensable [9]. Additionally, possess the gearless drivetrain less rotating machines than conventional geared drivetrain, leading to lower failure rates and consequently to lower maintenance costs [9]. Other mentionable advantages include; no costs related to gear such as replacement or repairs as well low vibration and flicker levels [35]. The major disadvantage of this design is the high weight as also the uneven weight distribution which accordingly can lead to problematic mechanical load [35]. Its weight and also large size can complicate the transportation, making it more costly [35].

2.2.1.3 Hybrid drivetrain

In order to combine the advantages of both previously explained drivetrain design, geared drivetrain and the gearless drivetrain, the hybrid drivetrain technology has been developed. The hybrid drive basically unified the gearbox and the generator in one compact system, reducing so the drivetrain length by about 35 percent and thus the overall length of the nacelle [11]. Unlike the conventional drivetrain, the hybrid drivetrain comprises either a two-stage gearbox or a single-stage gearbox [35]. The overall ratio varies thereby between around 10:1 and 40:1 [7]. The generator integrated

in the hybrid system is a permanent magnet generator that runs with speed between 150-400 rotations per minute [8, 11]. Figure 2.9 demonstrated a hybrid drivetrain.
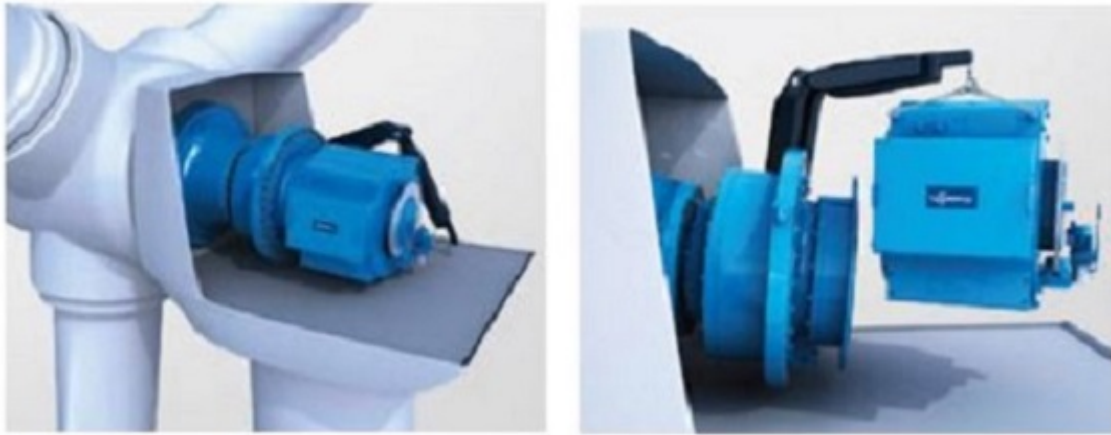
Figure 2.9: Hybrid drivetrain [11].

Besides the compact design the hybrid drivetrain has with respects to the other existing technologies following advantages:

- Flexible integration, the hybrid system can be also integrated in existing nacelle enabling the utilisation of the saved space to house other technical equipments such as converters or transformers [11].

- Highest efficiency of all available technologies [11].

- Ease of maintenance and repairs, through modular design [11].

Despite all these benefits, the hybrid design shows also some crucial drawbacks, as such the cost of the system, which is the most expensive among all types as also the still immaturity of this technology [35].

2.2.1.4 Conclusion of comparison between geared and gearless drivetrain

Altogether, the previously presented three drivetrain types feature relevant benefits as also some drawbacks. As already mentioned the drivetrain with gearbox is the eldest among the three main drivetrain designs and still dominates the wind turbine industry. The Figure 2.10 shows a market research released by SKG Austria AG comparing both types of drivetrain in a period between 2001-2008.
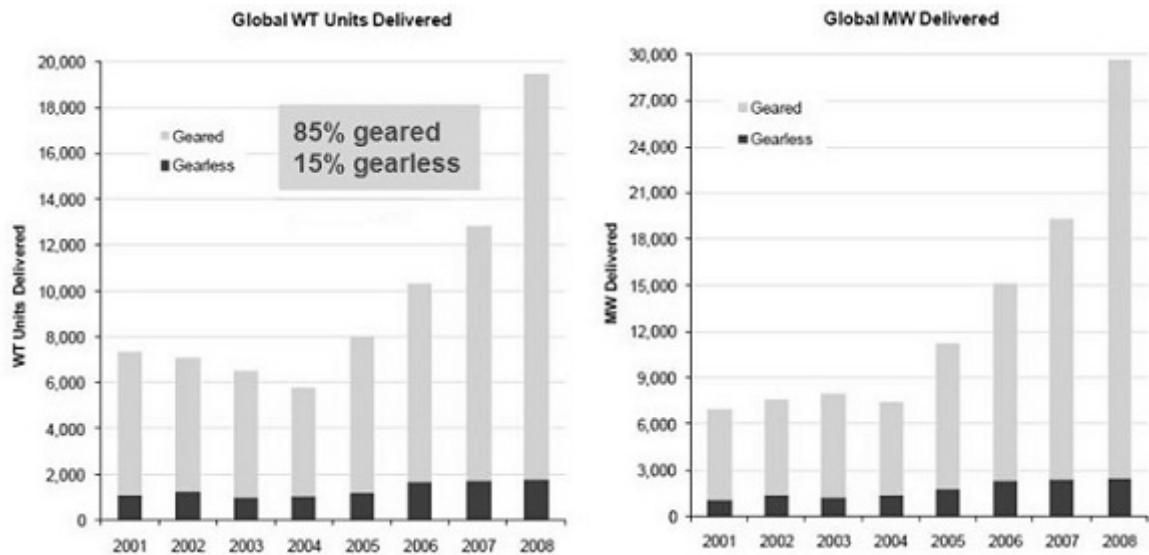
Figure 2.10: Market comparison between geared and gearless drivetrain [8].

As it can be observed the geared drivetrain accounts for 85 percent of the wind turbine installations between 2001-2008 and it was responsible for a global MW delivered of about 30,000 MW compared to 3,000 MW from the gearless in 2008 [8].

However, as the prior generations of wind turbine are aging, particularly the geared drivetrains, the importance of an accurate inspections, maintenance and repair methods are gaining more significance [36]. Therefore, the study of the feasibility of inspecting mechanical failures of wind turbines by using a mobile-robot equipped with sensor devices will be focusing on the geared drivetrain design. Furthermore, it will be also demonstrated in this study the feasibility of applying the inspection methods to the other drivetrain types. The next chapter will examine the typical turbines failures and will give an overview of currently used inspection methods.

Chapter 3

Literature Survey

The determination of the inspection procedures, which will be executed by the sensor device have been identified initially by studying the typical mechanical failures of the wind turbine. The inspection with the sensor device has as main objective to detect in advance any damage of the wind turbine nacelle components, in order to enable the plan of effective and accurately maintenance operations and repairs. In this connection, the captured data from the sensor device are sent to a control system, from where the plant condition can be continuous monitored. Furthermore, this approach not just improves the quality of the maintenance and repairs operation but also avoids undesirable additional downtimes of the plant. In the following chapter, the main wind turbine mechanical failures and the inspections, which have to be performed will be outlined. Moreover, it will be presented the state-of-art inspection techniques and technologies in the wind turbine sector.

3.1   Wind Turbine Failures

As previous mentioned, the wind turbines are designed for a life span of about 20 years. However, numerous of studies have shown that some equipments in the nacelle interior as such the electrical system, hydraulic systems or drive train present very high failure rates, requiring so frequently repairs or replacement. Figure 3.1 shows a graph of the failure rates and the downtime per failure for the main wind turbine subassemblies published in the research article *Wind turbine downtime and its importance for offshore*

deployment [13]. It should be noted that the mean annual downtime days is plotted alongside the downtime per failure [13].
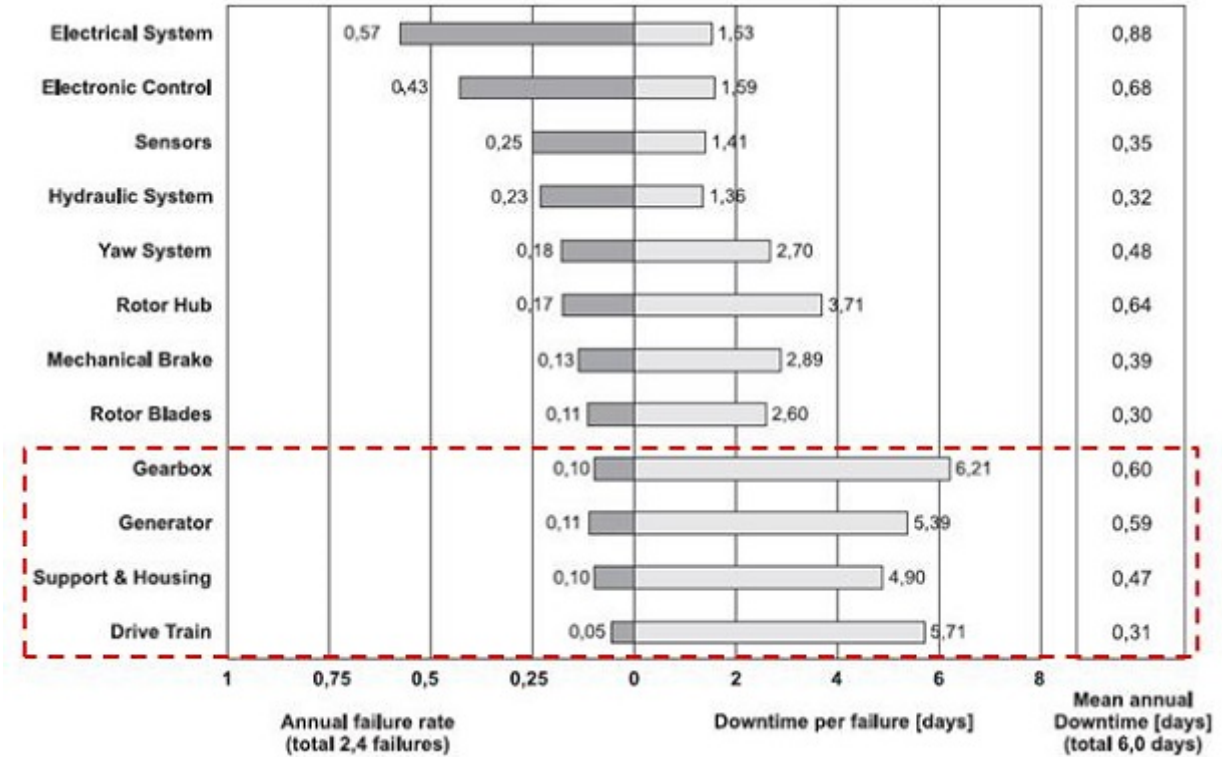
Figure 3.1: Failure rates and downtimes of European Wind Turbines [8].

The graph presented in Figure 3.1 highlighted the importance of consider both aspects; failures rates and downtime per failure [13], since they are both oftentimes not necessary respective to each other. According to this graph, the highest failure rates are found in the electrical system and electronic control, followed by the sensors and hydraulic system. The mechanical components such as, the gearbox, generator, support & housing and drivetrain, which are framed in red, show the lowest failure rates, but at the same time it can be observed that these components possess the longest downtime per failure. The downtimes basically represents the period needed for regular maintenance as also the period of malfunctions [10]. The mean annual downtime varies between 0.88 day (electrical system) and 0.3 day (rotor blades) [13]. All in all, it becomes clear that, on the one hand, the mechanical components feature a relative lower failure rate compared to the electrical and electronic system, but on the other they show a considerable long downtime. In order to estimate the failure severity the authors of the research article

18

Wind turbine downtime and its importance for offshore deployment used the downtime duration, which is based on the *WMEP* database [12, 13]. The *WMEP* also known as *Scientific Measurement and Evaluation Program* is a large monitoring survey for onshore wind turbine in Europe, which had been managed in the period from 1989 to 2006 by the Fraunhofer Institute for Wind Energy and Energy System Technology in Kassel, Germany [13]. The *WMEP* database possess 64,000 maintenance and repairs reports from 1500 wind turbines, which have been documented and analysed [13]. According to the research article *Wind turbine downtime and its importance for offshore deployment* the severity of the failure can be subdivided in [13]:

- **Minor failures**: occurring frequently but with a short downtime [13].

- **Major failures**: occurring seldom but with a long downtime [13].

The downtime duration of 1 day has been employed to distinguish the failures between minor or major, as downtime duration longer than 1 day is assumed to be related to high production losses and costs, since the the service team will inspect the wind turbine at least twice [13]. Hence:

- **Minor failures**: downtime duration $\leq$1 day [13].

- **Major failures**: downtime duration > 1 day [13].

Figure 3.2 shows the result of this analysis. As it can be observed in the graph shown in the Figure 3.2 the failures and downtimes are divided into minor and major. Comparing to the graph in Figure 3.1, it can be see that for example from the overall failure rate of the electrical system (0.57) (see Figure 3.1), 0.45 accounts to minor failures and 0.12 to major failures. The same applies to the mean annual downtime, demonstrated on the right-hand-side of the graph, for example the mean annual downtime of the electrical system (0.88 days) (see Figure 3.1) has been divided in mean downtime duration of minor failures (0.08 days) and mean annual downtime duration of major failures (0.8 days). By comparing the mean annual downtimes duration of the components minor failures it becomes clear that the electrical system (0.08 days) and the electronic control (0.05 days) mean downtime duration are counted among the longest downtime duration. All in all, the minor failures accounts for approximately 75 % of the total

failure and for 5 % of the total downtime whilst the major failures accounts for about 25 % of the total failures and for 95 % of the total downtime [13].
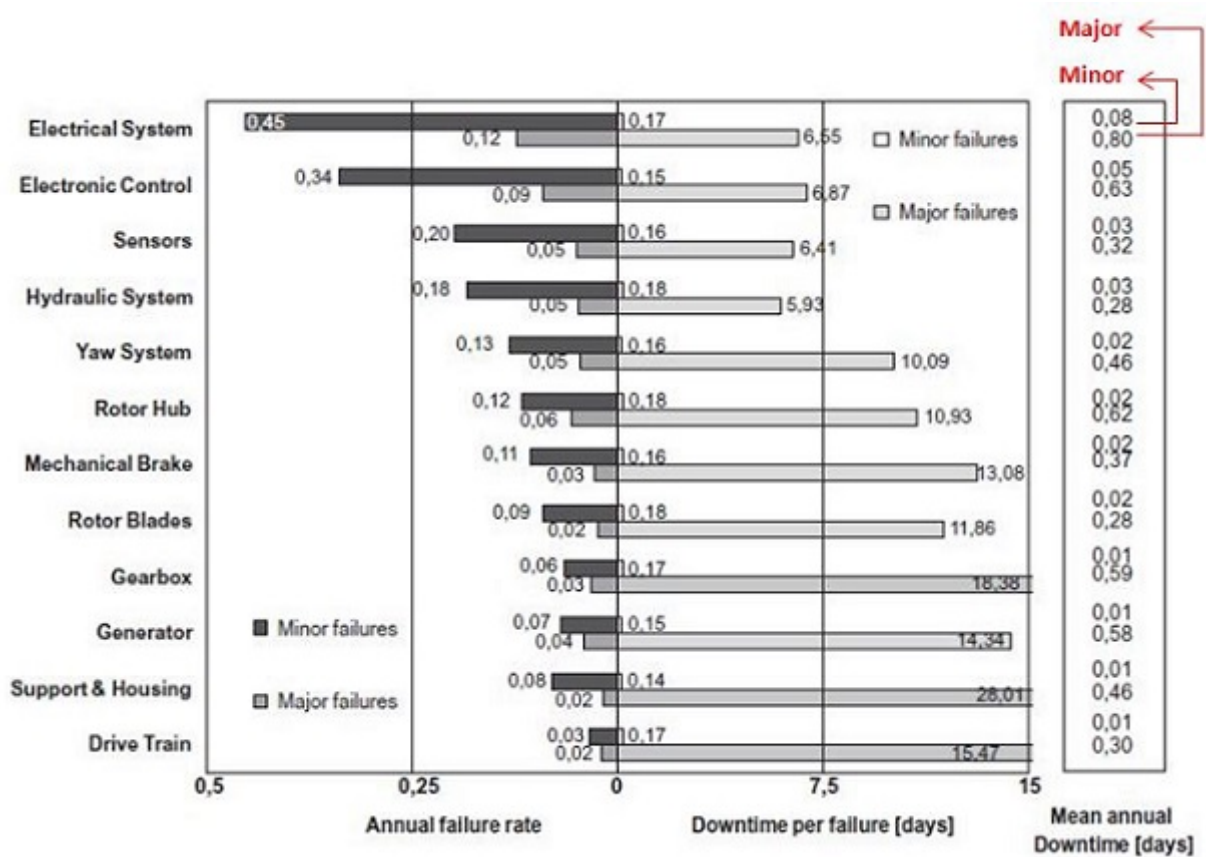
Figure 3.2: Severity of subassemblies failueres [13].

The mechanical components within the nacelle, including the gearbox, drivetrain, generator and the mechanical brake, represent 15 % of the total minor failures and 21 % of the total major failures. The minor mechanical failures are responsible for 3.5 % of the total minor failures downtime, while the major mechanical failure are responsible for 32.3 % of the total major failures downtime.

Overall the mechanical components within the nacelle are responsible for 16 % of the total failures and 25 % of the total downtime duration. These value are significatly large particularly for components within the nacelle, which are consider to be the heart of the wind turbine. Therefore ist is from imense impotance to inspect and detect these failures at an earlier stage, in order to increase the wind turbine reliability and decrease cost and risks.

3.1.1 Cause of wind turbine failures

The root causes of these failures are diverse. In principle, the root causes can be subdivided into two causes; external factors, such as icing, lightning or storm, and internal factors, as for example the failure of components or of the control system. Two third of all wind turbine plant failures lead eventually to a downtime of the plant [12]. In one third of the downtime case, the plant can be taken into operation within a short-term, sometimes after only half day [12]. In other cases the downtime lasts longer, particularly, when there is a requirement for repairs or replacements [12]. Since the early 90's the *Institute for Solar and Energy Supply Technology (ISET)* has documented, also as part of the *Scientific Measurement and Evaluation Program WMEP*, the plant operation of 1500 wind turbines (by 1998) of different designs and size [12]. It has been recorded any kind of malfunctions, repairs, causes and effects on the wind turbine and its operation. These have been reported straight by the operators of the supported wind turbines [10]. Figure 3.3 demonstrated a result of this research, where the main failure causes of an operational wind turbine are shown. As it can be seen 12 percent
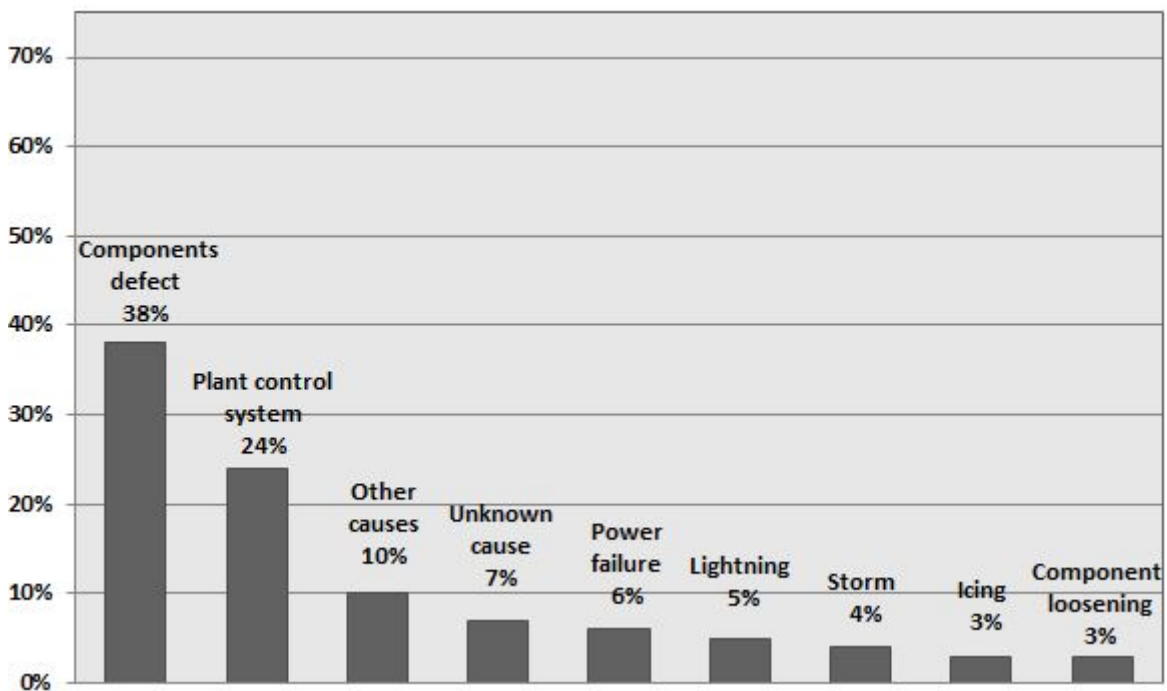
Figure 3.3: Failure causes of an operational wind turbine [12].

of the failure has been caused by external factors, especially old wind turbines, which

often do not possess a lightning protection are affected [12]. Wind turbine, which are equipped with a lightning protection can usually be taken into operation after a short-time [12]. The most failures, accounting for more than 71 percent, are caused by internal factors. It is remarkable that the components defect, which mostly corresponds to technical components in the nacelle, accounts for almost 40 percent of the failure causes. The failures of the technical components can be considered as severe, since those mostly cause a plant downtime and require immediately repair or replacement.

3.1.2 Impacts of wind turbine failures

The wind turbine failures have different impacts on the wind turbine operation. Figure 3.4 shows a further result of the research carried out by the *Institute for Solar and Energy Supply Technology (ISET)* in Kassel [12], where the main impacts of the failure are presented.
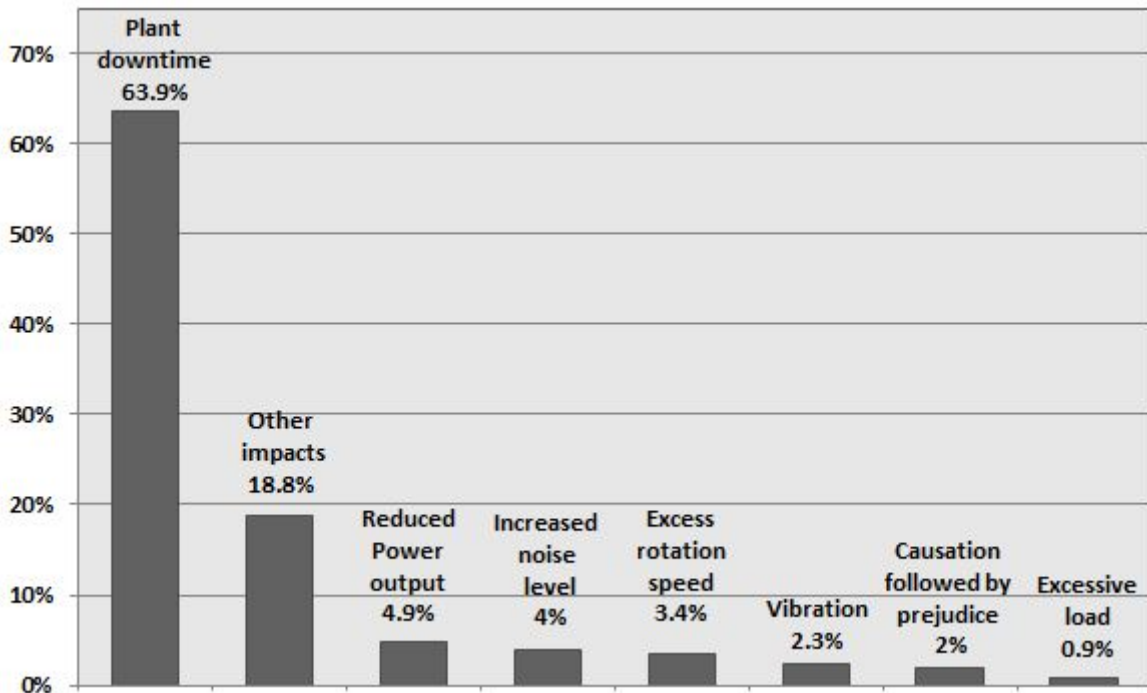
Figure 3.4: Impacts of wind turbine failures [12].

As it can been see, the most frequent impact on the wind turbine operation as a consequence of failure is a total downtime of the plant. Consider to be the nightmare of wind turbine operators, the plant downtimes, are more likely to occur in period of

high wind speed and accordingly after a high wind speed period [25]. The impact of a downtime on the economical performance is immensely, as the wind turbine stop for this period the generation of power.

The *Institute for Solar and Energy Supply Technology (ISET)* in Kassel [12] has furthermore published, as also part of the German *Scientific Measurement and Evaluation Program*, the main occurred failure sources of a wind turbine plant [12]. These failure sources are shown in Figure 3.5, where they are pointed to the corresponding components of the wind turbine model that has been modelled as part of this study.
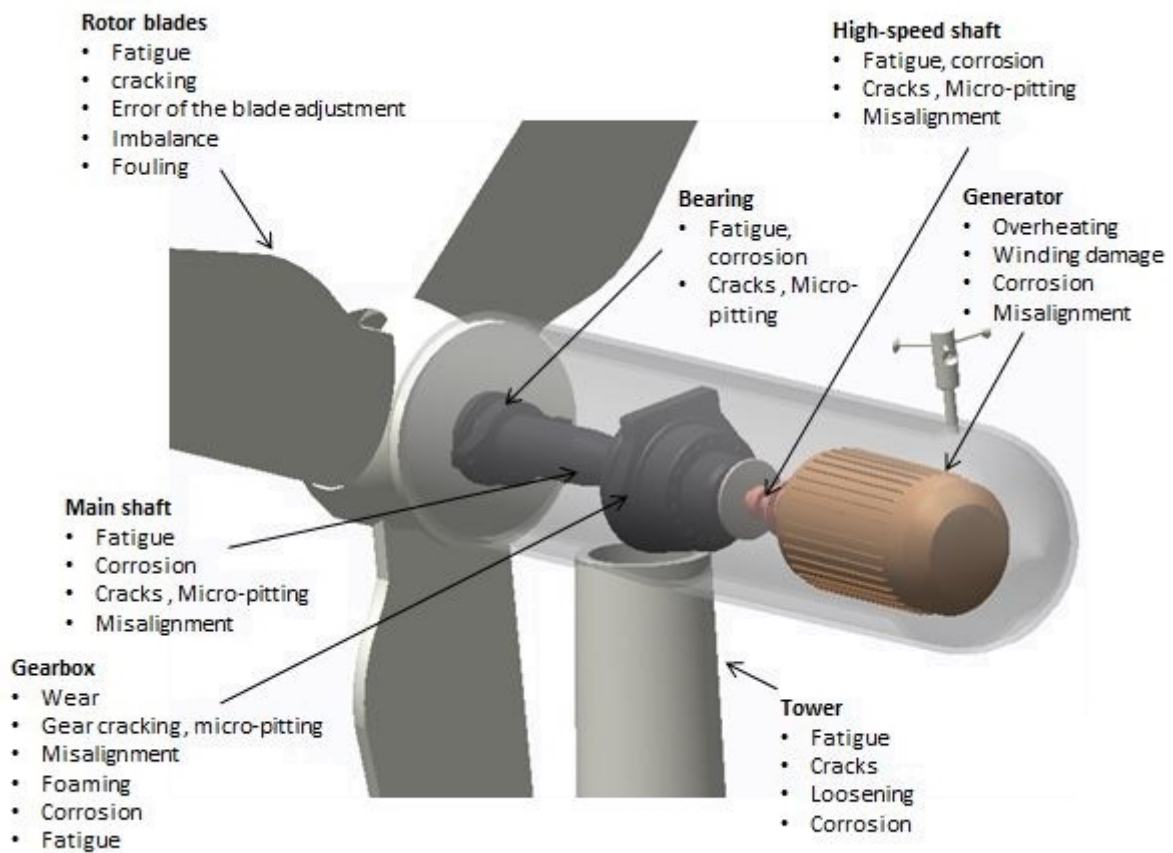
Figure 3.5: Failure sources of a wind turbine plant.

In the Figure 3.5 can be see that the mechanical failures; micro-pitting, corrosion and misalignment occur more frequently. As already mentioned, this study will focus on the mechanical failures of the nacelle components. The following section 3.2 will explain in more details the main mechanical failures of the wind turbine nacelle components.

23

3.2 Mechanical failures within the nacelle

3.2.1 Micro-Pitting

As its can be see in the Figure 3.5 the phenomenon micro-pitting can be found on several components, such as on the bearing, main shaft and high-speed shaft and specially on the gears. Micro-pitting also known as grey staining or frosting is a wear and tear phenomenon, which occurred on the surface areas of heavily loaded metallic component [58]. By observing with unaided eyes, the affected area displays a frosted or dull grey appearance hence the names grey staining or frosting [58]. The cause of this appearance can be recognized under high magnification of the affected area, where a large number of very small pores and micro-cracking can be observed [58]. Figure 3.6 shows examples of micro-pitting at an early and advanced stage.
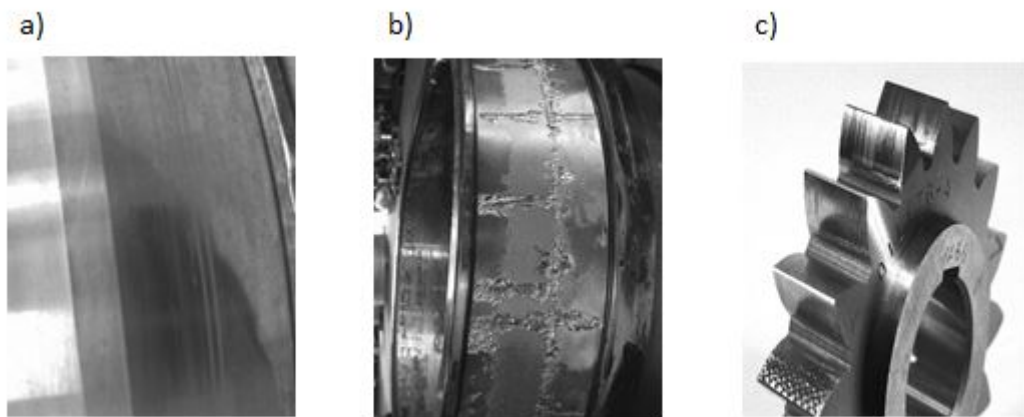
Figure 3.6: Micro-pitting appearance, a) bearing (micro-pitting at an early stage), b) bearing (micro-pitting at a advanced stage), c) gear (micro-pitting at an early stage) [62, 63].

Micro-pitting can be caused by many factors, although roughness and lubricant selection are the main sources [14]. Generally the components surface, for example the teeth of the gears, are separated by a layer of a lubrication oil called Elastohyfrodynamic (EHD) [59]. Due to high temperature, excess load, high speed or water, the required oil (EHD) viscosity can decrease, rising so the probability of micro-pitting [59]. The severest consequence of micro-pitting is the alteration of the components shape through the wearing. Since, the load is not evenly distributed over the surface and concentrates

just on a small area [14]. This can damage the component, for example the gears when they move through the mesh [14]. Furthermore, micro-pitting can cause vibrations, noise, misalignment as also severe fatigue failure [14].

The essential measurement to avoid micro-pitting is to select the proper oil lubricant [14]. Thereby, the oil viscosity plays a significant role [14]. Moreover, it should be consider the operation conditions, as such temperature or speed as these have an significantly affect on the viscosity. The optimisation of geometry and metallurgy of the component can also minimize the chance of micro-pitting [64].

3.2.2 Corrosion

Corrosion is a chemical reaction or electrochemical reaction between a material and its environment, which can cause a remarkable alteration of its surface shape leading often to serious consequences [66]. This phenomenon occurs usually on metallic material. According to Figure 3.5, corrosion affects several components of the wind turbine, including the main shaft, high-speed shaft, generator, gearbox, as well the tower, which is often partly made of steel (See also Chapter 2.2). However, specially affected from corrosion are offshore wind turbines, as the salt in the water and air increases the conductivity making the material more reactive [65]. Offshore wind turbines have therefore additionally, the challenge to avoid the corrosion issues on the base of the turbine, which is placed under water and as well on the tower, which is partially sprayed with seawater.

The currently main applied methods to avoid the corrosion of wind turbine components are: the surface coating, which usually consist of a cooper-nickel alloy (CuNi 90/10) [65] and makes the components material resistant against corrosion, the dehumidification systems and heating system. The dehumidification system has the purpose to reduce the humidity level of the air. As soon as the humidity level decreases to a certain value, the salt is physically unable to absorb enough moisture to initiate the corrosion process [67]. This measurement also decreases the possibility of an electric short-circuiting. The heating system has also as aim the reduction of the relative humidity. Although compared to the other methods, the heating system can be relative cost-intensive, making it a less attractive option.

3.2.3 Misalignment

Misalignment is common problem found in the wind turbine drivetrain. According to Figure 3.5 misalignment issues affect the main components within the nacelle, including the generator, gearbox, main shaft or high-speed shaft. It is also remarkable that all these components belong to the rotating machinery group, where generally misalignments occur. In order to rotate freely and avoid any additional unwanted forces to the system, which can lead to serious damage of the equipments, the rotating machinery have to be proper aligned to each other [16]. The process of alignment is nothing less than making the components co-linear under normal operating condition [16]. On the other hand some components, require a certain defined misalignment, to allow an effective lubrication when operating [18].

Basically, there are four misalignment types, which distinguish from each other in terms of angularity and offset in the vertical (side view) and horizontal (plan view) [18]. These four types are systematically illustrated in the Figure 3.7.

Vertical angularity   Vertical offset

Horizontal angularity   Horizontal offset
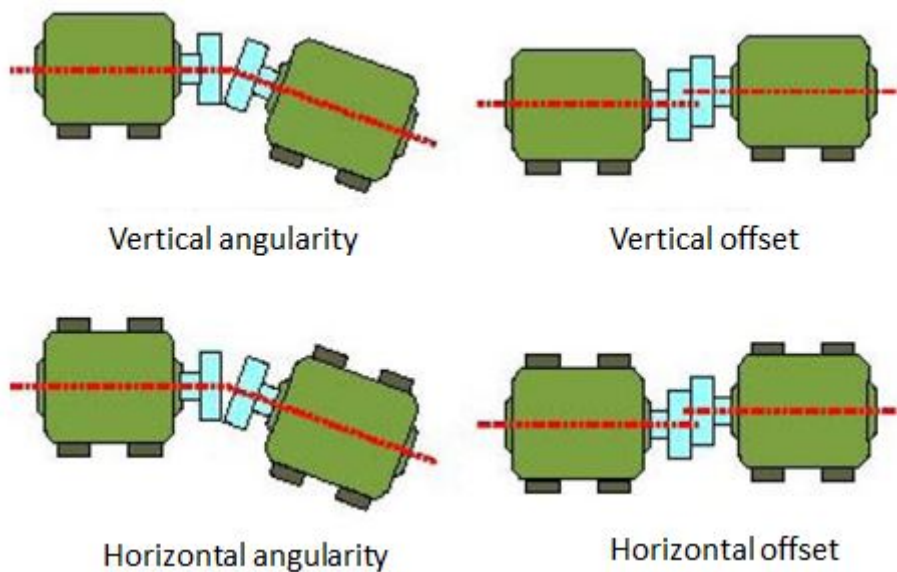
Figure 3.7: Misalignment orientation types [18].

Angularity is a term used to characterize the angle between two rotating axis [18]. The term offset characterize the distance between two rotating axis at a certain point [18]. The measurement of the alignment condition under normal operating condition is crucial as it can modify when the machine is operating. This can be caused by many

factors, such as thermal growth, piping strain, foundation movement, machine torque and so on [18]. Shaft alignments, for example, are measured when the machine is „cold"or in other words out of operation, consequently the value measured are not necessarily the alignment condition of the machine [18]. Section 3.3.2 will explain in more details how misalignment measurement respectively alignment methods are performed.

3.3 Inspections within the nacelle

In order to avoid all those in the previous chapter mentioned failures and consequently downtimes and costs, it is necessary to perform regularly inspections. As already mentioned, due to an early, effective and accurate inspection, the maintenances operation, repairs and replacement can be exact planned in advance, reducing so the downtime period. The inspection requirements are different from component to component. The expert advisory committee of the German Federal Association for Wind Energy released in 2007 a report [15] including a table with the required inspection tasks and inspection scope for wind turbines. Based on this table, the following table (Table 3.1) has been compiled. It should be mentioned that the Table 3.1 has been partly compressed and slight modified, as also due to the research within this study additional inspection tasks and methods came to attention. The Table 3.1 provides besides the inspection tasks per component also the inspection intervals according to the size of the plant.

No	Component	Inspection Task	Inspection Interval		
			annually	every 2 years	every 4 years
1	Hub	cracks, corrosion, coating	> 1.5 MW	0.3 − < 1.5 MW	< 0.3 MW
2	Main shaft	cracks, corrosion, coating, alignment	> 1.5 MW	0.3 − < 1.5 MW	< 0.3 MW
3	Screw fitting shaft-hub	cracks, corrosion, clamping torques	> 1.5 MW	0.3 − < 1.5 MW	< 0.3 MW
4	Axel journals	cracks, coating	> 1.5 MW	0.3 − < 1.5 MW	< 0.3 MW
5	Rotor bearing	Noise, sealing, lubrication, lubrication tank, lightning protection, shaft nut	> 1.5 MW	0.3 − < 1.5 MW	< 0.3 MW

Table 3.1: Wind Turbine inspection task and intervals [15].

No	Component	Inspection Task	Inspection Interval		
			annually	every 2 years	every 4 years
6	Gearbox	Noise, visual inspection control of: abrasion, gearing, micro-pitting, wear debris analysis	> 1.5 MW	0.3 − < 1.5MW	< 0.3 MW
7	Drivetrain	Vibration analysis: constant measurement and capture of vibration data on different points of the drivetrain	> 1.5 MW	0.3 − < 1.5MW	< 0.3 MW
8	Lubrication oil supply	Condition monitoring, function and temperature difference measurement. Visual inspection of: oil level, foaming, filter contamination, debris analysis, function test of fluid pump	> 1.5 MW	0.3 − < 1.5 MW	< 0.3 MW
9	Coupling and brake	Visual inspection control of: condition monitoring, abrasion, alignment	> 1.5 MW	0.3 − < 1.5 MW	< 0.3 MW
10	Torque arm	Motion, alignment, condition monitoring of rubber bearing	> 1.5 MW	0.3 − < 1.5 MW	< 0.3 MW
11	Generator (drivetrain with gearbox (See also 2.2.1.1))	Bearing noise, sealing, fixing on bed plate, vibration, motor connection box, alignment	> 1.5 MW	0.3 − < 1.5 MW	< 0.3 MW
12	Generator (gearless (See also 2.2.1.2))	Corrosion, sealing, inspection of crack on supporting body, air gap, bolted assembly	> 1.5 MW	0.3 − < 1.5 MW	< 0.3 MW
13	Temperature condition	Inspection of maximum bearing and lubrication oil temperature	> 1.5 MW	0.3 − < 1.5 MW	< 0.3 MW

Table 3.2: Wind Turbine inspection task and intervals [15].

The wind turbine inspections state-of-art technology relies mostly on visual and vibration analysis inspection. Generally, the key issues of wind turbine inspections are following:

- The wind turbine has to be shut down for the inspection operations, which con-

sequently results in a cost increase.

- Repeatedly requirement of technicians climbing the wind turbine, specially off-shores, sometimes under extreme weather condition, which besides causing more downtime also increases the risk of personal injury.

- Lack of effective and accurate inspection.

The key challenge is to find inspection methods to avoids those issues. Inspection or condition monitoring is nothing less than the periodic view of the machine operating condition [18]. Basically, the inspection methods can be divided in offline and online inspection. An offline inspection means that the wind turbine has to be shut down for the inspection period and/or requires the attention of a operator [21]. On the opposite an online inspection can be carried out while the wind turbine is operating and usually the measurements devices are permanently integrated in the wind turbine system [20, 21]. Since the downtimes of wind turbine are very expensive, the interest in automated remote inspection methods is becoming more popular.

In the following sections 3.3.1-3.3.3 some inspection methods will be discussed. Thereby, the state-of-art technology for each method will be presented.

3.3.1   Vibration inspection

The vibration analysis inspection delivers several informations about the machine condition. It can help for example, to detect if the condition of the machine has changed, diagnose the cause of the change and classify its condition [18]. Besides that, this method has the advantage of allow the inspection to be performed when the machine is running, avoiding so additional downtime [18]. By definition vibration means the movement of a point, due to internal or external excitation, oscillating about a fixed reference point [18]. It can be classified in: friction vibration (e.g. vibration from a bearing to a bearing house), free body vibration (e.g. shaft vibration), meshing and passing vibration (e.g. gear mesh vibration and blade pass vibration) [18].
Basically, all those vibration types can be found in the wind turbine drivetrain. The frequency along the drivetrain varies from component to component, as it consists of

several different components and each component has a particularly frequency [18]. This is exemplary illustrated in the Figure 3.8. As it is shown in the graph, the condition of each component is indicated through its frequency amplitude [18].
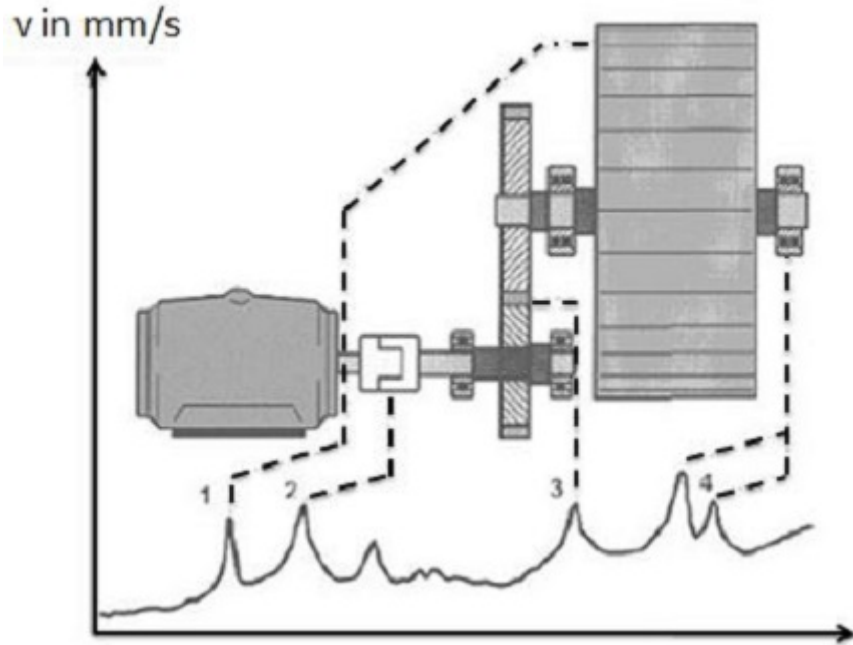
Figure 3.8: Example of frenquency variation within a machinery [18].

The conversion of the obtained vibration signal into an amplitude representation of the individual frequency components, is called vibration frequency spectrum [18]. This conversion is carried out through the Fast Fourier Transform (FFT), which is an algorithm that basically breaks down a time domain function into its frequency domain components [18]. The vibration frequency spectrum analysis has the capability to regulate each vibration component so that the machine spectrum can be subdivided into separate components, as it can be see in Figure 3.9 [18]. This allows an easier detection of mechanical failures within the system [18]. The frequency is hereby defined as [18]:

$$F[Hz] = \frac{RPM}{60} \tag{3.1}$$

This equation enable the definition of the fundamental frequency, which is the primary rotating speed of the machine or shaft [18]. The fundamental frequency is defined as (1x RPM) or as Hz (e.g an 1,200 generator would be 20Hz (1x 1,200)) [18]. Several machine failures happen at few multiple of the fundamental frequency [18].
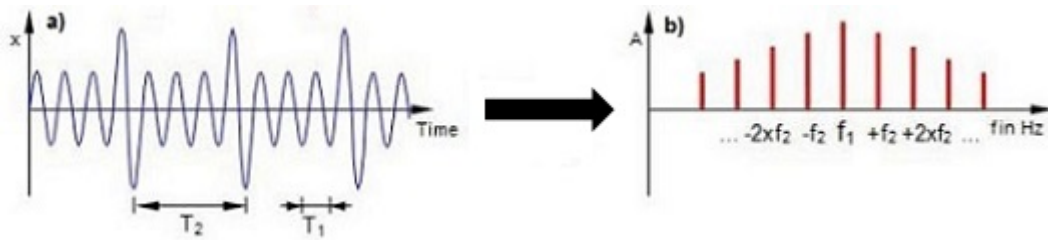
Figure 3.9: Time signal converted in spectrum, here as example a cracked/broken tooth (local problem), a) time signal, b) spectrum [18].

3.3.1.1   On-site vibration monitoring

The on-site vibration measurement and monitoring is usually carry out by a compact portable device equipped with metering sensors. An example of a vibration measuring instrument is the VIBSCANNER (VIB 5.400) from Prüftechnik [19]. Besides of measure the vibration, vibration velocity, displacement and acceleration, this device is also able to measure the temperature, rotation speed [RPM] as well the shock pulse (bearing condition). The VIBSCANNER vibration measuring instrument basically consist of a data collection and a transducer, which are shown in the Figure 3.10.

Figure 3.10: Example vibration measuring instrument (VIBSCANNER),a) built sensor on the top of the data collector, b) data collector, c) transducer with coded measurement location [18].

The Measurement is carried out by placing the transducer, the measuring sensor, in the measurement location. The measurement location has to be an exposure part of

the component, that reflects its vibration. The obtained data are then displayed in the data collector device and can be analysed immediately. Furthermore, the measurement should be conducted with the machine running, when the components have reached their usual operating condition, regarding the speed, temperature, load, voltage and pressure [18].

3.3.1.2 Remote vibration monitoring

The remote vibration measurement is carried out by devices, which are installed in the wind turbine system and consists usually of connection box and several sensors, which are installed on different components of the wind turbine. The connection box is assembled near the measurement location and posses several sensor lines [17]. Figure 3.11 shows an installation example of a connection box with three sensor lines:
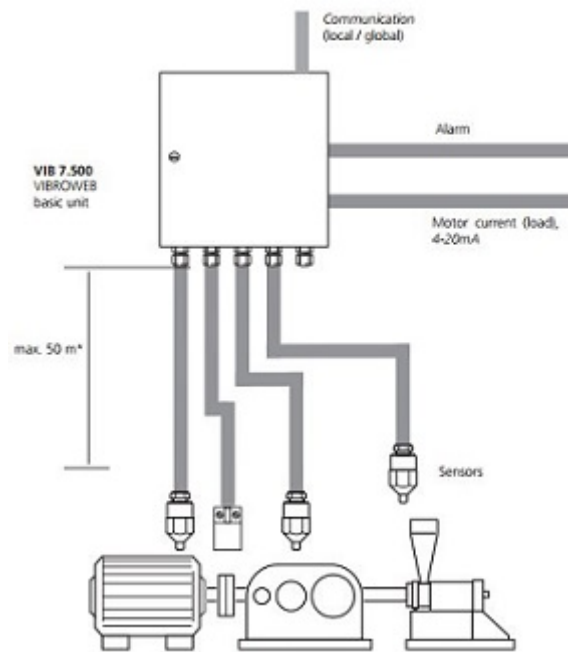
Figure 3.11: Installation example of a remote vibration measurement[17].

The system allows a continuously measurement of the vibration and other parameters, such as the speed, load or temperature. The obtained data are then transmitted to a remote control room and are consequently sent via Internet to the wind turbine operator and Telediagnosis-Partner [20], where the data can be analysed.

3.3.2 Laser system inspection (Misalignment)

The current method to measure misalignment within the wind turbine nacelle is means a portable laser system. The laser system consists mostly of a data collector with display, two laser both with a built-in detector and different types of bracket to support the laser/detector [18]. Figure 3.12. shows the misalignment measurement principle.
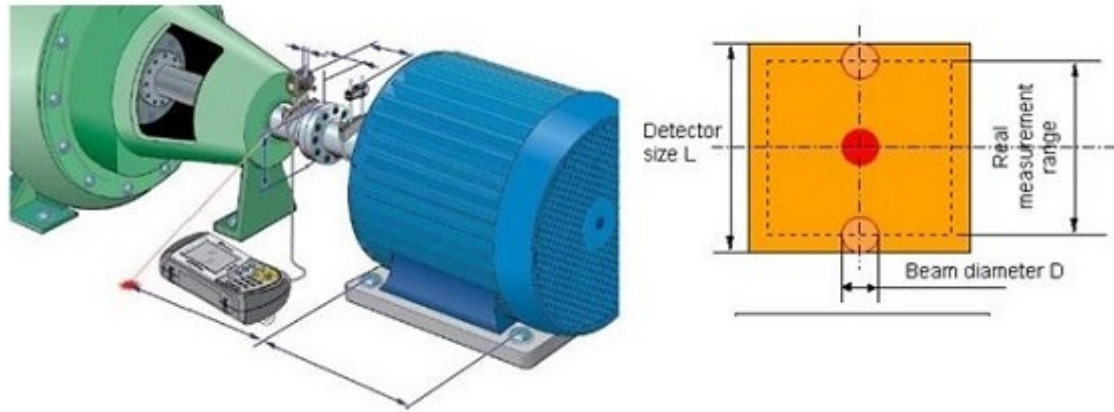
Figure 3.12: Misalignment measurement method [18].

In this process, the lasers send a beam of light, which is detected by the detectors. The deviation is consequently shown on the data collector display, as it can be see in the Figure 3.12. The alignment tolerance depends on the component and its rotating speed. Figure 3.13 shows a table with suggested alignment tolerances [18].

Short "flexible" couplings

Type	RPM	metric [mm]	
		Acceptable	Excellent
Offset	750 900	0.19	0.09
	1200 1500 1800	0.09	0.06
Angularity	750 900	0.13	0.09
	1200 1500 1800	0.07	0.05

Spacer shafts and membrane (disk) couplings

Type	RPM	metric [mm]	
		Acceptable	Excellent
Offset	750 900	0.25	0.15
offs B / offs A	1200 1500 1800	0.12	0.07
Angularity (mrad)	750 900	2.5 (mrad)	1.5 (mrad)
alpha / beta	1200 1500 1800	1.2 (mrad)	0.7 (mrad)

Figure 3.13: Suggested alignments tolerances for a short coupling [18].

3.3.3 Inspection with Infrared (IR) Thermometer

A further method to detect mechanical failures is by using an infrared thermometer sensor. A case study carried out by the Infraspection Institute in the U.S. has examined the thermal difference from mechanical stressed components [16]. The aim of the study was to detect misalignment of machinery components as for example couplings, shafts bearings and so on [16]. In this connection, the temperature of the components, which were misaligned, have been measured by taking thermographic photography of them [16]. The misalignment level has been varied and at each misalignment interval thermographic photographies were taken [16]. This survey was carried out in a series of components and all measured components, without exception showed a considerable temperature risen [16]. Figure 3.14 shows an example of misalignment detection with an infrared thermometer. As it can be observed in the Figure 3.14 the temperature rises
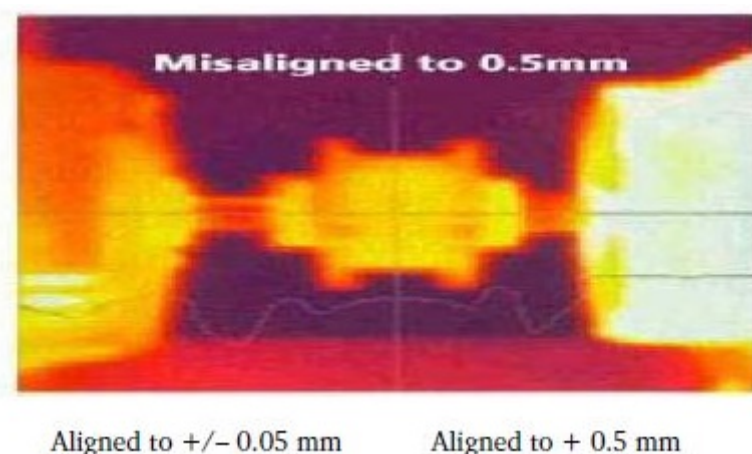
Figure 3.14: Thermographic photography of misalignment (misaligned to 0.05mm and 0.5mm).

significantly with the increase of the misalignment level [16]. Not only the temperature of the coupling changes but also the temperature of the components [16]. As this components are not designed to operate at high temperature for prolonged periods of time, this level of misalignment can result in a total loss [16]. According to Table 3.2 the inspection with infrared thermometer is a method which is not currently applied for the detection of mechanical failures in the wind turbine nacelle interior area. Although there are some projects regarding this (See also Section 3.3.4.2.5). However, inspection with an infrared thermometer is currently mostly applied for the detection of failure on

the wind turbine rotor blades. In other fields the evaluation of mechanical failure with the infrared thermometer is already widespread. The mechanical failures, which can be detected with this type of sensor include, besides misalignment, for example gearbox failures, overload, lubrication, wear and so forth [71]. Moreover, once the infrared thermometer has identified a temperature difference of the component as a result of mechanical stress, the infrared energy is converted into real time full colour display [71]. And according to the severity the of the failure the colour of the components varies enabling so an accurately diagnosis. This can be see in the Figure 3.15 [71]. Furthermore the infrared thermometer is also able to detect any thermal anomalies in
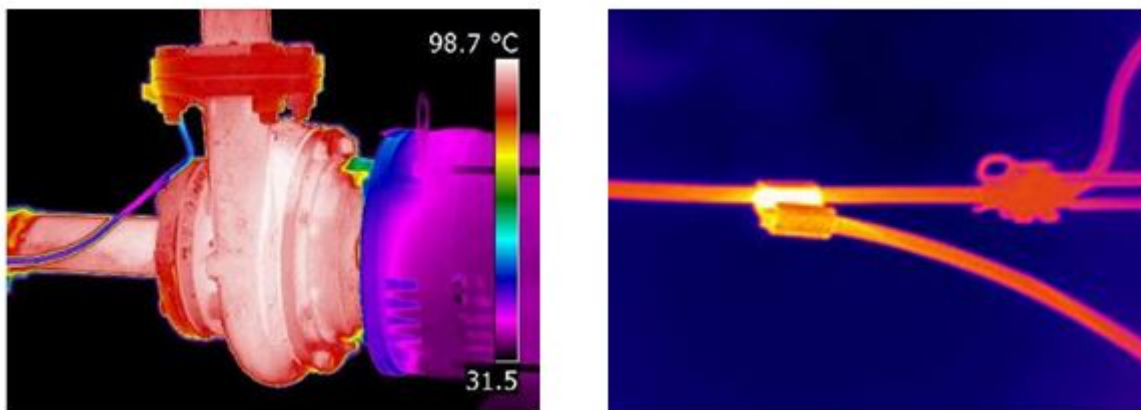
Figure 3.15: Example of thermographic photography of a gearbox and an electrical system [71].

the electrical system, as it is shown in the Figure 3.15 [71]. As previous mentioned, the electrical system features the highest failure rates among the components in the nacelle interior area and in addition to that, it causes a considerable long downtime (See also Section 3.1). However, the state-of-art technologies of infrared thermometer systems are normally very compact and features a light weight and in addition to that they are able to conduct a stable and accurately measurement in a temperature measuring range between -50°C to +2220°C [30]. Moreover, the measurement with an infrared thermometer can be conducted contact-free and autonomous [22]. These characteristics make the infrared thermometer a considerable attractive alternative for the inspection of wind turbine nacelle interior area, specially as combination with further measurement instruments.

3.3.4 Visual inspection

3.3.4.1 Offline visual inspection

The offline visual inspection requires the operation of a experienced technician team. The technician team first inspects the condition of the components by viewing the visible area within the nacelle. The condition monitoring of the not visible and not accessible areas of the nacelle components is inspected by using a portable videoscope instrument. The videoscope instruments basically consists of a micro camera and a display, where the images can be assess immediately. Figure 3.16 show an example of a videoscope instrument for visual inspection of wind turbines components, as well a technician inspecting the gearbox interior.

Figure 3.16: Example of a videoscope instrument for visual inspection of wind turbines components, as well a technician inspecting the gearbox interior [68, 69].

As it can be see the camera is equipped with a variable LED light, which can illuminate small and dark spots of the components interior [68, 69]. The images obtained are sharp and clear, allowing the technician to diagnose the condition of the component effectively [68]. This type of inspection is applied for severals components of the wind turbine, specially for the gearbox, is this inspection methods essential for the maintenance.

3.3.4.2 Visual inspection with Mobile-Robot (state-of-art technology)

As previous mentioned, worldwide researches for wind turbine inspections are giving more and more attention to remote automated inspection methods. Specially for

offshore wind turbine, where the access is more limited resulting in significantly cost increase. Therefore, since 2009, the German Wind Technology Management GmbH have been working in cooperation with the Bremen Center for mechatronics, represented by the Bremen Institute for structure and manufacturing plant, on the conversion of the so called Robot supported Offshore-Service-System also known as *ROSS* [22]. This robot has been so designed to be able to carry out a visual inspection of the wind turbine nacelle interior area [22]. In this connection, the visual inspection is conducted by using a camera system. The captured images or videos can be consequently analysed by experts and in combination with other measured data the experts will be able to diagnose the plant condition effectively [22]. The design and abilities of *ROSS* have been decided by analysing the technical and economic aspects of different concepts, Variant 1-4, which will be demonstrated in this study [22]. Regarding the economic aspect, it has been considered the installation costs, manufacturing costs, and future operation costs. For the technical aspect it was from great significance that the monitoring system possess an adjustable angle of view [22]. Moreover, the system should offer the possibility to integrate further sensors [22]. In the next step, it will be presented the developed and investigated variants 1-4 by the German Wind Technology Management GmbH, the Bremen Center for mechatronics and the Bremen institute for structure and manufacturing plant (called in this study the *ROSS* developer team).

- **Variant 1**: Distributed installed video system (similar to a building video monitoring), which either are fixed cameras or are remote-controlled swiveling cameras [22]. The cameras are so located to be able to cover the necessary monitoring points [22].

- **Variant 2**: Robot systems equipped with a camera. The robot is remote-controlled and is able to move free within nacelle [22]. The robot enable so a full visual inspection [22].

- **Variant 3**: Combination of Variant 1 and Variant 2, the camera system is able to move within nacelle but on a defined path [22]. This method can be realised, for example, by using available structures like a hoisting crane, whose beam hoist can be amplified with a telescopic [22].

- **Variant 4**: The monitoring points can be reached by guiding the camera system on railways [22]. The railways possess straight path as also winding paths [22].

Figure 3.17 shows the Systematical illustration of the 4 variants.
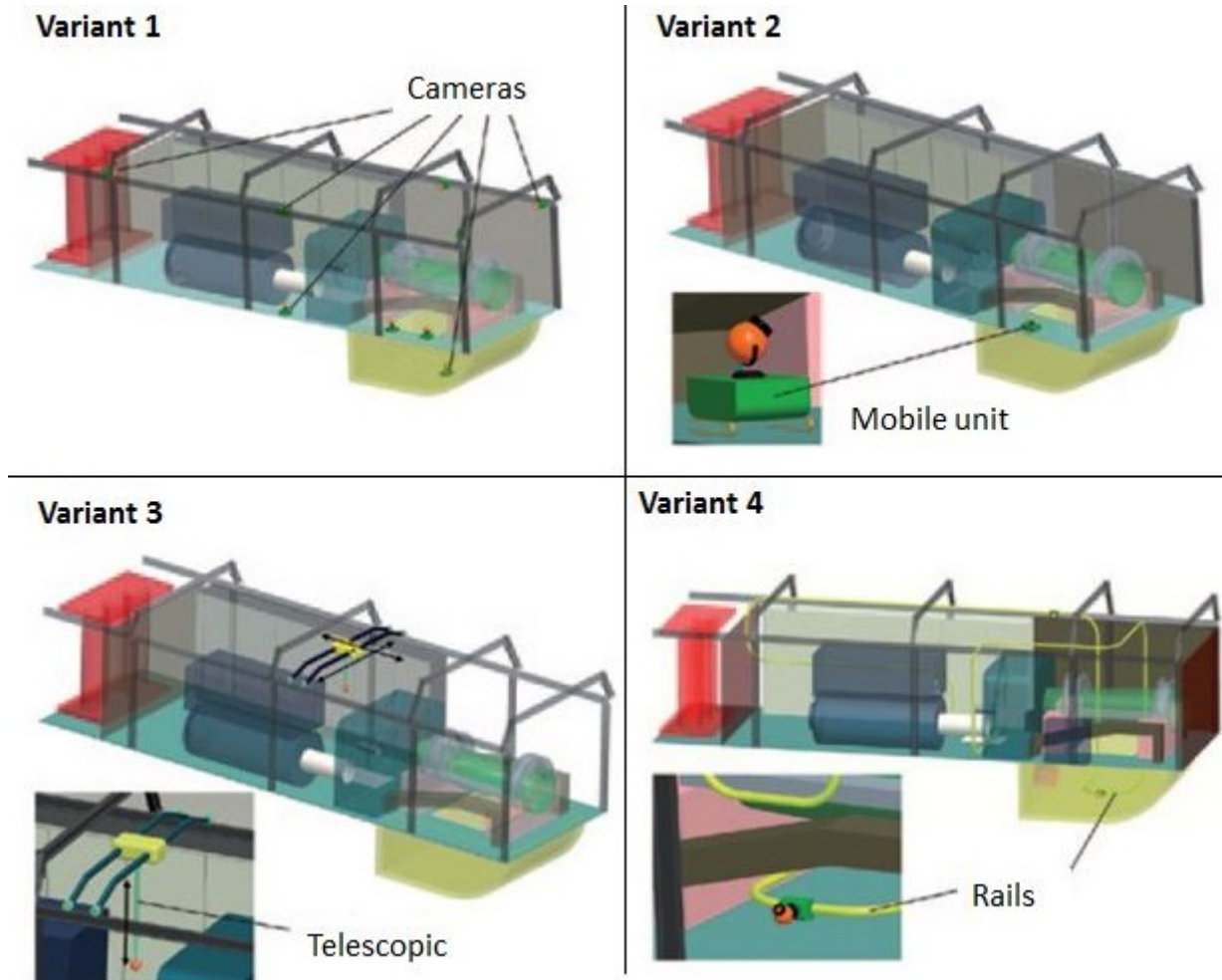
Figure 3.17: Systematical illustration of the 4 variants analysed by the Ross Team developer [22].

After creating the four variants the *ROSS* developer team has made a comparison between them. It has been detected that the variant 1 with the fixed installed camera system, has compared with the other variants a limited angle view [22]. Moreover, the installation of further cameras is complex and expensive [22]. Variant 2 featured, compared with the others, a relative low process reliability [22]. Variant 4 showed the best option, regarding the economic and technical aspects. Figure 3.18 shows a graph created by the *ROSS* developer team. The graph presents the quality rating of the four

variants regarding the technical aspects (plotted on the x-axis) and economic aspects (plotted on the y-axis).
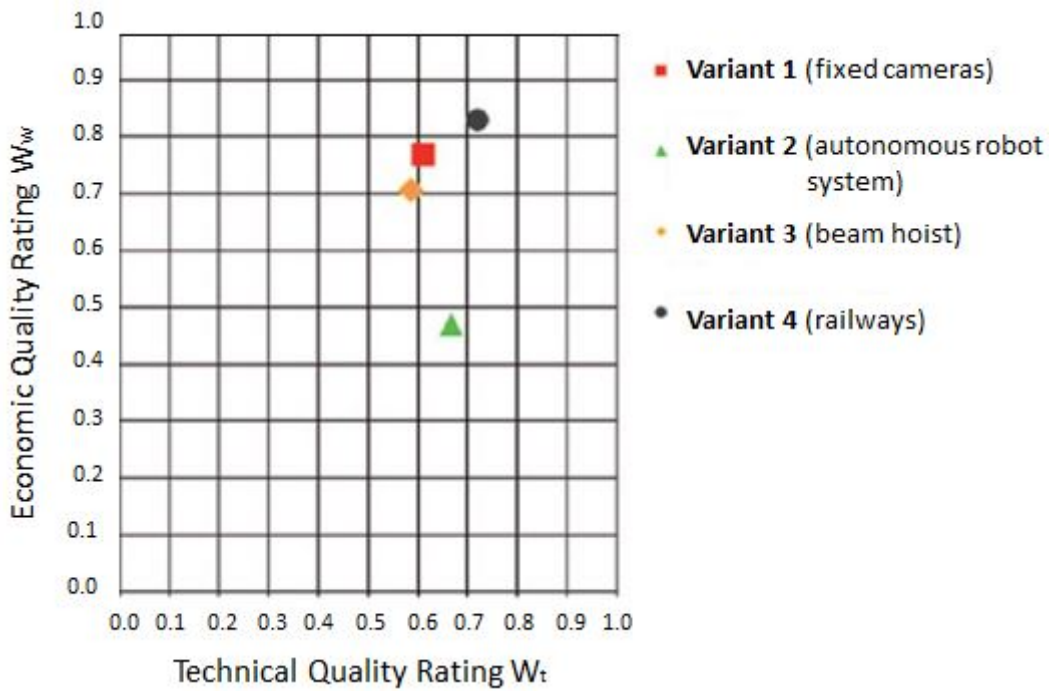
Figure 3.18: Quality rating between all four variants, regarding the technical and economic aspects conducted by the Ross Team developer [22].

As it be observed in the graph of Figure 3.18, the Variant 4 is the most feasible option among the others. Followed by Variant 1 and 3. Variant 3 has the main disadvantage of requiring multiple cameras to be installed within the nacelle. Variant 2 is because of its low reliability the less attractive option.

Based on this finding, the mobile-robot equipped with measuring devices in the inspection procedure demonstration, which will be carried out in this study (see also Section 5.3), will be also supposed to move on railways within the nacelle. As next it will be described in more details the configuration of the robot *ROSS*, such as the railway, camera system and the data transmission.

3.3.4.2.1 Railway within the nacelle

The railway, for the locomotion of the robot *ROSS*, chose by the *ROSS* developer team, is made of aluminum standard profile and has a quadratic cross-section with a

T-groove lateral profile [22]. This can be see in the Figure 3.19. *ROSS* also called as the inspection train consists of a drive wagon, a supply wagon and a camera wagon [22]. The railway has four T-grooves and each of them has a function. As it can be see in the Figure 3.19, in the T-grooves, which is located right under the drive wagon, is a gear rack integrated [22]. A drive pinion gear, which is mounted on the drive wagon, grabs the gear rack and transmits hence the torque for the locomotion [22] and as well the holding torque at standstill on the railway [22]. The T-groove on the opposite side has the task to hold the railway on the nacelle wall structure [22]. The lateral T-grooves have the task to guide the drive wagon [22]. In the lateral T-grooves are of each side two wheel integrated. The wheels are responsible to limit the mobility levels of the drive wagon. Due to the preloading of the wheels by springs, the drive wagon is able to drive horizontal and vertical curves [22].
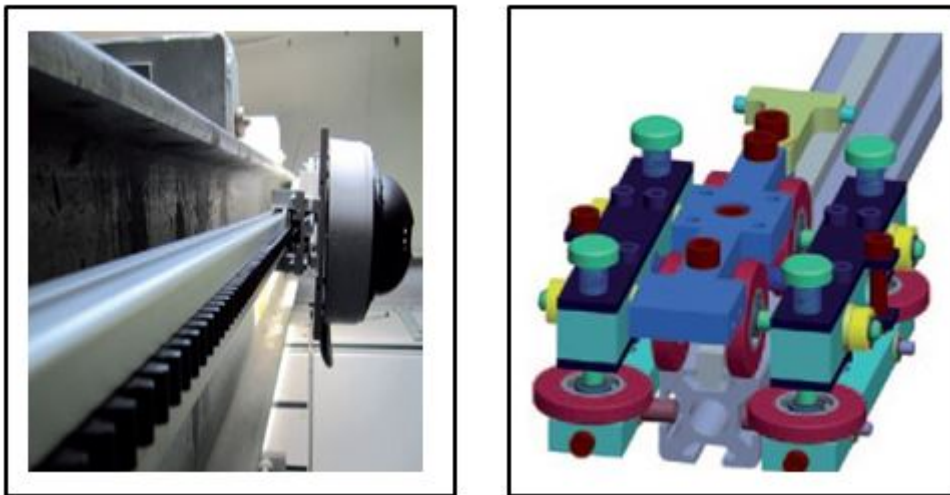
Figure 3.19: Railway and mobile-robot developed by the Ross Team [22].

In order to reach every spot of the nacelle interior and complete a successful inspection, the system has been so designed to enable the drive wagon to operate upside down, collateral, at stillstand and drive any railway inclination [22].

3.3.4.2.2 Camera wagon

The camera system, a digital camera with a powerful optical zoom and adjustable perspective, is mounted on the camera wagon [22]. The camera system is fixed on a

rotary-swivel unit that enables the camera to inspect the components of the nacelle from different angle of view [22].

3.3.4.2.3 Supply wagon

The energy for the robot is supplied by an accumulator mounted on the supply wagon [22]. This enables *ROSS* to operate completely autonomously and wireless [22]. The accumulator energy supply lasts 90 minutes, according to the range of the railway [22]. The charge of the accumulator can be succeeded in the charging station [22]. To do so the inspection train drives to the bottom of the nacelle, where it can connect to the battery charger autonomously [22]. Furthermore, the supply wagon is equipped with the required power electronics and the communication module [22]. An integrated micro controller is responsible for the activation of the hardware and communication between inspection system and the host computer [22].

3.3.4.2.4 Data Transfer

The host computer is installed with a java server. This can scan continuously the currently state of the micro controller via telnet [22]. The images taken by the camera system are sent to the host computer, where they can be further edited [22]. The robot can be manually remote-controlled or preprogrammed. The remote-controll is succeeded from the control room. The inspection can be live observed per video stream. The inspection points are marked with so called RFID transponders along the railway [22]. The RFID transponder automatically identify and localize the inspection points and thus simplify the collection of data [70]. The RFID transponders are identify by a miniature receiver, which is mounted on the inspection system [22]. Both allow the automatic acknowledgment of the defined inspection points [22].

3.3.4.2.5 ROSS inspection tasks and conclusion

Due to the high zoom power, *ROSS* is able to conclude several inspection tasks including among others: read fill levels and type labels, screw connections tests, hose

connections tests etc [22]. All in all, the robot ROSS has been developed with the purpose to be simple, that means reliable and not cost intensive but effective. The *ROSS* developer team plans to expand the robot with further integration of measuring instruments, as for example with a contatc-free infrared thermometer sensor [22].

3.4   3D-Laser-Scanner

As already mentioned the aim of this study is to evaluate the feasibility of inspecting the mechanical damages of the nacelle components with sensor devices, this include among other devices, a 3D laser scanner. Thereby, the 3D laser scanner is supposed to be mounted on an autonomous robot, which will be located in the nacelle interior area. The 3D laser scanner to be integrated on the robot is a very light and compact equipment. A laser scan is used for accurate profile measurement and examination of a variety of different surfaces [23]. The measurement principles of the laser scanner is carried out according to the laser triangulation for the 2D profile detection [23]. The emitted laser beam is expanded, means particular lenses, forming so a laser line, which is projected onto the target surface [23]. The laser line is reflected on the target surface to an optical system, which projects it onto a sensor matrix [23]. This principle is systematically illustrated in Figure 3.20.
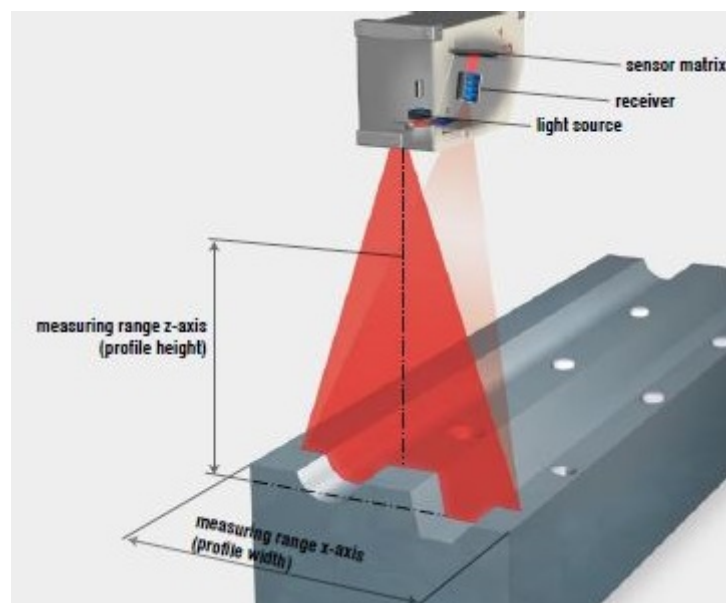
Figure 3.20: Measuring principles [23].

Besides the distance information (y-axis) the scanner also calculates the position alongside the laser line (x-axis) [23]. The laser system is usually designed for industrial use and capable to scan several surface structure specially shiny metallic surface. This enables a precisely surface assessment of the nacelle components, in order to detect mechanical failures, since the most mechanical failures can be diagnosed by evaluating the surface as for example micro-pitting, corrosion, fatigue and so forth. Furthermore it also allows a precise inspection of the components geometric, enabling so the detection of further anomalies such as loose screw, weld seam profile (see Figure 3.21) hose connections etc. Due to its compact design and light weight the laser can be easily mounted on a mobile robot. For this purpose the 3D-Laser-Scanners are usually equipped with robot-compatible cables [23]. The data obtained can be analysed in 3D or 2D display. The Figure 3.21 shows the measurement of a weld seam profile as an example.
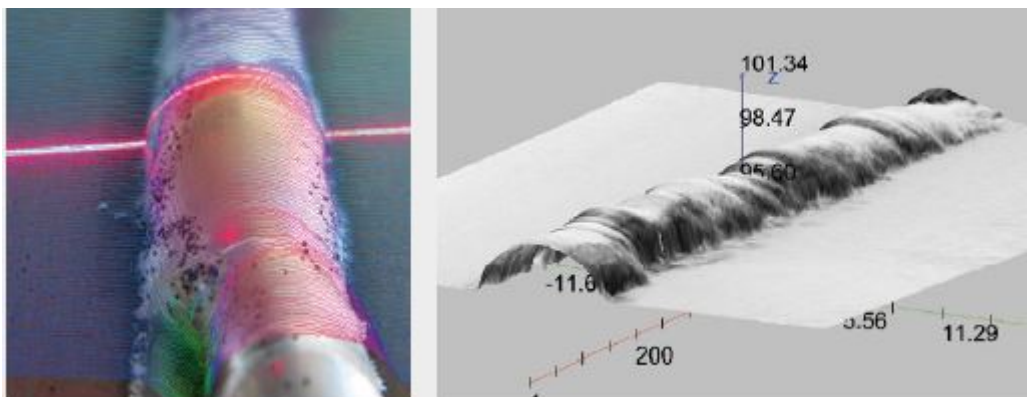
Figure 3.21: Measuring example (weld seam profile) of a 3D-Laser-Scanner [23].

All in all, the laser scanner can be a feasible alternative for the permanent inspection of the nacelles components in order to increase the reliability and avoid downtime-induced productivity loss.

On the basis of these findings, presented in this chapter, a methodology for the evaluation of the feasibility of inspecting mechanical failures within the wind turbine nacelle by using sensor devices has been developed. The following chapter will demonstrate the research methodology used in this study.

Chapter 4

Methodology and Contribution

Based on literature review presented in the previous chapter, this study will investigate the feasibility from a technical and economic point of view of inspecting the nacelle components by using a mobile robot equipped with sensor devices. As previous mentioned, in addition to the literature review, experiments will be conducted with a 3D laser scanner, in order to evaluate the accuracy of the obtained 3D images and the potential application of the 3D laser scanner to inspect the mechanical damages. The overall evaluation within this study consists of 5 stages:

- **Selection of components samplings for the experiments**: Samplings, that correspond the nacelle components, regarding the geometric, metallurgy, and as well components, which have experienced similar mechanical stress as wind turbine components.

- **Optical analysis of the samplings with 3D CNC Vision Measuring Machine**: In order to identify failures and as well obtain a comparison to the 3D laser scanner analysis. In this connection, the geometric deformation will be precisely measured.

- **Visual analysis of the samplings with 3D laser scanner**: Analysis of accuracy and precision of the obtained data. Additionally, the data will be analysed and compared in a CAD program.

- **Demonstration of inspection procedure (CAD-Model)**: Demonstration of the monitoring procedure within the nacelle with a mobile-robot equipped with

measuring devices.

- **Feasibility evaluation**: Technical and economic feasibility of inspecting nacelle components with a mobile-robot, which is equipped with the previous introduced sensor devices, either as single or combination.

The following flowchart displays the overall project methodology applied in this study.
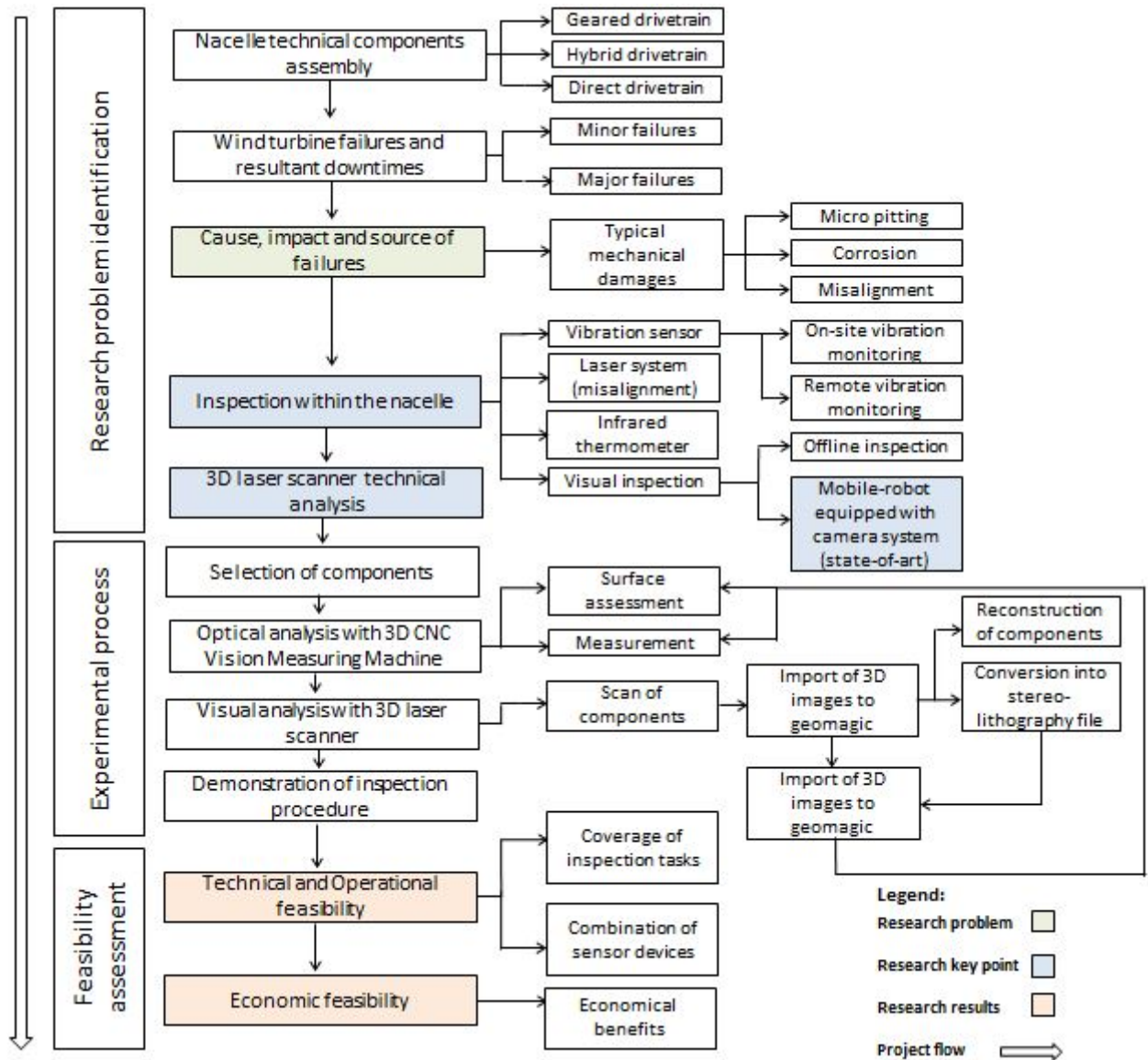
Figure 4.1: Project methodology.

The following sections 4.1-4.5 will explain each methodology stage of the experimental process and feasibility assessment adopted in this study.

4.1 Selection of components samples

As previous mentioned, by the selection of the components samplings it was from great importance that these correspond the nacelle components, regarding the geometric and metallurgy. Furthermore, it has been selected components which have experienced similar mechanical stress as those find in the wind turbine nacelle components. Based on the literature review, where the typical mechanical failure have been highlighted, the most common occurred mechanical failures within the nacelle include: micro-pitting, corrosion, fatigue as well misalignment. Therefore the component samplings selected for the analysis were part of rotating machineries and some of them were partly subject to mechanical stress. However, some of the samplings have not been used, which enable a significant comparison, between used and new components. The followings sections will demonstrated the analysed samplings within this study.

4.1.1 Main shafts

Within the wind turbine nacelle, the main shaft (low-speed shaft) and the high-speed shaft are permanently under mechanical stress (See also Section 2.2 and 3.1). In order to obtain a comparison between a new and a wear shaft, the shafts in the Figure 4.1 have been analysed. The two shafts only differ from each other in their lengths, shaft a) is about 1cm longer then shaft b), expect of that both are equal regarding their metallurgy and geometric. These shafts are mechanical components of a motor vehicle. As the main shaft also called drive shaft the illustrated shafts have the task to transmit the torque and rotation from a component of the drivetrain to another component, usually between driving and driven wheels [72]. The main shaft belongs to the rotating machinery and are subject to several type of mechanical stress include shear and torsion [73]. Moreover a shaft is subject to misalignment, corrosion, micro-pitting and wear. The sampling selected have different usage times. While shaft a) has only about 2,000 mile on it, shaft b) features around 10,000 mile on it. The wear difference between both can be easily noticed with unaided eyes. Specially on the part, which was connected to the driven wheel and transmitted the whole force. This parts are highlighted in the Figure 4.1. As it can be observed in Figure 4.1, shaft b)
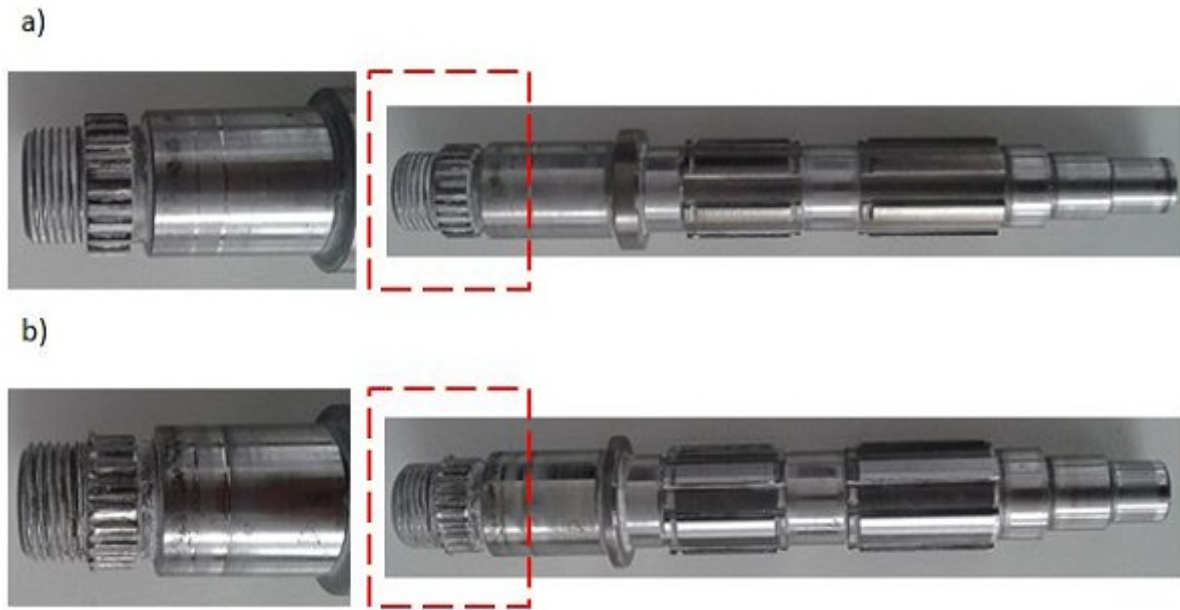
Figure 4.2: Motorcycle main shafts, a) 2,000 mile, b) 10,000 mile.

looks compared to shaft a) relatively worn. In the framed area of Figure 4.1 it can noticed that shaft b) is strong deformed. The main objective of analysing these shafts is to verify the accuracy of the obtained data, in this case, the deformation of shaft b). In this connection both shaft have been analysed with the optical 3D CNC Vision Measuring Machine and the 3D laser scanner.

Moreover, a further shaft has been analysed. The shaft, which can be see in Figure 4.2, belongs to a car machinery and has about 15,000 miles on it. As the previous shown shafts, this shaft was subject as well to several type of mechanical stress, as such torsion and shear. This shaft shows severe wear, which is highlighted in the Figure 4.2. The aim of analysing this shaft is to verify the precision of the acquired data of the highlighted part, in this case the strongly worn part of the component.
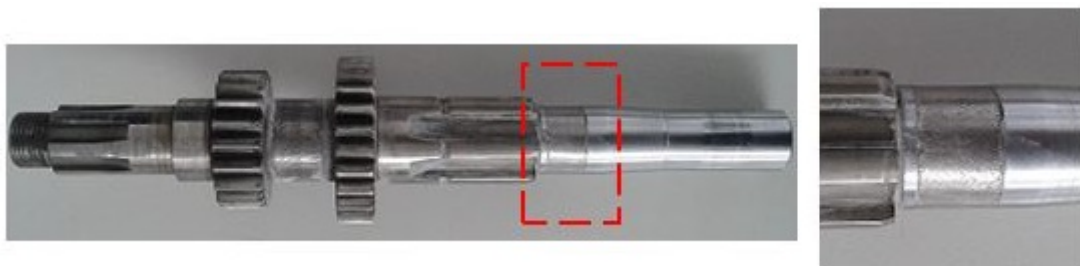
Figure 4.3: Automobile main shaft (severe wear).

4.1.2 Gears

Within the wind turbine nacelle, the gears can be found in the gearbox interior area (See also Section 2.2.1.1). A gear is basically a toothed wheel, which belongs to the rotating machinery components. In the wind turbine system the gears have the task to increase the rotation speed of the rotor blades, in order to achieve the generator required speed (See also Section 2.2). Thereby the gears are subject to great mechanical loads, specially the teeth, which mesh with each other in order to transmit the force. Figure 4.3 shows the examined gears within this study. The gears in Figure 4.3 have different
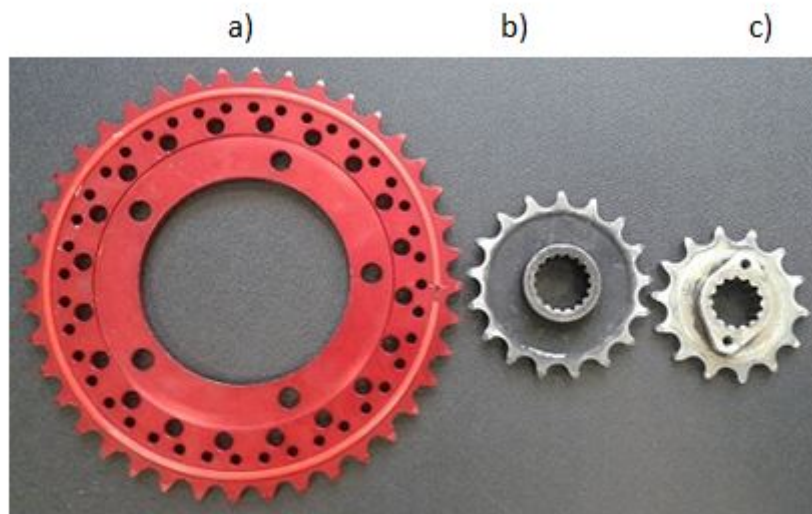
Figure 4.4: Different aged gears, a) not used, b) and c) used

time of use. While gear a) is not used, the gears b) and c) have been used for some time. The teeth of both used gears are strongly degraded by wear and tear. In this connection, it will be analysed the deformation of the teeth profile of the gears.

4.1.3 Impeller of a centrifugal pump

The workpiece shown in Figure 4.4 was part of a impeller of a low pressure centrifugal pump. The impeller, which was a second hand component, failed after a short time in operation. Metallurgy specialist pointed out fatigue as the cause of the failure. In addition to that, it has been identified that the drive shaft connected to the centrifugal pump impeller was not properly fixed. This eventually led to a misalignment and

consequently to a high vibration.

As it can be observed in the Figure 4.4, impeller features a highly porous surface. This is mostly a result of a sand casting manufacturing process. Moreover, the impeller features several deep cracks. And at some places there are signs of a collision and also frosting of slight micro-pitting damage on the top surface.
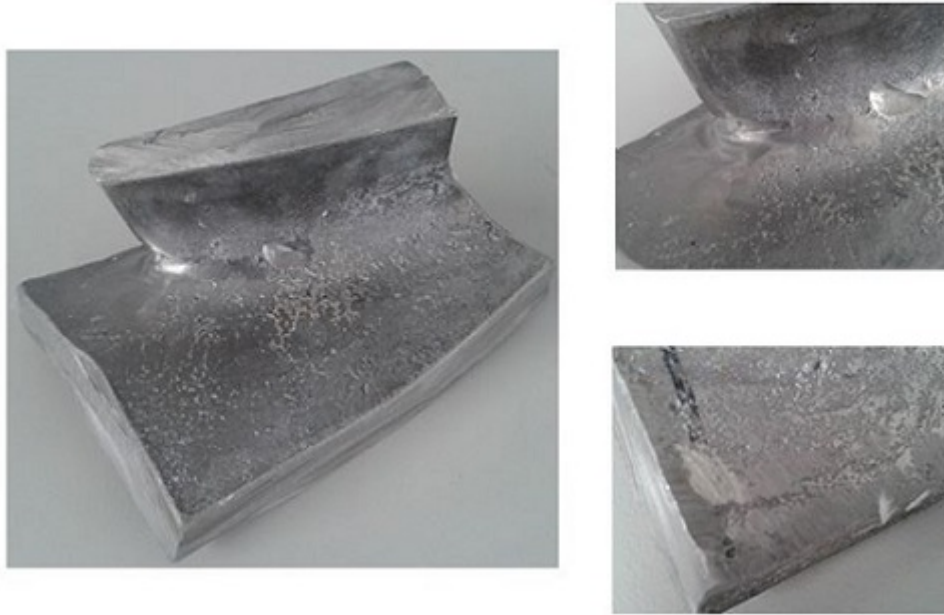
Figure 4.5: Part of a impeller of a low pressure centrifugal pump.

The aim of analysing this workpiece is as well to verify how the 3D laser scanner displays this failures.

4.2   Optical analysis (3D Vision Measuring Machine)

The 3D CNC Vision Measuring Machine used within this study, allows high accurate, non-contact, 3D measurements of workpieces [24]. Furthermore, the system is provided with a color CCD-camera, which permits the observation of workpieces and the acquisition of high resolution color images [24]. The acquired color images can be stored as bitmap images [24]. In order to identify failures of the previous demonstrated samplings and as well obtain a comparison to the 3D laser scanner analysis the 3D CNC

Vision Measuring Machine has been used.

In this connection, the surface condition of the samplings has been accurately studied. In addition to that, the geometric deformations of the workpieces have been measured.

4.3   Visual analysis (3D laser scanner)

As previous explained in section 3.4 a 3D laser scanner permits a precise scanning of a variety of different objects and in addition to that it allows an accurate surface assessment [23]. In order to evaluate the accuracy of the laser scanner and the feasibility of detecting with it mechanical failures, the demonstrated component samplings have been scanned. In this process, specially the anomalies of the component samplings have been exactly examined.

Once the component samplings have been scanned, the acquired digital data have be imported to a CAD program. Basically, a digitised data obtained from the 3D laser scanner can be immediately compared with the CAD data or rather with a reference model, if available [78]. In this connection the deviation or any anomalies of the components can be exactly analysed [74].

As within this study there were no CAD data of the component samplings available, the investigation of the anomalies could be succeeded by comparing old with new component samplings. Generally, the use of a CAD program enables the measurement and examination of any kind of anomalies including cross-sectional variation and as well the position and geometric of the component [74].

4.4   Demonstration of inspection procedure

Based on the literature review and experiments, it will be demonstrated theoretically the inspection procedure within the nacelle. Aim of this section is to transmit a visual introduction of the inspection approach. At this juncture, it will be modeled in a CAD program the nacelle interior area of the wind turbine and additionally the inspection system.

4.5 Feasibility assessment

Lastly, a technical and economic feasibility assessment of inspecting nacelle components with a mobile-robot, which is equipped with the previous introduced sensor devices will be conducted. In this connection, it will be evaluated from a technical and as well economic point of view the possibility of equip the mobile-robot with sensor devices either as single or combination.

The results obtained through this experimental analysis will be demonstrated and evaluated in the following chapter 5. The economic and technical feasibility assessment will be discussed in the subsequently chapter 6.

Chapter 5

Results and evaluation

As part of this work, several component samplings have been experimentally studied by using two type of measurement methods; These are: an optical analysis with 3D CNC Vision Measuring Machine and a visual analysis with 3D laser scanner. In order to evaluates the feasibility of inspecting mechanical failures with a 3D laser scanner the results of both methods have been compared with each other. In this chapter it will be demonstrated and evaluated the results acquired from the experimental study. Furthermore, it will be indicated the appropriate inspection method for each component failure.

5.1 Optical analysis with 3D CNC Vision Measuring Machine

Figure 5.1 shows the optical analysis of the automobile main shaft with the 3D CNC Vision Measuring Machine. In this connection, it has been focused on the damage caused by wear on its surface. As it can be observed in the images, the shaft is strongly degraded by wear and tear, which eventually resulted in a significantly alteration of its cross-section in the same area. In the worst case scenario the reduction of the cross-section can lead to a serious misalignment. The suggested alignment tolerance range, of a short coupling for example, is between 0.07-0.19 mm (See also Section 3.3.2). According to 3D laser scanner manufacturers, a laser scanner system is able to verify alignments of a variety of different components such as tooling dies, moulds, metal

casting and so on [28]. This also requires a very precise capture of 3D shapes. Taking into account that the 3D laser scanner is able to capture such accurately 3D shape, it can be assumed that the 3D laser scanner is also capable to detect misalignment of components within the wind turbine nacelle. Moreover, the primary consequence of a misalignment is a increase of the vibration frequency and accordingly of the temperature of the components. In this process, the failure can be also detected with vibration sensor or with a infrared thermometer system.
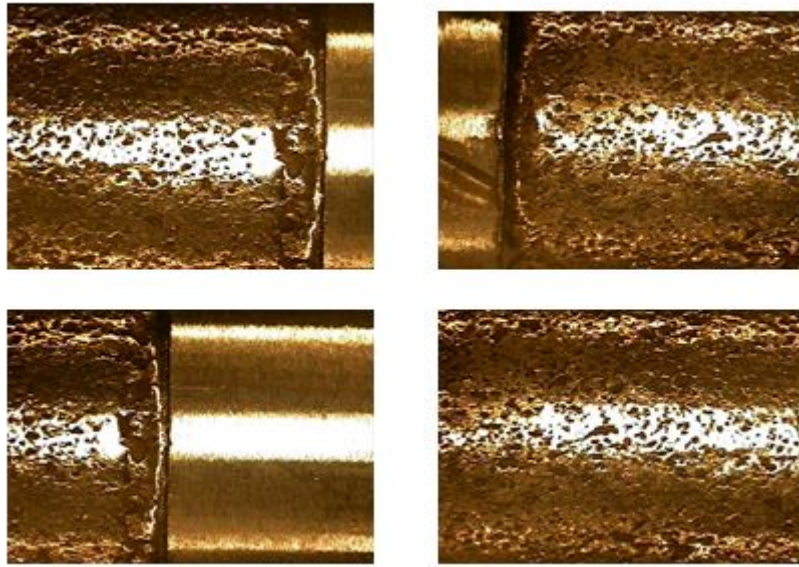
Figure 5.1: Optical analysis of an automobile main shaft with a 3D CNC Vision Measuring Machine.

Figure 5.2 shows the optical analysis of the previous demonstrated gears with the 3D CNC Vision Measuring Machine. In this connection, it has be studied used and unused gears. As it can be seen in the images the used gears shown in comparison to the unused gear significantly profile deformation, particularly the teeth profile of the gears. The images show that, with increasing ages the degree of deformation on the mechanical components becomes worse. The deformation of the teeth profile can cause a considerable decrease of the torque transmission. The primary consequence of that is a low performance of the gearbox leading to significantly low production yield. At an advanced stage the deformation of the teeth profile may result in a total loss of the gearbox. The first signs of anomalies in the gearbox interior area are the change

of the vibration frequency and consequently, high noise level and the change of the temperature. A visual inspection of the interior area of the gearbox is currently only possibly by using a videoscope (See also Section 3.3.4.1), which requires the operation of a technician. For an autonomous remote inspection of the gearbox interior area it is recommendable to use vibration sensor or an infrared thermometer system, as the 3D laser scanner is unable to access the problematic interior area.
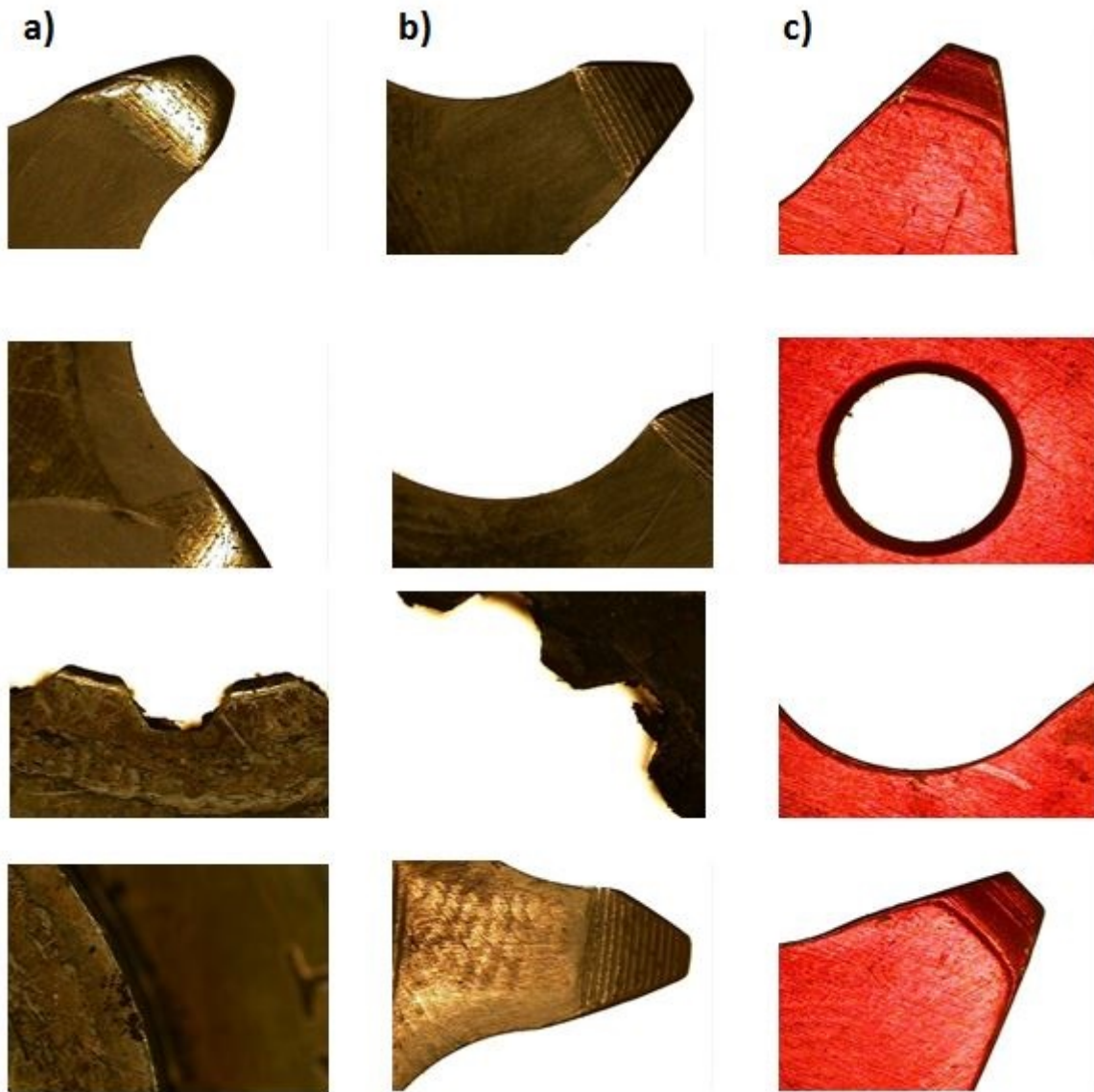
Figure 5.2: Optical analysis of different aged gears, a) 5 years, b) 2 years c) unused.

Figure 5.3 shows the optical analysis of the previous demonstrated motorcycle main shafts with the 3D CNC Vision Measuring Machine. As already mentioned the main shafts have different miles on it. By observing the images in Figure 5.3, which show

the heavily used area of the shafts the so called gear ring, it can be noticed that shaft b) is compared to shaft a) strongly deformed. The measuring with the 3D CNC Vision Measuring Machine delivered a reduction of the gear ring tooth by approximately 0.763mm and a width expansion of about 0.912mm.

Figure 5.3: Optical analysis of motorcycle main shaft, a) 2,000 mile b) 10,000 mile.

As the previous presented gears, the deformation of the shafts have similar consequences. At an early stage the anomaly may result in a low performance of the components leading also to significantly low production yield. Furthermore, the deformation can cause a misalignment and subsequently higher vibration frequency and higher temperature. Therefore, it is recommendable to detect this kind of anomalies by analysing the alignment of the shaft, with the 3D laser scanner, vibration sensor or infrared thermometer system.

5.2 Visual analysis with 3D laser scanner

The laser scanner used for the experimental analysis, scanned the components at six different view angle intervals: 0, 60, 120, 180, 240, 300, 360. In this connection, the target workpiece was placed on an automated turntable, which is direct connected to the 3D laser scanner system [28]. Figure 5.4 shows an example of obtained 3D data from the scanning process. The different view angle intervals of the shaft can be seen on the top hand right corner of the figure.
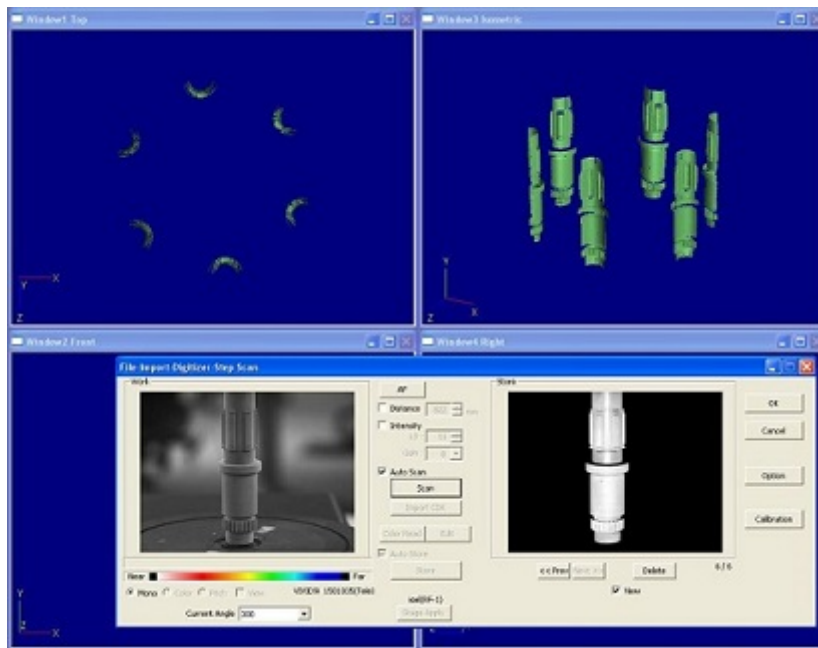
Figure 5.4: 3D data from the scanning process.

Once the components have been scanned the next step was to import the data to a 3D Inspection and Metrology software. This software enables the measurement of the components, analysis of deviation and tolerances, as well graphical comparison between digital images [81]. Furthermore, the software has an integrated complete toolbox, which allows performing the reconstruction of the 3D scanned data. In this connection, the digital images of the six angular intervals of the component were placed into the software for the reconstruction process [82]. Figure 5.5 shows the performed reconstruction of the analysed motorcycle shaft. Lastly, the edited scanned 3D data have been direct imported to a CAD program. In the CAD program the components images data could be investigated after anomalies by comparing old with new compo-
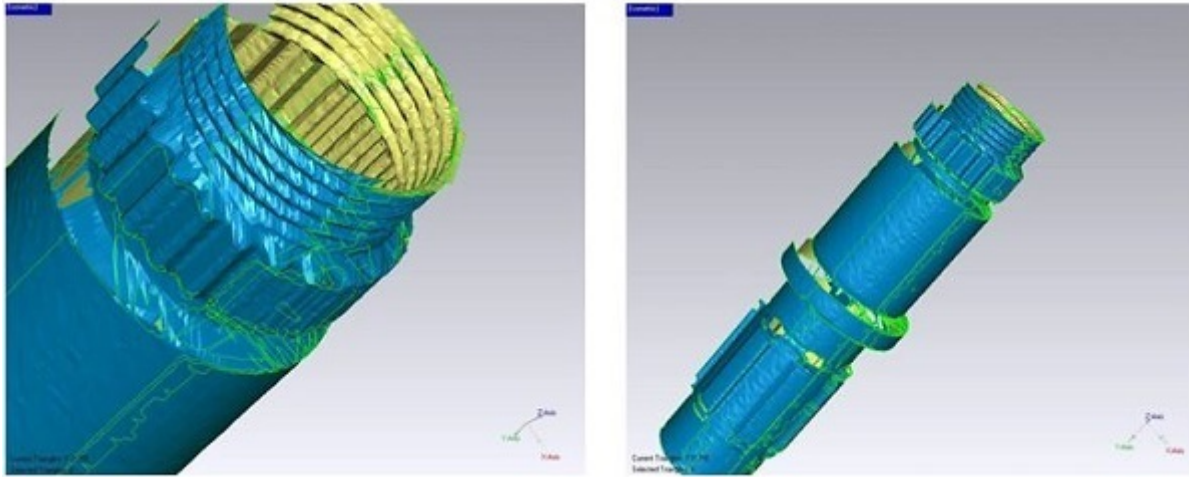
Figure 5.5: Reconstruction of scanned 3D data.

nent samplings or by measuring and analysing their geometric and surface. Figure 5.6 shows the motorcycle main shaft (2,000 mile) analysis with the CAD program. The images in Figure 5.6 demonstrates the component from two different view angles. By observing the main shaft in Figure 5.6, in particular the gear ring and the screw thread, it can be see that images obtained from the 3D laser scanner display a detailed shot of the component.

Figure 5.7 and Figure 5.8 show both motorcycle main shafts (2,000 miles and 10,000 miles) analysis with the CAD program from the same view angle. Here it can be noticed that shaft b) is compared to shaft a) strong deformed in the gear ring part. By changing the display modes to *shading with reflection* the program delivered a more enhanced image of the 3D components, which can be see in Figure 5.6.

As previous mentioned, the 3D image obtained from the 3D laser scanner can be immediately compared with the CAD data, if available, in order to detect any anomalies of the components. In this connection, as there were no CAD data of the component samplings available, the investigation of the anomalies have been carried out by comparing the new shaft (shaft a)) with the old shaft (shaft b)). The result of this analysis can be seen in Figure 5.9. Thereby, the 3D images from both shafts have been inserted in each other. Shaft a) is highlighted in green and shaft b) in white. As it can be see, shaft a) leaps out into view in the areas where shaft b) is deformed, allowing so an immediately and accurately diagnosis of the component failure.
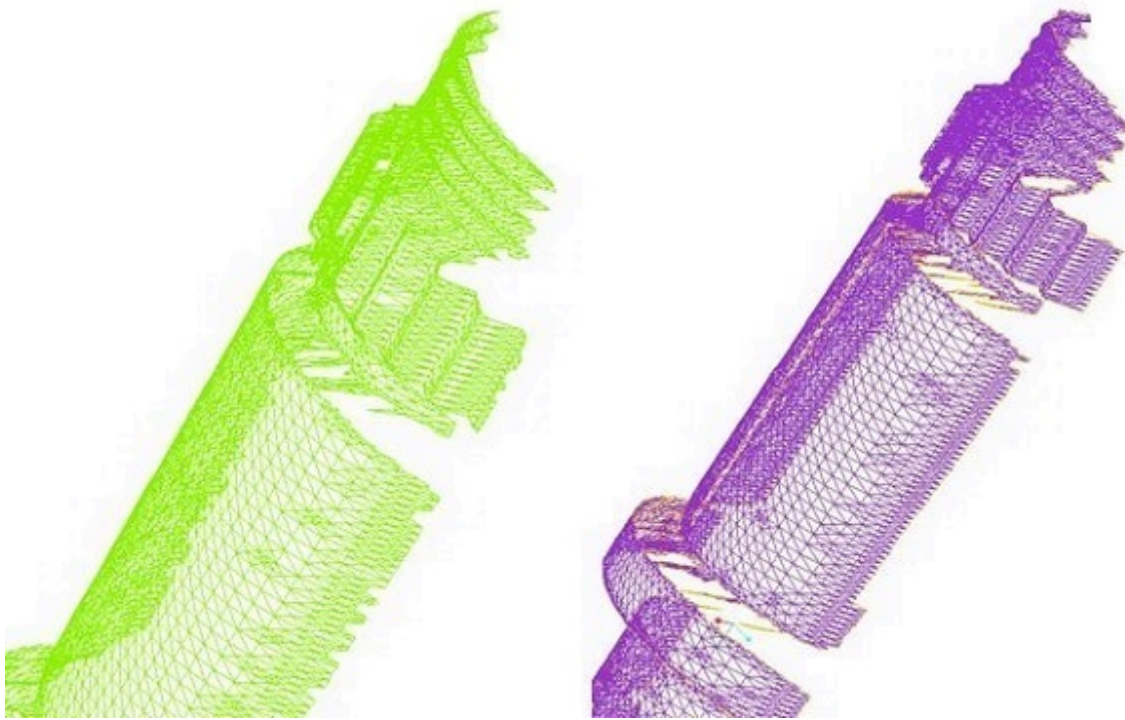
Figure 5.6: Motorcycle main shaft (2,000 mile) analysis in CAD program.
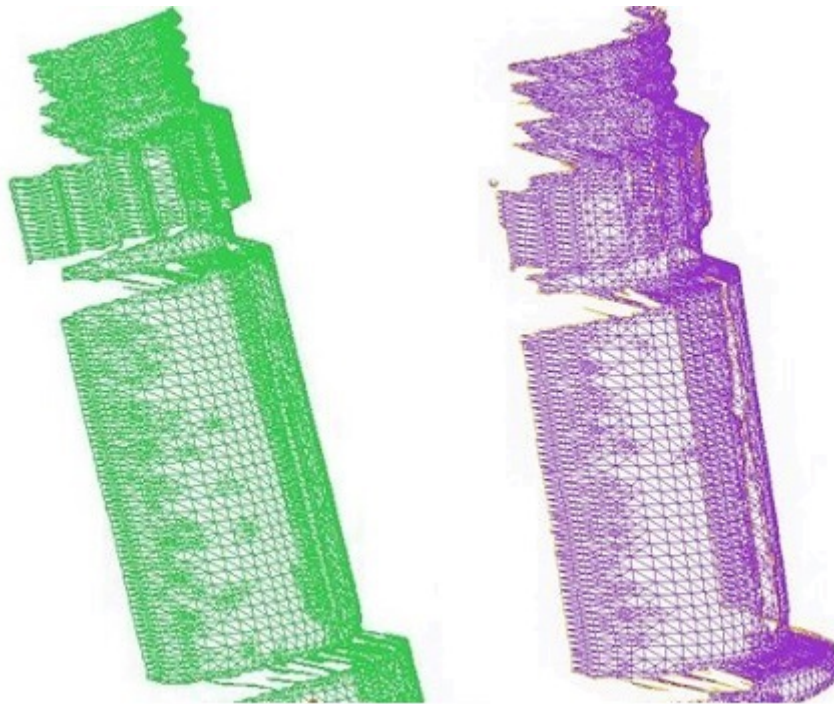
Figure 5.7: Motorcycle main shafts analysis in CAD program, a) 2,000 mile, b) 10,000 miles.
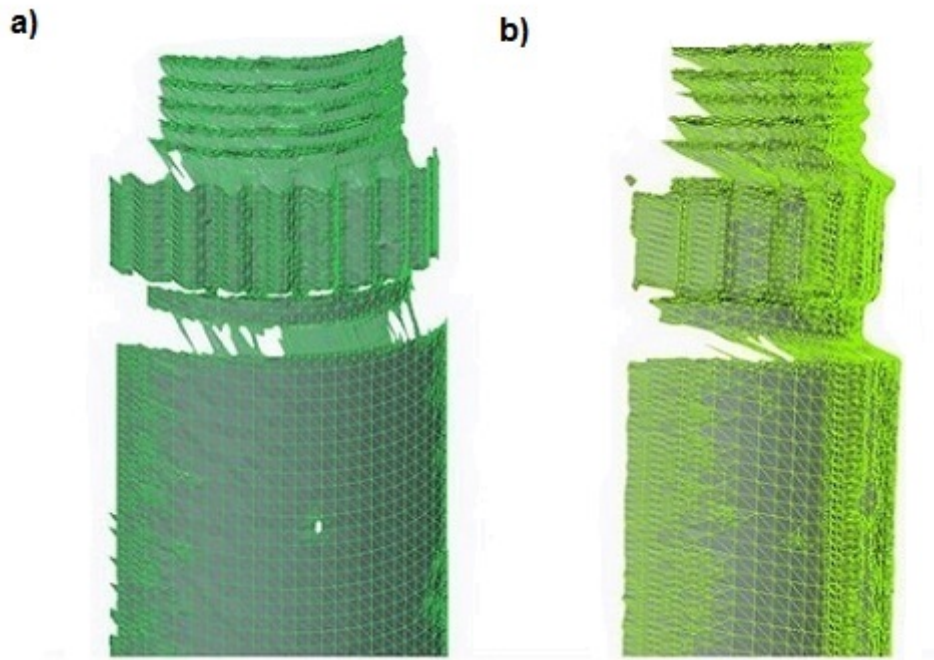
Figure 5.8: Motorcycle main shafts analysis in CAD program, *shading with reflection display mode*, a) 2,000 mile, b) 10,000 miles.

Figure 5.9: Motorcycle main shafts inserted in each other.
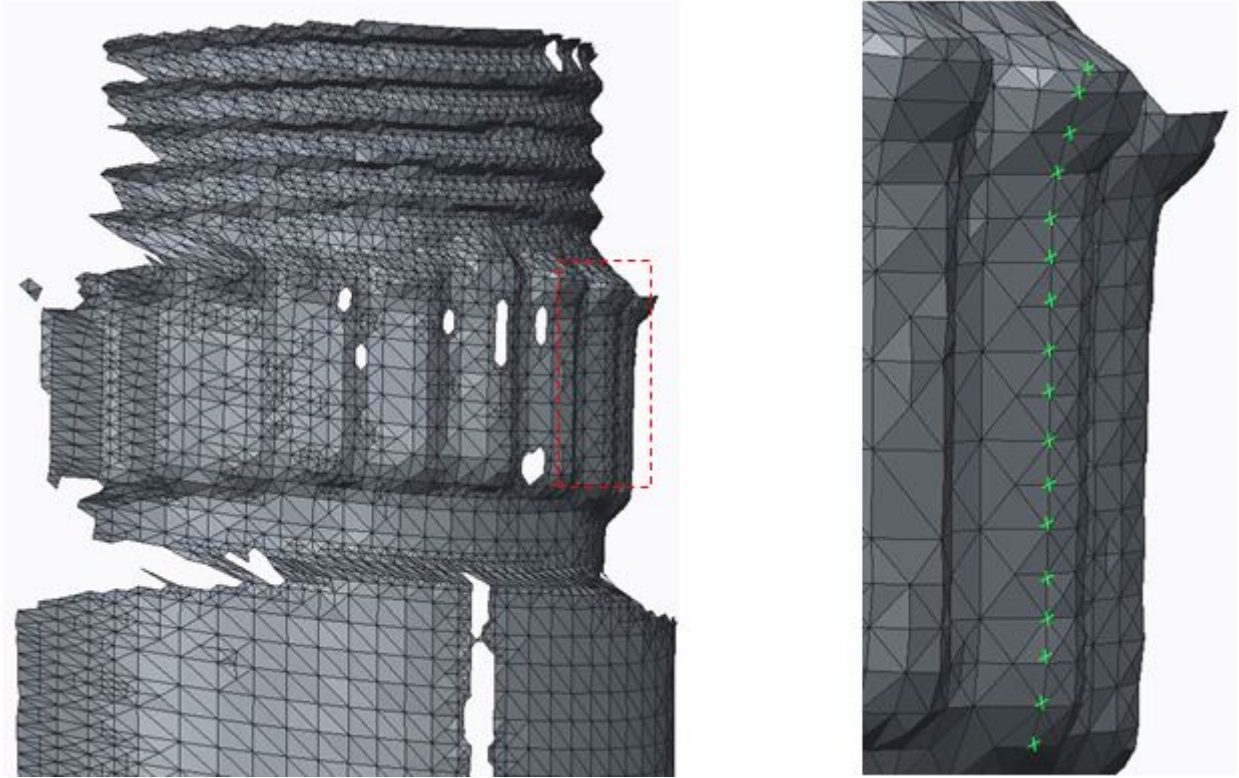
Figure 5.10: Motorcycle main shaft (10,000 mile) measurement in CAD program.

Point	X-coordinate	Y-coordinate	Z-coordinate
1	203.648	223.691	-128.567
2	203.732	229.555	-130.231
3	203.813	239.952	-138.296
4	203.925	250.834	-144.656
5	204.107	262.773	-147.262
6	204.332	275.354	-147.568
7	204.540	287.684	-148.760
8	204.773	300.387	-148.609
9	204.998	312.967	-148.889
10	205.215	325.435	-149.563
11	205.430	337.858	-150.392
12	205.656	350.443	-150.625
13	205.864	362.761	-151.816
14	206.082	375.226	-152.470
15	260.328	388.118	-151.552
16	206.500	399.894	-154.702
17	206.586	410.393	-162.544

Table 5.1: Coordinates of displayed points in Figure 5.8 (in mm).
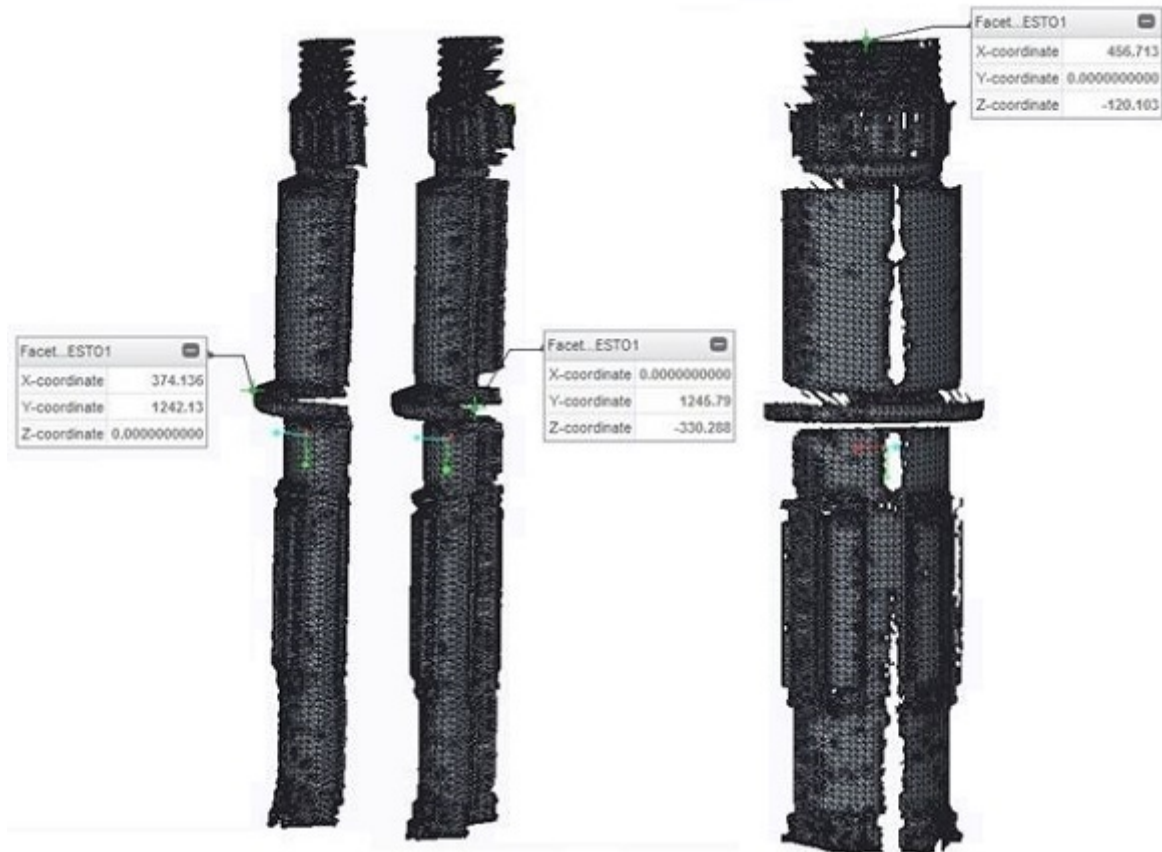
Figure 5.11: Motorcycle main shaft (10,000 mile) coordinate system in CAD program.

Figure 5.10 shows the measurement of the main shaft (10,000 mile) conducted in the CAD program. In this connection, the highlighted area of the shaft, which displays the deformation, was considered in details. Table 5.1 shows the coordinate of the shown points in Figure 5.10. Based on the coordinates of those points, the deformation level of the shaft could be consequently accurately defined. The coordinate axis origin locations of the component are shown in Figure 5.11. By comparing the z-coordinate of point 1 to the z-coordinate of point 15, it could be determined that the level of deformation of this area is exactly 2,6135 mm. The analysis conducted with the 3D CNC vision measuring machine delivered, however, a deformation level of 0.856 mm (see also Figure 5.3). Based on this results, it can be concluded that the measurement with the 3D laser scanner is, compared to a 3D CNC vision measuring machine or to a video camera system, very precise and thus best suitable for the inspection of the nacelle components regarding the measurement aspects. Furthermore, due to the high level of precision, the 3D laser scanner can be applied for the detection of misalignment, which occurs

with high frequency (see also Figure 3.5) and requires a very precise measurement (often 0.1 mm) (see also Figure 3.13). Figure 5.12 shows the measurement of the main shaft (2,000 mile) conducted in the CAD program. The corresponding coordinates of the shown points in Figure 5.12 are displayed in Table 5.2. Here, it can be observed, that on the opposite to the deformed main shaft, the y-coordinates barely change. It should be noticed at this point, that the coordinate axis origin locations of the (2,000) shaft differs from the previous shown(10,000) shaft.
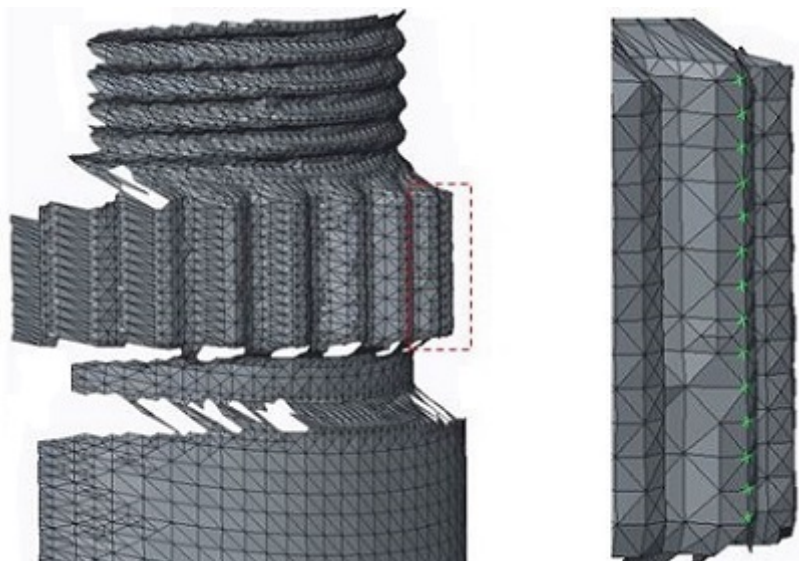
Figure 5.12: Motorcycle main shaft (2,000 mile) measurement in CAD program.

Point	X-coordinate	Y-coordinate	Z-coordinate
1	195.465	227.119	-119.770
2	195.682	239.566	-120.465
3	195.902	252.065	-120.967
4	196.106	264.313	-122.353
5	196.343	277.058	121.959
6	196.564	289.558	-122.429
7	196.788	302.103	-122.728
8	197.022	314.800	-122.469
9	197.241	327.265	-123.039
10	197.468	339.844	-123.183
11	197.700	352.499	-123.042
12	197.919	364.953	-123.620
13	198.133	377.345	-124.413
14	198.373	390.109	-123.842

Table 5.2: Coordinates of displayed points in Figure 5.8 (in mm).

Figure 5.13 shows the 3D images of the impeller part in two different display modes, *(no hidden mode and shading With Edges mode)*. The *shading With Edges* display mode creates a shaded image of the component and highlighted the edges [29]. As it can be observed in the 3D image, the porous surface of the impeller is clearly displayed. On the other hand the several deep cracks, which could be easily seen with unaided eyes, can not be distinguished in the 3D image. Figure 5.14 shows the 3D images of
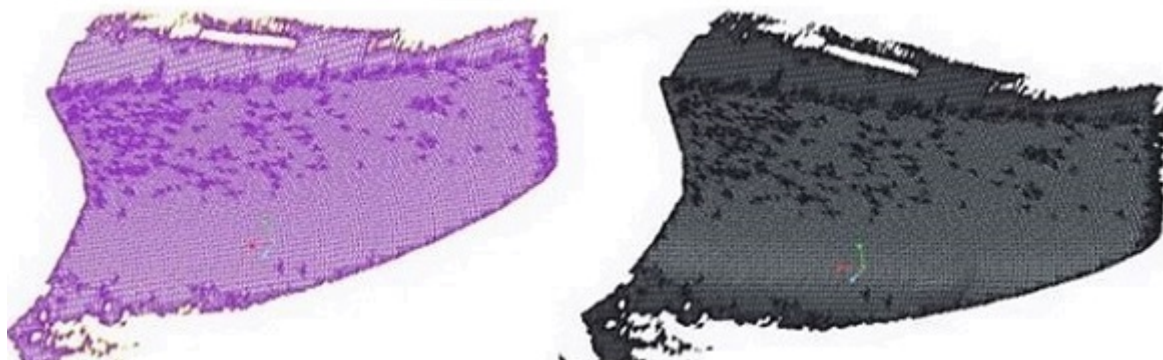
Figure 5.13: Analysis with CAD program of a impeller part.

the automobile main shaft in two different modes, *(shading with reflection mode and shading With Edges mode)*. The aim of analysing this shaft was to verify the precision of the 3D images of the strongly worn part of the component. As shown in Figure 5.14, the abrasion of the shaft, which is framed in red in the image, can be clearly seen.
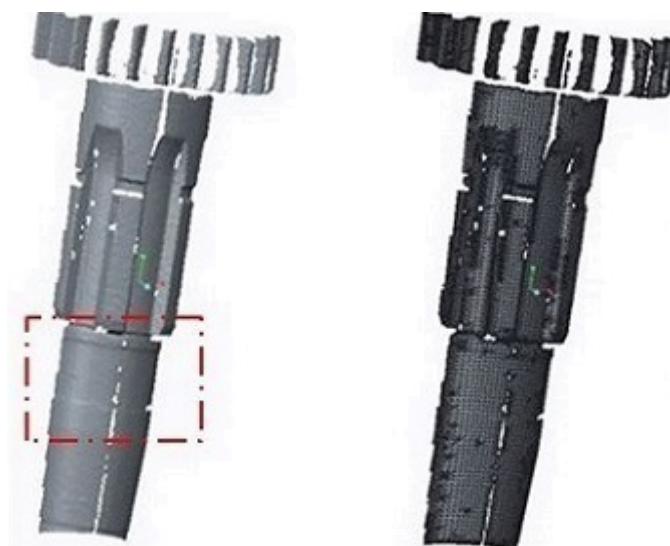
Figure 5.14: Analysis in CAD program of automobile main shaft.
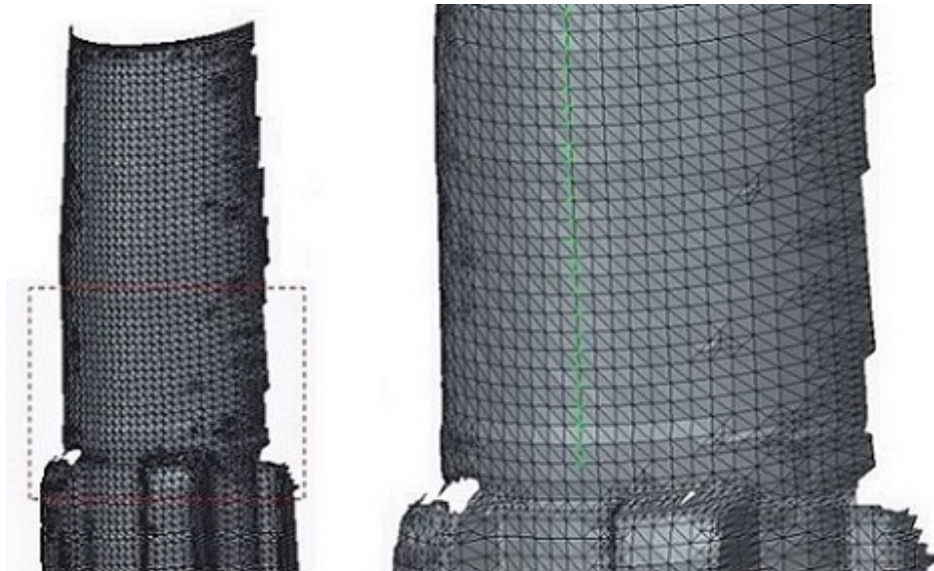
Figure 5.15: Automobile main shaft measurement in CAD program..

Point	X-coordinate	Y-coordinate	Z-coordinate
1	32.1787	22.1360	-19.6862
2	32.1710	23.1572	-19.7259
3	32.1596	24.1404	-19.6306
4	32.1517	25.1599	-19.6679
5	32.1392	26.1310	-19.5310
6	32.1287	27.1214	-19.4655
7	32.1187	28.1180	-19.4240
8	32.1082	29.1075	-19.3577
9	32.0957	30.0778	-19.2215
10	32.0859	31.0742	-19.1834
11	32.0728	32.0373	-19.0217
12	32.0613	33.0168	-18.9225
13	32.0510	34.0065	-18.8628
14	32.0392	34.9818	-18.7497
15	32.084	35.9663	-18.6725
16	32.0177	36.9512	-18.5984
17	32.0070	37.9364	-18.5267
18	31.9961	38.9187	-18.4447
19	31.9854	39.9028	-18.3714
20	31.9746	40.8845	-18.2900
21	31.9630	41.8598	-18.1843
22	31.9525	42.8437	-18.1138
23	31.9413	43.8217	-18.0212
24	31.9319	44.8152	-17.9917
25	31.9255	45.8365	-18.0755

Table 5.3: Coordinates of displayed points in Figure 5.15 (in inch).

64

Figure 5.15 shows the measurement of the automobile shaft conducted in the CAD program. The corresponding coordinates of the shown points in Figure 5.15 are displayed in Table 5.3. Here, it can be observed, that the z-coordinates of the damage area barely change. The damage area can be clearly seen with unaided eye in the 3D image, shown in Figure 5.14. However, the identification of this deviation by observing the coordinates is in this case not possible, since the deviation is minimal and superficial. Figure 5.16 shows the obtained 3D image of the unused gear. It can be seen, that the gear profile and surface are in best condition.

Figure 5.16: 3D image of the unused gear.

Figure 5.17 shows the captured 3D image of the used gear. Here, the deformation of the teeth profile can be clearly observed, in particularly by comparing it to the unused gear of Figure 5.16. The 3D images of the gears are shown in different display modes.

Figure 5.17: 3D image of the used gear.

5.2.1 Conclusion of visual analysis with 3D laser scanner

Based on these experimental results, it became clear that the inspection with a 3D laser scanner within the wind turbine nacelle is thoroughly feasible, as it enables the detection of even very specific damage and in additional to that it offers the possibility to import acquired 3D images to a CAD program for a detailed analysis. The analysis of component damages in the CAD program not just simplifies the monitoring but also improves the detection of any anomalies. However, it should be mentioned at this point that the 3D laser scanner used in these experiments had the disadvantage of being unable to scan shinny surfaces. Therefore, the component samplings had to be first covered with a white powder spray. This obviously led to a loss of the data details, which can be partly seen in the previous shown 3D images, as some part of the 3D object present surface gaps.

5.3 Demonstration of inspection procedure

Based on the literature review and experiments, it will be demonstrated theoretically the inspection procedure within the nacelle. As previous mentioned the aim of this section is to transmit a visual introduction of the inspection approach. Therefore, it has been modelled in a CAD program the nacelle interior area of the wind turbine and additionally the inspection system. It should be noticed at this point, that the modelled systems demonstrated in the following Figures 5.18 and 5.19 are not based on proven scientific facts and therefore only aim to present theoretically the inspection performance. Since the determination of the exactly inspection procedure with a mobile robot requires careful consideration of multiple criteria. The same applies to the design and technical features of the mobile-robot. The modelled systems demonstrate a mobile robot equipped with a 3D laser scanner in Figure 5.18 and mobile robot equipped with a infrared thermometer in Figure 5.19. Furthermore, the modelled mobile robot moves on railways as this has been pointed out from the Ross team developer (See also Section 3.3.4.2) to be the most suitable inspection method, in terms of the technical and economic issues [22]. The following chapter will further analyse the feasibility of inspecting mechanical damage with a mobile-robot equipped with sensor devices.
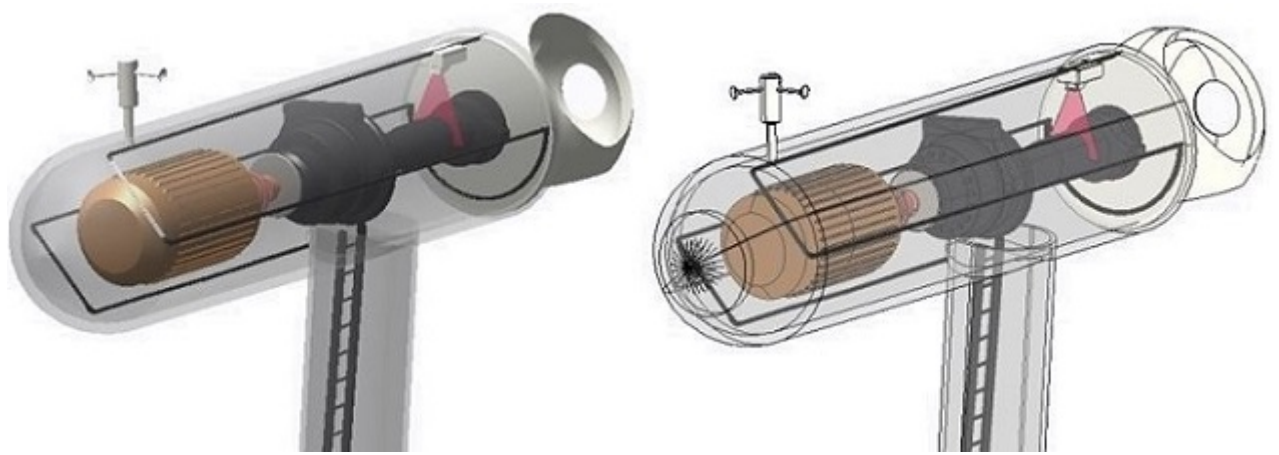
Figure 5.18: Modelled system for visual demonstration of the inspection procedure (3D laser scanner).
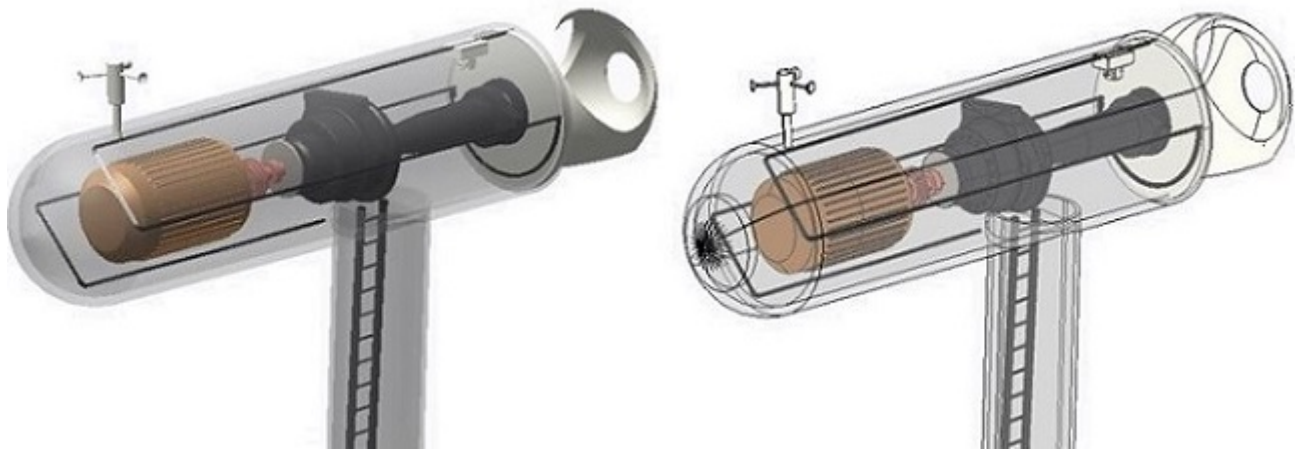
Figure 5.19: Modelled system for visual demonstration of the inspection procedure (Infrared thermometer).

Chapter 6

Discussion

In this chapter, the feasibility and effectiveness of the introduced sensor devices as inspection equipment for wind turbine periodical condition monitoring will be evaluated.

„Feasibility assessment is the disciplined and documented process of thinking through an idea from its logical beginning to its logical end to determine its practical viability potential, given the realities of the environment in which it is going to be implemented."(Vincent Amanor-Boadu, 2003) [26]. In general, a feasibility assessment consists of three stages of evaluation and each stage faces a key question [26]. The first stage is the operational feasibility, which concerns about the question „Will it work?" [26]. The following stage is the technical feasibility, this stage answers the question „Can it be applied?" [26]. However, the first and second stages together are in most cases consider to be the actual overall technical feasibility [26]. The third and last stage is the economic feasibility, which responds the question „ Is it economical recommendable to implement it?" [26].

In this study the technical and operational feasibilities will be analysed as one single stage. The evaluation to be conduct as part of this work will focus on the issue of finding the best appropriate measurement device or best recommendable combination of devices to prevent failure within the wind turbine nacelle. The measurement devices to be evaluated include:

- 3D laser scanner

- Infrared thermometer system

- Video camera system

- Vibration sensor

All those measurement instruments have been introduced in the previous chapters. In this connection, it had been summarised the technical abilities related to inspections within the wind turbine, as well the currently applications and the viability of integrate the device on a mobile robot.

6.1   Technical and Operational feasibility

Based on the experiment results and the knowledge acquired through the literature review, a feasibility assessment has been carried out. Aim of the feasibility evaluation is to identify the most suitable device, regarding the technical and economic aspects, to be integrated on a mobile robot in order to inspect the wind turbine nacelle components. The technical feasibility assessment focused on following criteria:

- Inspection tasks, which can be conducted by the device.

- Automation potential and robot compatibility.

- Data accuracy.

- Reliability in terms of: maintainability, availability and failure.

The first and main step of the technical and operational evaluation was to analyse which inspection tasks can be conducted by each device system and accordingly their accuracy in doing so. Based on the literature review, the following table, which summarises the inspection tasks in the wind turbine nacelle and correspondingly which device is able to accomplish it, has been established. It should be noted at this point, that the four studied devices detect some failures at different stages of development. In particular, the „external" damages, which begin to occur on the surface causing at an early stage hardly any noticeable variance on the components operation condition. The detection of a damage at an advanced stage means not necessary the result of a

total loss, but it definitely reduces the period of the maintenance planning process. The „X" in brackets means the detection of the damage by the measurement device in a slightly advanced stage of development. Moreover, it should be noticed, that the table consider, besides the inspection tasks for mechanical damage of the nacelle components, also the inspection task for the electrical system within the nacelle.

Inspection task	Infrared Thermometer	3D-Laser-Scanner	Video Camera System	Vibration Sensor
Misalignment detection	X	X		X
Gearbox Failure (Interior area)	X			X
Wear	(X)	X	(X)	(X)
Corrosion		X	(X)	
Cracks	(X)	(X)	X	(X)
Micro-pitting		X	(X)	
Fatigue	(X)	X	X	(X)
Loose screw		X	X	
Debris		X	X	
Electrical system	X			
Oil level test and read fill levels	(X)	X	X	(X)
Winding damage (Generator)	X			X
Overheating	X			

Table 6.1: Coverage of inspection tasks by each sensor devices.

By observing the Table 6.1, it can be noticed that the infrared thermometer and the vibration sensor detect oftentimes the damage, listed in the table, at a slight advanced development stage. However, the infrared thermometer and vibration sensor have essential advantage of being able to detect „internal" damages, which are for visual inspection devices, as the 3D laser scanner and the video camera system, unobtainable.

In addition to that, it is also remarked that the video camera system and 3D laser scanner are on the one hand nearly able to complete the same inspection tasks within

the wind turbine nacelle, but on the other hand they differ from each other in the quality and accuracy of captured images, as the 3D laser scanner, due to its precisely captured image, is capable to detect in many cases the damage at an earlier stage than the video camera system. Based on Table 6.1, the percentage of the inspection tasks each device are capable to cover has been defined. The following graph in Figure 6.1 displays the percentage inspection task range coverage by each measurement device.
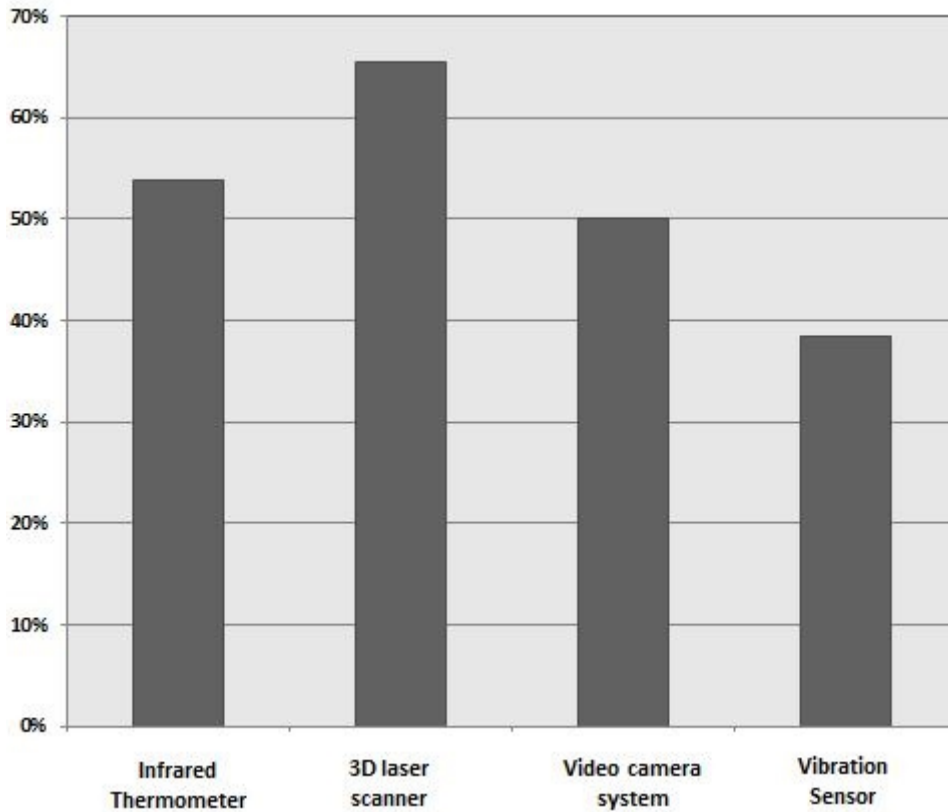
Figure 6.1: Percentage inspection task range covering by single measurement device.

As show in the Table 6.1 and in the graph of Figure 6.1, none of the four devices are able to accomplish all required inspection tasks. The highest percentage among the four devices shows the 3D laser scanner, which covers the inspection tasks within the nacelle by around 65 percent, followed by the infrared thermometer system with more than 50 percent. However, a combination of several devices, that complement one another, is the most technical feasible option.

In order to find the most suitable combination of devices for a successful inspection, the following graph in Figure 6.2 has been plotted. The graph basically shows the per-

centage inspection task coverage by the six possible combinations between the devices.
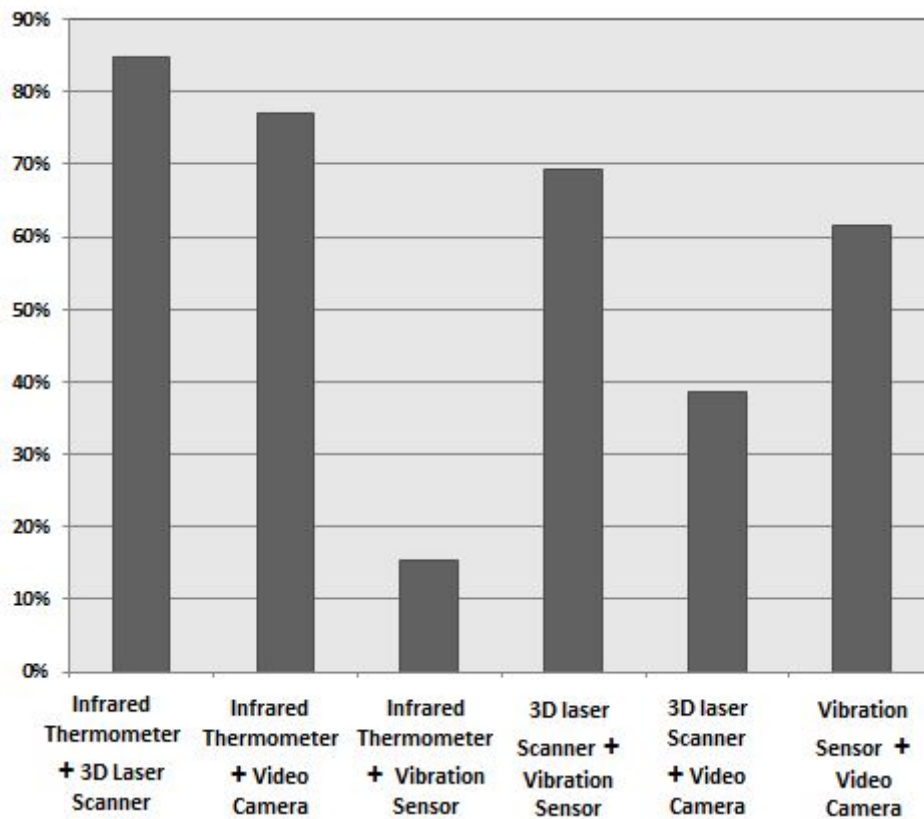
Figure 6.2: Percentage inspection task range covering by combination of measurement devices.

As it can be seen in the graph of Figure 6.2 the coverage value increased significantly by combining two devices with each other. According to the graph, the inspection task coverage by the combinations of *Infrared thermometer + Vibration sensor* and *3D laser scanner + video camera system* have a relative low coverage value. This is explained by the fact that the infrared thermometer and the vibration sensor of the first combination are both more suitable to detect the „internal" damage of the components as long as the other two devices, 3D laser scanner and video camera system, are more applicable for the detection of „external" damage.

This on the other hand can be confirmed by observing the coverage value of remaining combinations, which contain a mixture of both type of damage detection, „internal" and „external". As result of this analysis, the best suitable combination of measurement devices for the inspection of the wind turbine nacelle interior area is the combination of the *Infrared thermometer + 3D laser scanner*.

In relation to the failure rates and its resultant downtimes, the coverage value of the combinations, however, show slight different value. Based on the information obtained from the graph in Figure 3.1 the following graph, presented in Figure 6.3, has been established. Basically the graph outlines the failures frequency of nacelle components and the resultant downtimes.
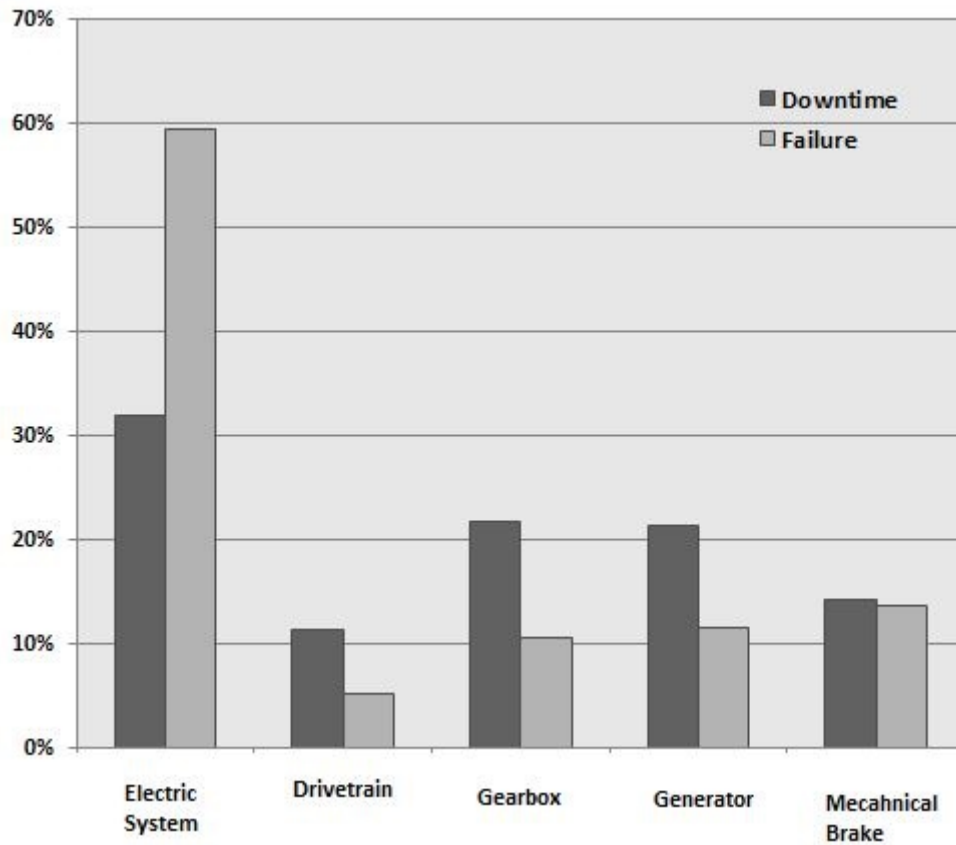
Figure 6.3: Failures frequency and the resultant downtimes.

By taking into account the in Figure 6.3 shown failure frequency and downtime periods and the in Table 3.2 shown wind turbine inspection tasks per component, the percentage inspection task coverages of the six combinations have been redefined. In this connection, the coverage value has been redefined, basically by calculating the frequency of failure, which happen to occur per component. The result of this analysis is graphical demonstrated in Figure 6.4. It should be noted at this point, the dark grey bar represents the coverage value in relation to the downtime as long the light grey bar displays the coverage value in relation to the failure frequency.
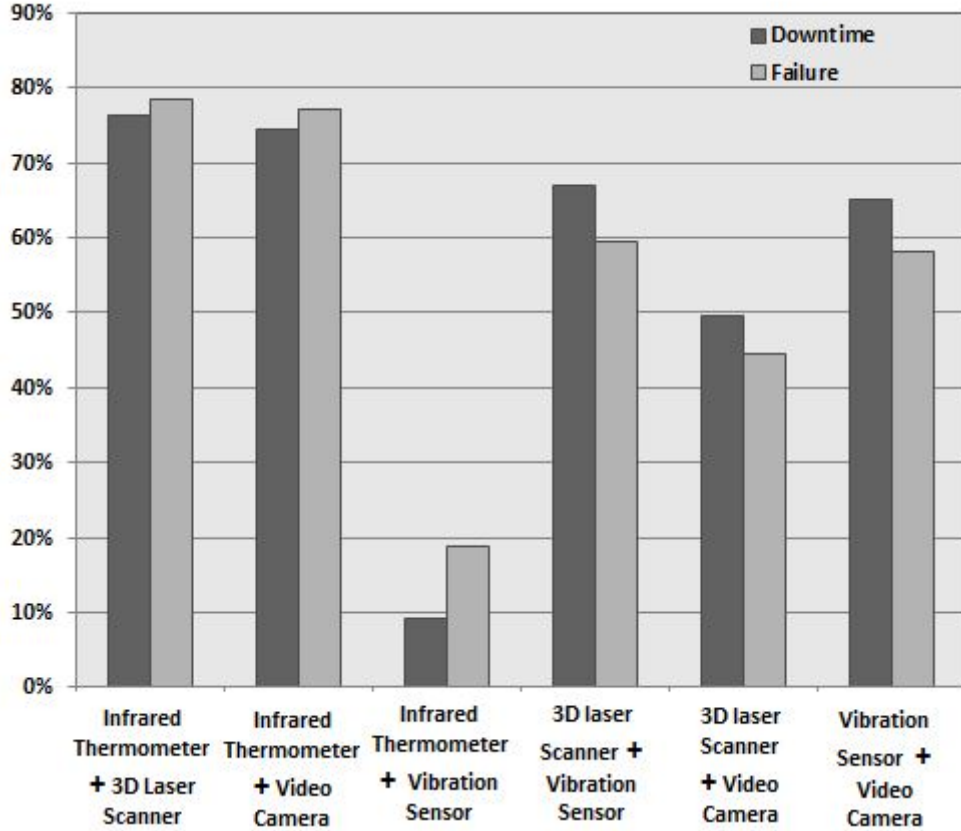
Figure 6.4: Coverage value in relation to the downtime and failure frequency.

Although the values change slightly the combination of the devices *Infrared thermome-ter + 3D laser scanner* remains the most suitable for the inspection of the components in the nacelle in terms of accuracy and tasks execution, followed by the combination of the devices *Infrared thermometer + Video camera system.*

Besides from the inspection tasks execution and the accuracy of the obtained data it is also from great importance that the devices are reliable, robot compatible and also feature automation potential. As previous shown, the four devices evaluated in this study presents fully robot compatibility technology regarding the integration of trans-mission channels, and their dimension and weight. The four devices feature usually several interfaces for signal input and output including among others: USB, Ethernet, analog/digital output and input, trigger interfaces and so on [30]. These enable a com-plete parametrisation and remote monitoring of the devices, as also the adjustment of signal processing functions [30].

6.2 Economic feasibility

The final decision of whether or not a project is going to be implemented depends on its costs and revenues. The economic viability of inspecting the wind turbine nacelle interior area with a mobile robot equipped with sensors devices has been conducted, in the framework of this work, by considering the following factors:

- Revenue through energy production

- Cost for operation and maintenance (O&M)

- Cost of downtimes

- Cost of devices installation and maintenance

Aim of this economic feasibility evaluation is also to identify the most suitable device, regarding the economic aspects, to be integrated on a mobile robot. The first step of the economical evaluation was to defined the energy production of a wind turbine in typical year of operation. The amount of energy captured by a wind turbine can be calculated as [31]:

$$E = C_p \cdot 0.5 \cdot A \cdot \rho \left[\int_{T_1}^{T_2} V_\infty{}^3 \cdot dT + V_\infty{}^3 \left[T_2 - T_3 \right] \right] \tag{6.1}$$

where, C_p is the power coefficient, ρ the air density, A the rotor swept area, V_∞ is the wind speed, T_1 number of days at cut-in speed, T_2 number of days at rated speed and T_3 number of days at cut-out speed [31]. However, the cut-in speed is the speed at which the rotor blades starts to rotate and the wind turbine begins to generate energy, this speed is usually between $3 - 4 \frac{m}{s}$ [79]. The rated speed is the maximum wind speed at which the wind turbine is able to produce energy without causing any damage to the system, and it is typically between $7 - 12 \frac{m}{s}$. The cut-out speed is the wind speed at which the wind turbine is brought to stillstand to avoid any damage because of high wind, this speed is generally around $25 \frac{m}{s}$ [79]. It has been assumed for the calculation of the energy production that the power coefficient C_p is constant between the cut-in speed and rated speed [31]. It should be noted at this point, that the data used for the economic feasibility are captured from an offshore wind turbine and have been

obtained from the Strathclyde University [31]. The speed exceedence curve at the site of this wind turbine has been approximated by the following equation [31]:

$$T_i = \left(\frac{60}{V_\infty}\right)^2 \tag{6.2}$$

Herewith the number of day at cut-in speed, rated speed and cut-out speed can be calculated [31]. The following graph shows the speed exceedence curve for this analysis.
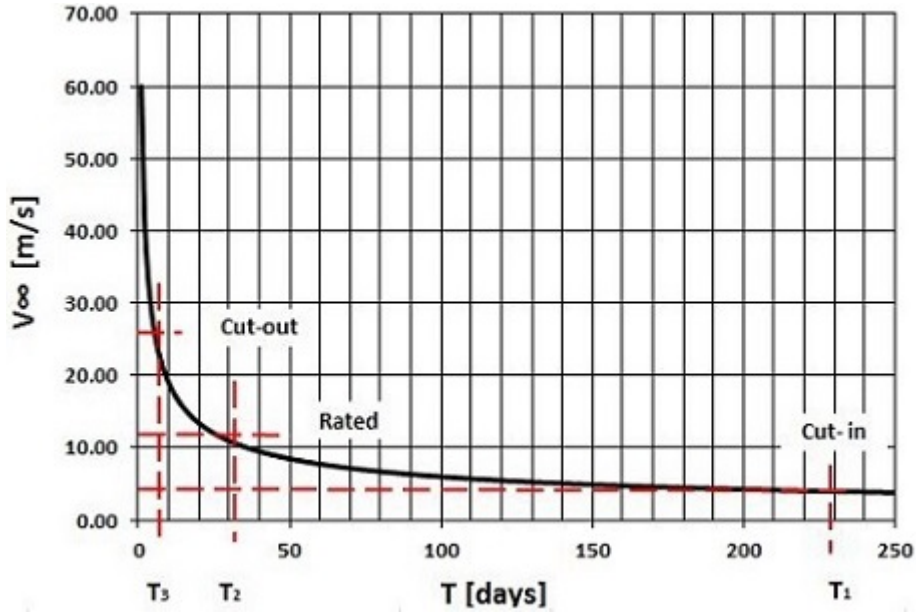
Figure 6.5: Speed exceedence curve.

The following table shows the assumed data obtained from the Strathclyde University for the calculation of the, in the framework of this study, simulated wind turbine energy production [31].

Factor	Value
Wind Speed V_∞	$3.4\frac{m}{s}$
Rotor diameter D	$94m$
Cut-in wind speed V_1	$4\frac{m}{s}$
Rated speed V_2	$10.8\frac{m}{s}$
Cut-out speed V_3	$24\frac{m}{s}$
Power coefficient C_p	0.42
Air density ρ	$1.21\frac{kg}{m^3}$
Total cost of the turbine	2100000.00 £

Table 6.2: Assumed data for the calculation of the wind turbine energy output [31].

By substituting the values given in Table 6.2 in the Equation (6.1) it results that the energy production in a typical year of operation for a offshore wind turbine is approximately 141013.27 $kW - days$ or rather 3384318.4 kWh [31].

However, the capacity coefficient of the analysed wind turbine is defined by [34]:

$$\text{Capacity coefficient} = \frac{\text{Energy output in a typical year of operation}}{\text{Wind Turbine rated power output of installation}} \tag{6.3}$$

where the Wind Turbine rated power output can be calculated through [31]:

$$\text{Wind Turbine rated power output} = C_p \cdot 0.5 \cdot A \cdot \rho \cdot V_\infty{}^3. \tag{6.4}$$

The capacity coefficient of the wind turbine is the real energy output of the wind turbine as the proportion of the wind turbine maximum capacity [80]. By substituting the value in the equation (6.3) it results for the capacity coefficient $0, 174$ [31].

In order to estimate the cost of the electricity generated from the wind turbine with a total operation time of 20 years, the total cost of the wind turbine has to be divided by the amount of produced energy. In doing so the cost of the electricity generated from wind turbine is estimated to be approximately 3.1 $\frac{\text{Pence}}{kWh}$ [31]. This is reproduced in the following equation [33].

$$\text{Cost of electricity} = \frac{\text{Total cost of the wind turbine}}{20 \text{ Years} \cdot \text{Energy output in a typical year of operation}} \tag{6.5}$$

The total cost of the wind turbine given in Table 6.2 is assumed to cover the foundations and the electrical connections. However, the actual total cost of a wind turbine includes in reality far more than that. The additional costs include the operational and maintenance cost (O&M), unexpected downtimes and as well interest as in the most case the capital is loaned from a bank. In case of a loan, the annual repayment can be calculated by [31]:

$$\text{Annual repayment} = \frac{C \cdot r \cdot (1 + r)^n}{(1 + n) - 1} \tag{6.6}$$

77

where C is the capital loaned, r the interest rate and n the number of years for the repayment. By assuming a repayment over a period of 20 years, $n = 20$ and an interest rate of 4%, the cost of the electricity generated from wind turbine increases to approximately 4.56 $\frac{Pence}{kWh}$.

The operation and maintenance cost composed of a mixture of cost factors, these are: administration, repair, regular maintenance, spare parts and insurance [32]. However, the cost for regular maintenance and insurance are predictable costs, on the contrary to the cost for repair and spare parts, which are difficult to estimate [32]. The following graph in Figure 6.6 displays the percentage proportion of each factor [32].

- Insurance 13%
- Administration 21%
- Service (Maintanence & Repair) and spare parts 26%
- Others (Land rent, power from the grid) 40%
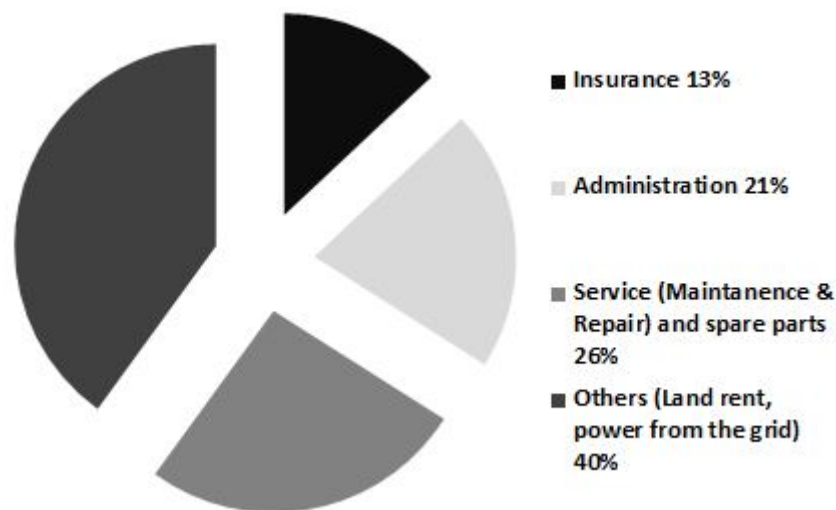
Figure 6.6: Operation and Maintenance cost factors [32].

However, numerous of studies have shown that the O&M cost increases with the age of the wind turbine. The overall O&M costs are usually approximately 1.2-1.5 eurocents per kWh over the total life span of the wind turbine [32]. Based on that, for the economic evaluation in this study it will be assumed an average cost for the O&M of 1.3 $\frac{Pence}{kWh}$. Therefrom are 0.169 $\frac{pence}{kWh}$ cost of insurance and estimated 0.13 $\frac{Pence}{kWh}$ cost of service.

In order to estimated the cost of unexpected downtimes, the energy production loss caused by the downtimes has been calculated:

$$E_{Lost} = \left[\frac{\text{Total Energy output [kW-days]}}{365} \right] \cdot \text{Downtime [days]} \cdot 24h \qquad (6.7)$$

The downtime days can be obtained from the graph in Figure 3.1. Finally, the loss of energy production due to downtimes is approximately 243856.37 kWh. This results in 7.2% of the total energy, which can be generated. The cost of downtime obtained through the calculation is 0.319 $\frac{\text{Pence}}{kWh}$.

The following table provides a briefly overview from the costs calculated for the economic evaluation.

Cost	Value
Cost of electricity (no loan)	3.10 $\frac{\text{Pence}}{kWh}$
Cost of electricity (repayment over 20 years)	4.56 $\frac{\text{Pence}}{kWh}$
O&M cost	1.3 $\frac{\text{Pence}}{kWh}$
Downtime cost	0.319 $\frac{\text{Pence}}{kWh}$
Insurance cost (included in O&M cost)	0.169 $\frac{\text{Pence}}{kWh}$
Cost of service (included in O&M cost)	0.13 $\frac{\text{Pence}}{kWh}$

Table 6.3: Costs calculated for the economic evaluation.

The overall cost of electricity per kWh from a wind turbine, in case of a repayment over 20 years is 6.18 $\frac{\text{Pence}}{kWh}$. This is reproduced in the following equation.

$$\text{Electricity Cost} = \text{Electricity cost (loaned Capital)} + \text{O\&M cost} + \text{Downtime cost}$$
$$(6.8)$$

According to the knowledges acquired from the investigation, the insurance companies are willing to decrease the insurance rate in case the wind turbine nacelle interior area is permanent inspected by a mobile robot. Furthermore, the inspection of nacelle components with a mobile-robot significantly decreases the downtime of the wind turbine. Therefore, it will be assumed in this study that through inspecting the wind turbine with a mobile-robot the insurance cost will be reduced by 15%, the inspection cost by 60% and the downtime cost by 50%. However, at this point it should also be consider for the economic evaluation, the cost for the mobile-robot. In the framework of this

study it will be assumed that the total cost of the mobile-robot is 20,000 £ and that it has an overall life span of 20 years. Finally, this results in a cost for the mobile-robot of 0.0295 $\frac{Pence}{kWh}$.

By taking into account these previous mentioned reductions, the electricity cost from the wind turbine decreases from 6.18 $\frac{Pence}{kWh}$ to 5.95 $\frac{Pence}{kWh}$. The following graph in Figure 6.7 shows the electricity cost difference between inspecting the nacelle components with a mobile-robot or with the conventional method.
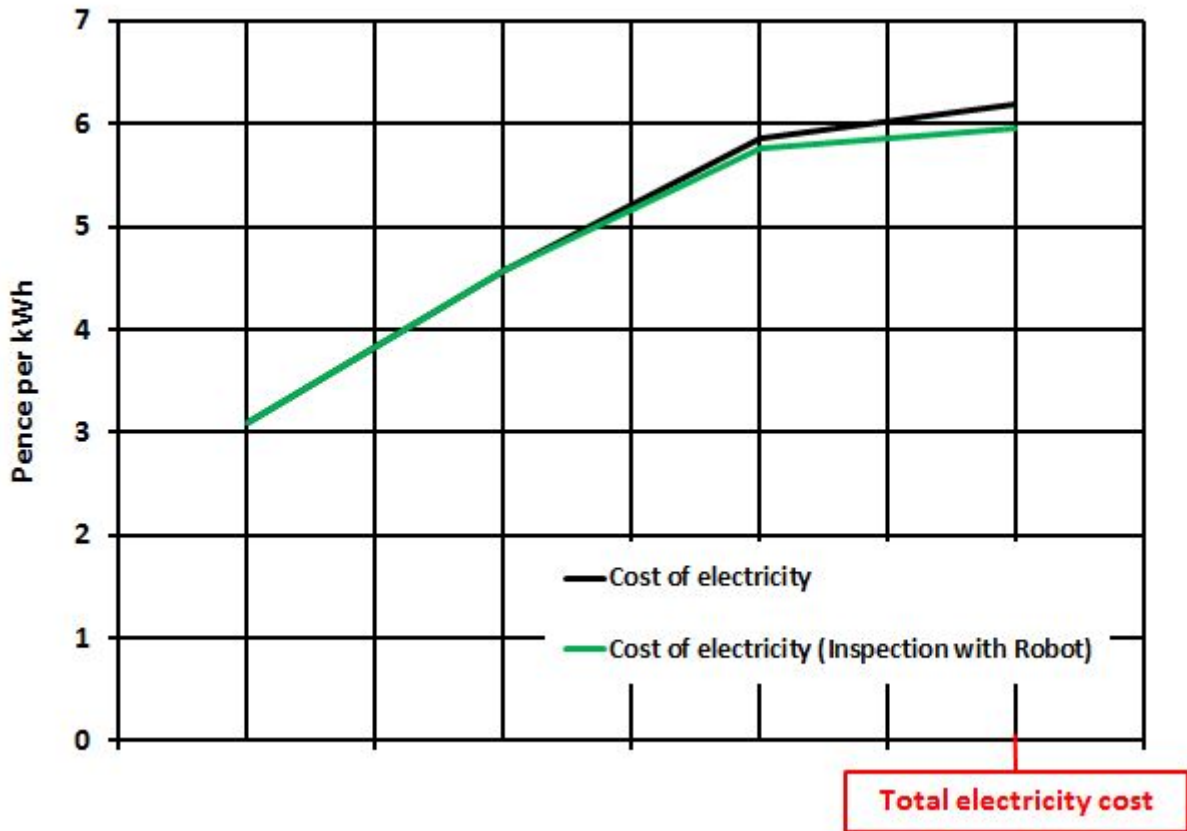
Figure 6.7: Difference of the electricity cost.

Based on this results, it can be confirmed, that the inspections of the nacelle components with a mobile-robot equipped with sensor devices reduce the electricity cost significantly. In this connection, the total electricity cost lows by 3.77%. Over the 20 years of operation this results in a saving of 158,199.03 £, which corresponds to 7.53% of the total wind turbine cost. According to this outcome, it can be concluded that the investment in a mobile-robot for inspections in the nacelle interior area is definitely long term economically feasible.

The results obtained from the technical, operation and economic evaluation have been combined together, in order to find the most suitable sensor device or rather the most suitable combination of sensor devices regarding the economic and technical aspects for the inspection of the wind turbine nacelle interior area. The graph in Figure 6.8 shows the technical and economic quality rating of the sensor device combinations established in this study.
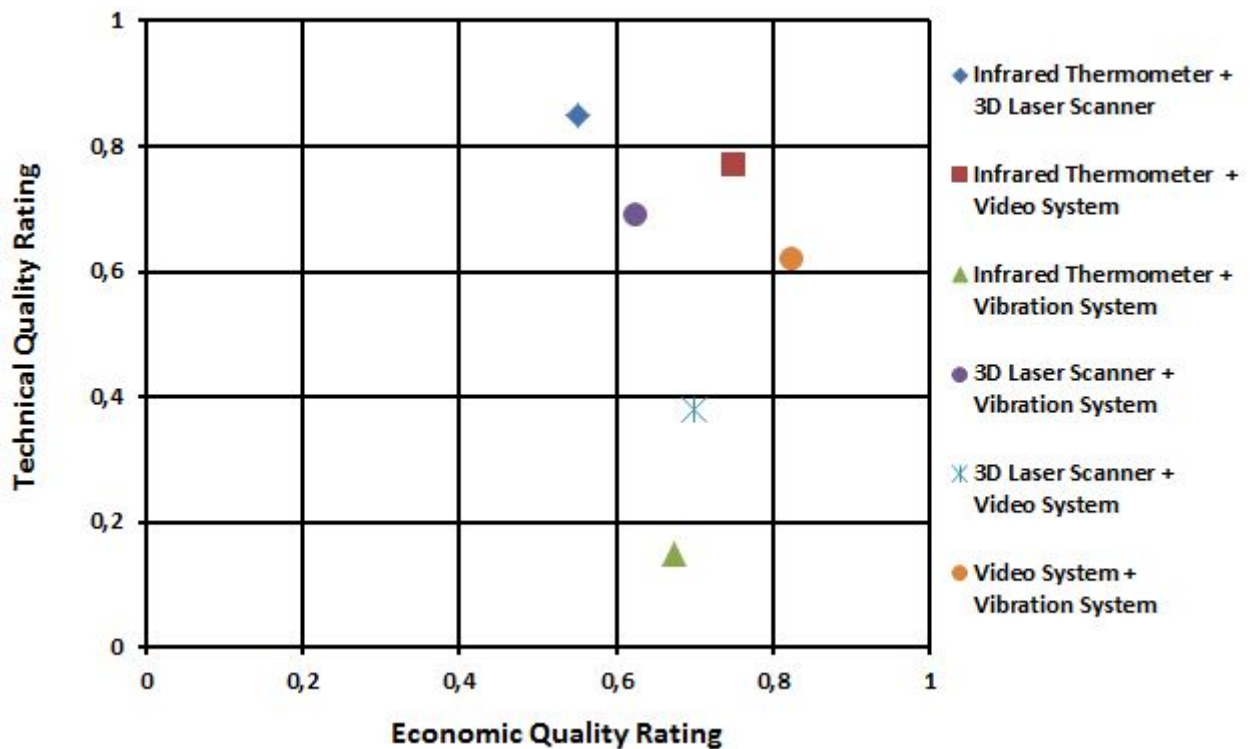
Figure 6.8: Technical and economic quality rating of sensor device combinations.

As it can be seen in the graph of Figure 6.8, the combination of the *3D laser scanner and infrared thermometer* features on the one hand the best technical quality rating but on the other hand the lowest economic quality rating compared to the other combinations. The second best combination, related to both factors, points the *infrared thermometer and the video system*. However, the economic quality ratings of the combinations differ only slightly from each other, while the technical quality ratings vary significantly from combination to combination. Over the long term, the slight variance of cost between the combinations are hardly distinguishable from each other and therefore negligible for the feasibility evaluation.

Chapter 7

Conclusion

The aim of this dissertation was to assess the technical and economic feasibility of inspecting the wind turbine mechanical damages by using a mobile-robot equipped with sensor devices. Thereby, only the integrated components in the nacelle interior area of the wind turbine has been considered. The overall evaluation process comprised of three main steps. Firstly, of a literature analysis, where the research problem and focus has been identified. Second of all, of an experimental analysis, due to experiments with a 3D laser scanner it has been analysed the accuracy of the acquired 3D images and evaluated the potential application of the 3D laser system as an inspection devices. In the last step of the evaluation process, a feasibility assessment has been carried out. Based on the conducted experiments and literature analysis, it could be highlighted, which inspection tasks can be performed by each sensor device or combination of sensor devices as well the therewith gained economic benefits.

In the literature analysis, it has been identified the failure frequencies and their severities as well resultant downtimes. Moreover, it has been presented the wind turbine failure impacts and sources. Based on that findings, the most frequent mechanical failures within the nacelle were highlighted and in more details explained. Furthermore, the inspection tasks to be conducted in the wind turbine have been demonstrated and consequently the several state-of-art inspection methods. Thereby, it has been discovered the project of inspecting the wind turbine nacelle components with a mobile-robot, which has been developed by the the German Wind Technology Management GmbH in cooperation with the Bremen Center for mechatronics, represented by the Bremen

Institute for structure and manufacturing plant [22]. This knowledge reinforced the viability of inspecting the wind turbine nacelle components with a mobile-robot.

The results obtained from the experimental analysis, which comprised of five steps, showed that the detection of mechanical damages with a 3D laser scanner is precisely and enables in comparison to other sensor devices specific measurement for the analysis. Accordingly, not just the surface assessment could be carried out but also due to monitoring of components coordinates in the CAD program other deviation could be easily and accurately detected. All in all, the analysis of component damages in the CAD program not just simplifies the inspection but also improves the detection of any anomalies.

Based on the literature and experimental analysis, the technical and economic feasibility assessment has been performed. The evaluation conducted focused on the issue of finding the best appropriate measurement device or best recommendable combination of devices to prevent failure within the wind turbine nacelle. The main step of the technical and operational evaluation was to analyse, which inspection tasks can be carried out by each measurement device and accordingly their precision in doing so. In this process, it emerged, that the 3D laser scanner covers the inspection tasks within the nacelle by 65 percent and showed therewith the highest amount. In order to increase the coverage amount, the measurement devices have been combined with each other and subsequently reanalysed. This analysis has shown, that the combination of the 3D laser scanner with a infrared thermometer device is the best suitable system, with a coverage amount of approximately 75 percent in relation to failure frequencies and downtimes. Furthermore, it has been considered in the technical and operational feasibility, the automation potential and robot compatibility of the devices and as well the data accuracy and their reliability in terms of: maintainability, availability and failure.

In the economic feasibility, it has been evaluated the economic benefits gained by applying the mobile-robot equipped with sensor devices as an inspection method. In this process, it emerged, that the electricity cost decreases from 6.18 $\frac{Pence}{kWh}$ to 5.95 $\frac{Pence}{kWh}$. Over the 20 years life time of the wind turbine, this results in a saving of 158,199.03 £, which corresponds to 7.53% of the total wind turbine cost.

Taken together, this study has shown that the inspection of mechanical damages within the wind turbine nacelle by using a mobile robot equipped with sensor devices is, in relation to the economic and technical aspects, thoroughly feasible. However, further research could assess experimentally the detection accuracy of offset and angularity misalignment of the drivetrain with a 3D laser scanner. Moreover, future experimental study in detecting mechanical damages with the other analysed sensor devices would be beneficial to determine their effectiveness and precision. Consequently, these findings will provide the required information for the determination of the monitoring points and procedure.

Bibliography

[1] **Fried, L.; Sawyer, S.; Shukla, S.; Qiao, L.:** *Global Wind Energy Council.* Brussels, 2012.

[2] **The European Wind Energy Association:** *Wind in Power, Annual Statistic 2012.* February 2013.

[3] **Ragheb, A.; Ragheb, M.:** *Wind Turbine Gearbox Technologies, Fundamental and Advanced Topics in Wind Power, Dr. Rupp Carriveau (Ed.).* ISBN: 978-953-307-508-2, InTech, 2011.

[4] **Winkelmaier,H.:** *Energiesysteme - Windenergie, 02 – Bauformen und Aerodynamik von Windkraftanlagen* WS 2005/06.

[5] **Zubiaga ,M.:** *Wind Energy, Energy Transmission and Grid Integration of AC Offshore Wind Farms* ISBN: 978-953-51-0368-4, InTech, 2012.

[6] **Dinner, H.:** *KISSsoft AG, Showing the teeth at the wind...* Switzerland.

[7] **Coultate, J.:** *Wind Turbine Drivetrain Technology and Cost Drivers.* Romax Technology, 2011.

[8] **Urban, A.:** *With or without gearbox? Drive train development for wind turbines (from a supplier perspective).* Technologie-Workshop (Windenergie - Quo Vadis?), Businnes Engineer SKF Austria AG, 2010.

[9] **Lönker, O.:** *Siemens testet Windenergieanlagen mit getriebeloser Antriebstechnik, Energy Sector Division Renewable Energy, Press.* Informations number: ERE200807.048 d, Press Sector Energy Siemens, Erlangen, 8. Juli 2008.

[10] **Hahn, B.; Durstewitz, M.; Rohrig, K.:** *Reliability of Wind Turbiines, Experiences of 15 years with 1,500 WTs.* Verein an der Universität Kassel e.V., 34119, Kassel, Germany.

[11] **Winergy:** *Windergy HybridDrive,Gearbox and Generator in one product.*

[12] **Schoofs, S.; Meyer, F.:** *BINE - Informationen und Ideen zu Energie und Umwelt, Fehlerfrüherkennung in Windenergieanlagen.* ISSN 0937-8367, Fachinformationszentrum Karlsruhe, Gesellschaft für wissenschaftlich-technische Information mbH, Eggenstein-Leopoldshafen, 1999.

[13] **Faulstich, S.; Hahn, B.; Tavner.P.J:** *Research Article, Wind turbine downtime and its importance for offshore deployment.* Wind Energ.2001; 14:327-337, published online 26 July 2010 in Wiley Online Library.

[14] **Mobil:** *Micro-pitting Can Lead to Macro Problems.* Exxon Mobil Corporation, 2006.

[15] **Bundesverband WindEnergie:** *Grundsätze für die Prüfung zur zustandsorientierten Instandhaltung von Windenergieanlagen.* Verabschiedet durch den technischen Sachverständigenbeirat des BWE, Osnabrück, 21. September 2007.

[16] **Berberian, P.:** *Wind Turbine Alignment FAQ.* Alignment Supplies, Inc.

[17] **Prüftechnik:** *VIBROWEB, VIBROWEB XP, Online Condition Monitoring for critical machinery and special application, Catalog.* Prüftechnik LTD, Ismaning, Germany, 2011.

[18] **Berberian, P.:** *An Engineer's guide, Making Maintenance Matter, Optimising Plant availability using laser shaft alignment, vibration analysis and dynamic balancing techniques.* Prüftechnik LTD, Edition 8.011, Burntwood, Staffordshire, 2002.

[19] **Prüftechnik:** *VIBSCANNER, Datenerfassung& Maschinendiagnose.* Prüftechnik LTD, Condition Monitoring, Ismaning, Germany, 2002.

[20] **Becker, E.; Poste, P.:** *Condition Monitoring application, Keeping the blades turning, Condition monitoring of wind turbine gears.* Ludeca INC., Prüftechnik LTD, Condition Monitoring, Ismaning, Germany, 2002.

[21] **Hyres, R.W.; McGowan, J.G.; Sullivan, K.L, Manwell, J.F., Syrett, B.C.:** *Condition monitoring and prognosis of utility scale wind turbines.* Energy Materials, VOL 1, NO 3, 2006.

[22] **Hetzer, K.; Schenck, C.:** *Auge auf See, Höhe Verfügbarkeit entscheidet off-shore über die Wirtschaftlichkeit. Eine robotergestützte Ferninspektion soll Serviceeinsätze reduzieren.* Deutsche Windtechnik Betriebsführung GmbH, Bremer Centrum für Mechatronik and the Bremer Institut für Structurmechanik und Produktionsanlagen, Ausgust 2011.

[23] **MICRO-EPSILON MESSTECHNIK GmbH & Co. KG:** *ScanCONTROL 2D/3D laser scanner (laser profile sensors).* Ortenburg, Germany.

[24] **Mitutoyo, CNC Vision Measuring System, Quick Vision:** *Advanced system architecture for higher levels of CNC vision measurement performance.* Bulletin No. 1953, USA, November 2008.

[25] **Chaves-Schwinteck, P.; Mönnich, K.:** *Temporal & Energetic Downtime Losses and its Influence on Wind Farm Economics.* DEWI Magazin NO.42, February, 2013, Oldenburg.

[26] **Vincent Amanor-Boadu, PhD:** *Assessing the Feasibility of Business Propositions.* Department of Agricultural Economics Agricultural Marketing Resource Center, Kansas State University, November 2003.

[27] **Pompe, B.:** *Windkraft.* University Greifswald, Institut für Physik Vorlesung Umweltphysik Bachelor of Science in Umweltwissenschaften, 6. Semester Fassung vom 25th September 2009.

[28] **Konica Minolta:** *Vivid 910, non-contact, 3-D Digitizer, Breakthrough in Process Innovation, Konica Minolta's VIVID 910 the ideal 3D capture device for industrial applications in product design and manufacturing inspection.* Konica Minolta Sensing , INC., Australia, 2001, 2002.

[29] **Randy H. Shih:** *Parametric Modeling with Creo Parametric, An Introduction to Creo Parametric 1.0.* Oregon Institute of Technology, SDC Publication.

[30] **Micro Epsilon:** *Mehr Präzision, Thermometer, Berührungslose Infrarot- Temperatursensoren.* Micro-epsilon Messtechnik GmbH& Co. KG, Ortenburg, Germany.

[31] **University of Strathclyde:** *Energy Resources and Policy, Assignment: Wind Power.* November 2012.

[32] **Krohn, S.; Morthorst, P.; Awerbuch, S.:** *EWEA, The European Wind Power Association, The Economics of Wind Energy, A report by the European Wind Energy Association.* March 2009.

[33] **University of Strathclyde:** *Energy Resources and Policy, Tutorial: Wind Power.* November 2012.

[34] **University of Strathclyde:** *Energy Resources and Policy, Handout: Wind Power.* November 2012.

[35] *Wattnow Magazin Feb. 2013 Edition, Wind Generator Technology).* Feb, 2013.

[36] **Kusiak, A.; Zhang, Z.:** *Gearbox Fault detection.* Department of Mechanical and Industrial Engineering at the University of Iowa. May 2012.

[37] http://www.spiegel.de/fotostrecke/windenergie-die-wichtigsten-player-der-zukunftsbranche-fotostrecke-60931-3.html (29.06.2013)

[38] http://www.energie-und-technik.de/erneuerbare-energien/technik-know-how/windenergie/article/78545/0/Roboter_inspiziert_Gondeln_von_Offshore-Windkraftanlagen/ (02.07.2013)

[39] http://www.nordex-online.com/en/products-services/hybrid-towers.html (04.07.2013)

[40] http://www.energienaturelle.ch/pdf/broschuren/ENM_technischebeschreibung.pdf (04.07.2013)

[41] http://www.windkraftanlage.de/ratgeber/genehmigung/bauarten/ (12.07.2013)

[42] http://www.windkraftanlage.de/ratgeber/genehmigung/bauarten/ (12.07.2013)

[43] http://en.wikipedia.org/wiki/Wind_turbine (15.07.2013)

[44] http://en.wikipedia.org/wiki/Darrieus_wind_turbine (15.07.2013)

[45] http://naturschutz.mareno.net/windenergie.html (15.07.2013)

[46] http://www.buchhandel.de/WebApi1/GetMmo.asp?MmoId=1068284&mmoType=PDF (15.07.2013)

[47] http://www.estw.de/cms/Unternehmen_Presse/Unser_Umweltbeitrag/Windparks/Windparks.html (15.07.2013)

[48] http://www.mmpa.org/Uploaded_Files/93/93934e74-9b35-4566-b5b4-dad8816fed46.pdf (19.07.2013)

[49] http://www.eng.iastate.edu/twt/Courses/Undergrad/packet/info/gears.htm (19.07.2013)

[50] http://www2.eng.cam.ac.uk/~mpfs/climate/IB_elective_windpower_gears_2012.pdf (19.07.2013)

[51] https://en.wikipedia.org/wiki/Epicyclic_gearing (19.07.2013)

[52] https://www.highpowermedia.com/RET-Monitor/2905/kers-epicyclic-gearing (19.07.2013)

[53] http://www.marketsandmarkets.com/Market-Reports/direct-drive-gearless-wind-turbine-market-805.html (19.07.2013)

[54] http://.eepublishers.co.za/article/siemens-228-04-siemens-launches-new-gearless-wind-turbine-for-low-to-moderate-wind-speeds.html (20.07.2013)

[55] http://www.can-cia.org/uploads/pics/turbine.jpg (21.07.2013)

[56] http://www.buykorea21.com/productImage/img20110629093208.jpg (21.07.2013)

[57] http://www.ecw.org/windpower/web/cat2a.html (22.07.2013)

[58] http://de.wikipedia.org/wiki/Graufleckigkeit (22.07.2013)

[59] http://en.wikipedia.org/wiki/Micro_pitting (22.07.2013)

[60] http://interdisciplinaryenergystudy.wiki.lovett.org/file/view/energyreportVertical-axis-wind-turbine.jpg/203903336/energyreportVertical-axis-wind-turbine.jpg (22.07.2013)

[61] http://s0.geograph.org.uk/geophotos/01/57/75/1577594_6fe65039.jpg (22.07.2013)

[62] http://homepage.ruhr-uni-bochum.de/Guenter.Luetzig/lmgk/lmgk-grafiken/Oel_fress_h.jpg (25.07.2013)

[63] http://rsta.royalsocietypublishing.org/content/368/1929/4829/F7.large.jpg (25.07.2013)

[64] http://www.renewableenergyworld.com/rea/news/article/2012/06/changing-a-gear-gearbox-lubrication-and-its-impact-on-wind-turbine-lifespan (25.07.2013)

[65] http://www.erneuerbareenergien.de/der-rost-und-das-meer/150/434/28766/ (26.07.2013)

[66] http://de.wikipedia.org/wiki/Korrosion (26.07.2013)

[67] http://www.cotes.com/dehumidifier-in-windmills.html (26.07.2013)

[68] http://www.windturbine-gearboxrepair.com/wind-turbine-gearbox-services-gearbox-inspection.html (31.07.2013)

[69] http://0101.nccdn.net/1_5/285/171/01e/3.9mmBrochure.pdf (31.07.2013)

[70] http://de.wikipedia.org/wiki/RFID (31.07.2013)

[71] http://www.irispdm.com/products.aspx?contentid=49 (04.08.2013)

[72] https://de.wikipedia.org/wiki/Antriebswelle (04.08.2013)

[73] https://en.wikipedia.org/wiki/Drive_shaft (04.08.2013)

[74] http://www.konicaminolta.eu/de/measuring-instruments/produkte/3d-messtechnik/range-7.html (07.08.2013)

[75] http://www.terramagnetica.com/wp-content/uploads/2009/08/size.jpg (10.08.2013)

[76] http://colortheearthturquoise.files.wordpress.com/2012/03/horizontal-and-vertical-axis-wind-turbines-1.pdf (10.08.2013)

[77] http://www1.eere.energy.gov/wind/inside_a_wind_turbine.html (10.08.2013)

[78] http://www.micro-epsilon.de/laser-scanner-profile-sensor/Software/scanCONTROL-Integration/index.html?item=1 (12.08.2013)

[79] http://www.wind-power-program.com/turbine_characteristics.htm (14.08.2013)

[80] https://www.wind-watch.org/faq-output.php (14.08.2013)

[81] http://geomagic.com/en/products-landing-pages/inspection (21.08.2013)

[82] http://finance.yahoo.com/news/media-video-advisory-geomagic-freeform-203800696.html (21.08.2013)